MECHANISMS OF FLASHOVER OF CONTAMINATED INSULATORS

by

Tsen-Chung Cheng

B.S., Massachusetts Institute of Technology
(1969)
M.S., Massachusetts Institute of Technology
(1970)
E.E., Massachusetts Institute of Technology
(1970)

SUBMITTED IN PARTIAL FULFILLMENT OF THE

REQUIREMENTS FOR THE DEGREE OF

DOCTOR OF SCIENCE

at the

MASSACHUSETTS INSTITUTE OF TECHNOLOGY

May, 1974

Signature of Author
Department of Electrical Engineering, May 24, 1974

Certified by
Thesis Supervisor

Accepted by
Chairman, Departmental Committee on Graduate Students

This thesis is dedicated to
my parents

MECHANISMS OF FLASHOVER OF CONTAMINATED INSULATORS

by

Tsen-Chung Cheng

Submitted to the Department of Electrical Engineering on May 24, 1974 in partial fulfillment of the requirements for the Degree of Doctor of Science.

ABSTRACT

Theoretical and experimental studies are carried out to investigate the problem of contamination flashover of transmission line insulators. To facilitate constructing mathematical models, experiments are categorized on one-dimensional, two-dimensional and real insulator cases.

For the one-dimensional model, instead of taking the conventional static approach, a comprehensive dynamic model is introduced where time is added as an explicit variable. To complete the physical picture, an arc growth equation, based on the power being fed in at the arc tip via either cathode or anode falls, is derived and proposed. The model's dynamic predictions are verified experimentally, thus establishing for the first time the important role played by electrode falls, especially the cathode, in contamination flashovers. The cathode fall is hence further studied theoretically and a mathematical model is completed, based partially on the principles of glow discharge. The model is capable of predicting quite accurately the cathode drops for different metallic surfaces and water.

For the two-dimensional model, experiments are done on the flat-plate with a variety of surface coatings under fogging conditions. A mathematical model, which is an improved version of previous theories, is constructed and correlated with experimental findings.

The effects of surface conditions on flashovers are also studied. Experiments are performed in uniform-field and flat-plate geometries. Extensive tests on times to flashover are carried out and results indicate that two operating regimes, the EHD regime and the Townsend breakdown regime, can be distinctly detected. Both regimes of operation are further studied theoretically. The threshold voltage is determined, and the effect of E-field on contact angle is investigated, culminating in a proposed elongation mechanism via contact angle hysteresis. The times to flashover are estimated theoretically and compared with experiments.

Throughout the above studies, high-speed motion pictures are utilized so that many physical phenomenon can be viewed in slow motion.

The conclusions of these studies establish very definitely the importance of the arc tip region and surface condition in causing contamination flashovers. They form the basis of suggestions for improving the insulator performance.

THESIS SUPERVISOR: Gerald L. Wilson
TITLE: Associate Professor of Electrical Engineering

ACKNOWLEDGEMENTS

I am greatly indebted to my thesis supervisor, Professor G.L. Wilson, for his guidance and help and his complete support throughout the course of this work. It has indeed been a privilege to work under him. I also wish to thank Dr. D. Jolly for his helpful advice and discussions. His active interest in this work has been an invaluable aid to its progress. Members of my thesis committee, Professors J. Trump and J. Melcher, have provided useful criticisms and suggestions throughout the course of this work.

Ed Los deserves a special mention for his excellent work on arc modeling which is vitally related to this thesis. His many helpful suggestions will long be remembered. D. Otten performed most of the experimental work in the linear model, for which I am most grateful. D. King provided much help during the experimental phases of this work and his skill in building equipment is especially appreciated. Other students have also contributed during the various experimental stages and to each of them, I wish to express my thanks. I am also proud to be associated with each and every member of the Electric Power Systems Engineering Laboratory. The financial support is provided by a grant from the National Science Foundation under the Research Applied to National Needs (RANN) Program.

The expert secretarial skills of Miss B. Smith is indispensable to the preparation of this thesis and all the

figure drawings were done by Mr. A. Giordani.

Lastly, I wish to thank my wife-to-be, Doris for her constant encouragements and her spending countless nights and weekends with me in my laboratory when we could be doing things of a more romantic nature.

TABLE OF CONTENTS

Page

TITLE PAGE 1

DEDICATION 2

ABSTRACT 3

ACKNOWLEDGEMENT 5

TABLE OF CONTENTS 7

LIST OF FIGURES 10

LIST OF TABLES 14

CHAPTER I - INTRODUCTION 15

- 1.1 Nature of the Problem 15
- 1.2 Scope of Previous Studies 18
- 1.3 Scope of Present Studies 20
- Bibliography 24

CHAPTER II - ONE DIMENSIONAL SIMULATION OF A CONTAMINATED INSULATOR - LINEAR MODEL 26

- 2.1 Introduction 26
- 2.2 Previous Theories 27
- 2.3 Recent Developments 37
- 2.4 Linear Model Experiments 39
- 2.5 Dynamic Theory of Contamination Flashover I 48
  - 2.5.1 Introduction 48
  - 2.5.2 Dynamic Arc Model 49
  - 2.5.3 The Discharge Growth Equation 51
  - 2.5.4 Normalization of the System Equations 54
  - 2.5.5 Initial Conditions 57
  - 2.5.6 Computer Simulation 60
  - 2.5.7 Comparison Between Theory and Experiment 63
  - 2.5.8 Discussion 69
  - 2.5.9 Limitations of the Model 73

Page

2.6 Dynamic Theory of Contamination Flashover II 75

2.6.1 Introduction 75
2.6.2 Theoretical Considerations 79
2.6.3 Computer Simulation 89
2.6.4 Comparison Between Theory and Experiment 89
2.6.5 Discussion 89

2.7 Studies of Cathode Fall Phenomenon 98

2.7.1 Introduction 98
2.7.2 Previous Research on Glow Discharges 101
2.7.3 A Model for Cathode Fall Region 107
2.7.4 Numerical Solution 112
2.7.5 Discussion 113
Bibliography 119

CHAPTER III - TWO DIMENSIONAL SIMULATION OF A CONTAMINATED INSULATOR - THE FLAT-PLATE 123

3.1 Introduction 123

3.2 Description of Experimental Apparatus 124

3.3 Experimental Testing Procedure 127

3.4 Discussion of Experimental Results 138

3.5 Theoretical Developments 142

3.5.1 Past Theories 142
3.5.2 Present Approaches 145
3.5.3 Discussion of Results 153

Bibliography 158

CHAPTER IV - SURFACE EFFECTS ON FLASHOVER PHENOMENON 159

4.1 Introduction 159

4.2 Theory of Behavior of a Water-Drop in an Electric Field 162

4.2.1 History of the Problem 162
4.2.2 Present Theoretical Approaches 164
4.2.3 Contact Angle Analysis 167

Page

4.3 Experiments on a Water-Drop in a Uniform Field 184

4.3.1 Description of Experimental Apparatus 184
4.3.2 Single Drop Tests in Uniform Field 188
4.3.3 Discussion of Theoretical and Experimental Results 190

4.4 Experiments on Flat-Plate Flashover in Fog 201

4.4.1 Description of Experimental Apparatus 201
4.4.2 Flat-Plate Tests in Fog 202
4.4.3 Discussion of Experimental Results 207

Bibliography 212

CHAPTER V - HIGH-SPEED PHOTOGRAPHIC STUDIES OF FLASHOVERS 214

5.1 Introduction 214

5.2 Linear Model Flashover 214

5.3 Flat-Plate Flashover 216

5.4 Insulator Testing 219

CHAPTER VI - SUMMARY, CONCLUSIONS AND SUGGESTIONS FOR FUTURE RESEARCH 222

6.1 Summary and Conclusions 222

6.2 Suggestions for Future Research 228

APPENDIX A - COMPUTER PROGRAM FOR DYNAMIC THEORY I 231

APPENDIX B - COMPUTER PROGRAM FOR DYNAMIC THEORY II 233

APPENDIX C - COMPUTER PROGRAM FOR CATHODE FALL REGION SIMULATION 235

APPENDIX D - COMPUTER PROGRAM FOR FLAT-PLATE SIMULATIONS 238

BIOGRAPHY 240

LIST OF FIGURES

		Page
Fig. 2.1	Obenaus Model	28
Fig. 2.2	Graphical Solution for Obenaus Model	29
Fig. 2.3	Rod Insulators (a) Standard long-rod (type VKL 75/14) (b) Antifog rod	32
Fig. 2.4	Equivalent Circuit Diagram for Dynamic Theories	36
Fig. 2.5	Critical Current of Breakdown Theory Compared With Experimental Data Points	40
Fig. 2.6	Linear Model	42
Fig. 2.7	A Sketch of the Linear Model	43
Fig. 2.8	Simplified Circuit Diagram for Experimental Set-up	45
Fig. 2.9	Experimental Set-up of Linear Model	46
Fig. 2.10	Streak Camera Record	47
Fig. 2.11	Scope Record	47
Fig. 2.12	Comparison Between Dynamic Theory I and Experiments	65
Fig. 2.13	Comparison Between Dynamic Theory I and Experiments	66
Fig. 2.14	Comparison Between Dynamic Theory I and Experiments	67
Fig. 2.15	Comparison Between Dynamic Theory I and Experiments	68
Fig. 2.16	Comparison Between the Static and a Dynamic E_a-I_a Characteristic for a Propagating Arc	71
Fig. 2.17	Bi-cylindrical Arc Geometry	80
Fig. 2.18	Experimental Results: Normalized Time Constants vs. Normalized Resistance	85

Page

Fig. 2.19 Comparison Between Dynamic Theory II and Experiments 91

Fig. 2.20 Comparison Between Dynamic Theory II and Experiments 92

Fig. 2.21 Comparison Between Dynamic Theory II and Experiments 93

Fig. 2.22 Comparison Between Dynamic Theory II and Experiments 94

Fig. 2.23 Comparison Between Dynamic Theory II and Experiments 95

Fig. 2.24 Comparison Between Dynamic Theory II and Experiments 96

Fig. 2.25 Electrode Regime of an Arc Discharge 100

Fig. 2.26 Glow Discharge Parameters 102

Fig. 2.27 Glow Discharge Parameters 103

Fig. 2.28 Steenbeck's Theory of Cathodic Voltage 106

Fig. 2.29 Calculated Discharge Parameters 114

Fig. 2.30 Calculated Discharge Parameters 115

Fig. 3.1 A Flat-Plate 125

Fig. 3.2 Inner Electrode 126
  (a) Side View
  (b) Top View

Fig. 3.3 Flat-Plate on Rotor 129

Fig. 3.4 Coating in Progress 129

Fig. 3.5 Plate Being Dried 131

Fig. 3.6 Plate in the Test Chamber 131

Fig. 3.7 Conductance of Flat-Plate as Function of Fogging Time 132

Fig. 3.8 Critical Resistivity vs. Voltage 135

		Page
Fig. 3.9	A Sample Visicorder Record	136
Fig. 3.10	A Sample Scope Picture	137
Fig. 3.11	Sketch of a Flat-Plate Arc Discharge	143
Fig. 3.12	Sketch of Current Flow from Arc Root to Outer Electrode	150
Fig. 3.13	Graphical Solution of Flat-Plate Theory	154
Fig. 3.14	(a) Comparison Between Flat-Plate Theory and Experiments	155
	(b) Comparison Between Flat-Plate Theory and Experiments	156
Fig. 4.1	A Sessile Drop	165
Fig. 4.2	Simplified Geometry of a Sessile Drop	165
Fig. 4.3	Computer Simulation of a Two-Dimensional Half-Cylinder	168
Fig. 4.4	Contact Angle Illustration	170
Fig. 4.5	Drop-Under Perturbational Change	170
Fig. 4.6	Simplified Circuit Diagram	186
Fig. 4.7	Experimental Set-up	187
Fig. 4.8	Parallel-Plate Set-up	189
Fig. 4.9	A Typical Scope Trace	191
Fig. 4.10	Time to Flashover for a Single Drop in Uniform Field	192
Fig. 4.11	Contact Angle Hysteresis	197
Fig. 4.12	Calibration of Test Chamber in Fog	203
Fig. 4.13	Time to Flashover for a Single Drop on a Flat-Plate	204
Fig. 4.14	Threshold Voltages for Various Surface Conditions	205

Page

Fig. 4.15 Time to Flashover for a Flat-Plate in Fog 208

Fig. 4.16 Time to Flashover for a Flat-Plate in Fig 211

Fig. 5.1 Linear Channel Flashover 215
   (a) Water Surface as Anode
   (b) Water Surface as Cathode

Fig. 5.2 Flat-Plate Discharges 217
   (a) Initial Discharges
   (b) Developed Discharges With Branching at the Arc Tip

Fig. 5.3 Flat-Plate Flashover 218

Fig. 5.4 Flashover of an Insulator With Metallic Bands on the Two Outermost Skirts 221
   (a) Geometry of Experimental Set-up
   (b) Initial Discharge Activities
   (c) Flashover

LIST OF TABLES

		Page
Table 2.1	Critical Discharge Quantities	31
Table 2.2	Dynamic Theory I - System Equations	55
Table 2.3	Normalized System of Equation	58
Table 2.4	Range of Input Parameters	61
Table 2.5	Characteristic Arc Time Constants	72
Table 2.6	Dynamic Theory II - System Equations	87
Table 2.7	Comparison Between Theory and Experiment	90
Table 2.8	Tabulation of α/P vs. E/P	110
Table 2.9	Glow Cathode Model - System Equations	111
Table 2.10	Comparison Between Theory and Experiment for Some Metallic Surfaces	117
Table 2.11	Water Cathode Fall Voltages for Various γ	118
Table 3.1	Composition of Slurry	128
Table 3.2	Flat-Plate Test Data	139
Table 4.1	Determination of Contact Angle of Water on Clean Plexiglas	172
Table 4.2	Determination of Contact Angle of Water on Teflon	173
Table 4.3	Determination of Contact Angle of Water on Greased Plexiglas	174

CHAPTER I

INTRODUCTION

1.1 Nature of the Problem

During the past decade, demand for electric power has been growing steadily. In order to meet such increasing demands, utilities must construct transmission lines of higher and higher delivering capacities and at higher levels of reliability. For a number of reasons, raising the transmitting voltage seems to be the most feasible method. Thus lines of 765 kV are already in operation in the U.S. Even higher voltages are being contemplated. But, overhead lines of high voltages are subject to two basic abnormal conditions which cause the most frequent flashovers and outages. They are:

1) overvoltages caused by switching surges and
2) abnormal electrical stresses in the insulating system caused by contamination of insulator surfaces.

In addition, lightning strokes may cause overvoltages; their harmful effects, however, have been reduced by the use of lightning arresters. All these abnormal conditions have been extensively studied. It is the purpose of this thesis to investigate in greater detail the physical mechanisms which are primarily responsible for the occurrence of contamination flashovers.

Contamination flashover is a form of arc discharge across the moist surface of an insulator upon which have been previously deposited soluble particulates so that it has become conducting. Once the arc discharge, which usually starts either from the central cap or pin, has bridged over the top porcelain surface and the creepage path beneath it, the insulating strength of that insulator is entirely gone. The result is that other insulators in series, with increased voltage stresses will be similarly affected and eventually an outage occurs. The necessary ingredients for a flashover are moisture and contaminant substances. The former is usually supplied by nature in the form of fog, dew, rain, ice and etc. The sources of contamination can range from industrial pollution to bird droppings. A recent survey by an IEEE Working Group[1] tabulated a great variety of such contaminants. With the presence of moisture and contamination, the flashover process is thought to occur as follows. During dry weather, pollutants are deposited on an insulator surface. When the surface becomes moist, some pollutants are dissolved and the surface starts to conduct electrically. The passage of leakage current produces ohmic heating and the area around the pin, where the electric field is the highest, starts to dry out. Subsequently, a dry zone is formed around the pin and low current arcs can now bridge this zone. The heat of the arc evaporates more water, enlarging the dry zone and the arc. Sometimes the arc lengthens to some extent and goes out. Other times, the arc grows until the insulator string is bridged and full fault current then flows, causing the circuit breakers to be tripped. This picture embodies the essence of what happens during a contamination flashover. After a flashover, the line may or may not be automatically reclosed, depending on whether the factors causing the fault have been removed or not. Frequently, it may be many minutes before the line can support voltage again. Also, quite often, the insulators involved are damaged by the arcs and must be replaced.

Many physical processes are involved in the above sequence of events. This thesis will focus attention on the electrical breakdown of the dry band and subsequent arc discharges propagating across the moist, conducting film.

The propagation of arcs across the film is also very much dependent upon the surface conditions. A new and clean insulator, as a rule, performs much better than an old and contaminated one. On the surface of the former, moisture tends to bead up, forming separate droplets. While, on the surface of the latter, moisture can wet the surface quite readily, thus increasing the leakage current and initiating arc discharges. The ability to maintain either a clean surface or a water-repellent one has therefore become a major criterion in the design of an insulator. Keeping an insulator clean can be accomplished by regular washing; while making the surface water-resistant can be achieved by greasing. Depending on locality, washing usually has to be performed fairly frequently, making it a costly operation. Greasing, on the other hand, is cheaper and must be done only once every two years or so. Furthermore, the improvement in insulator performance is far more significant.[2,3] Silicone grease is probably the most commonly used type and will also be used in our studies. The primary function of the grease is to break-up the moist film so that surface resistance increases. The physical processes involved, however, are more complex. Under the influence of electric fields, water drops can elongate in shape and coalesce with neighboring drops, reducing the water repellent property of the surface. Greasing is thus not totally effective against all kinds of flashover conditions. These physical mechanisms will be investigated below.

1.2 Scope of Previous Studies

The contamination flashover problem has been studied since the earliest days of outdoor power transmission. In the beginning, most of the studies were aimed at designing a better insulating unit either by increasing the leakage path or by lessening the collection of moisture. Thus anti-fog as well as oil-filled insulators were introduced. As pollution from industrial and agricultural sources has increased drastically in the last two decades and as transmission voltages are increased, the flashover problem has become more serious and more costly. It was clear that by mere trial and error in modifying the shapes of insulators, the best solution would not necessarily be found. Some basic understanding of the problem is required. The first quantitative theory was proposed by Obenaus[4]. The theory models the flashover process as an arc discharge in series with a resistance. Neumarker[5] worked out the mathematical steps involved and derived a critical voltage for flashover. Hampton[6] proposed that, for an arc running over a water resistor (a jet of water), instability (and hence flashover) would occur if the electric field in the arc was less than that in the water resistor. He further demonstrated that the arc-voltage gradient was higher than that for an arc in air. Alston and Zoledziowski[7] calculated a critical condition below which flashover was impossible, also for a uniform-resistor case. This can be shown to be the same as Hampton's if the same arc characteristic is used. McElroy[8] extended the calculations further to include the two-dimensional flat-plate which he designed.

Experimentally, numerous test methods were devised to simulate the natural conditions. Macchiaroli and Turner[9] proposed a standard test method. Kawai[10-12] at Project UHV performed an extensive series of tests to determine the performance characteristics of contaminated insulators. Because some parts of the leakage distance do not function during scintillations, he introduced the concept of "effective leakage distance". Both McElroy[8] and Jolly[13] tested suspension insulators in salt fog to determine the effects of porous surface layers, fog salt concentration, and surface conditions.

In the past few years, some considerations have been directed towards determining the physical causes behind flashovers. Wilkins[14] proposed a mechanism called "elongation by ionization and successive root formation". The theory proposes that elongation is produced by new ionization paths created at the tip of the discharge. Jolly derived a mathematical model which gives the critical voltage if it is assumed that the discharge root will move forward whenever the field strength at the root exceeds some constant value E_o.

Relatively little literature is available on the subject of surface conditions in relation to flashover voltages. Most of the information available is from test reports on greasing and washing insulators.[15-17] Tominaga[2] studied the moisture absorption process on contaminated surfaces.

Besides the U.S. and Britain, research on contamination flashover is also being carried in other countries, particularly Japan, Germany and France.

1.3 Scope of Present Studies

The present investigation was motivated by the need to understand the physical processes involved in a flashover. The study was carried out under a grant from the National Science Foundation. It became clear at the outset that, because of the complex nature of the problem, to fully explain, mathematically and physically, the flashover process for an insulator, is almost an insurmountable feat. The next best approach is to build simplified models so that the principal physical mechanisms can be determined and studied in a controlled manner. Their modes of operation, once understood, can then be used as a basis for designing improved insulators.

Our philosophy of approach is thus as follows: - to start from the simplest model, namely, a one-dimensional one so that the mathematical limitations to the physical model is minimized. Then a more complicated geometry is used, with a little less sophisticated model and so on. For the one-dimensional case, a linear channel model is employed. In such a model, an initial discharge is allowed to propagate over a salt water solution towards a grounded electrode. The propagation mechanism was studied and a physical growth equation derived. Then based on Mayr's and then Phillip's (later revised by Los) arc models respectively, two dynamic and comprehensive theories of propagation are constructed. These theoretical predictions were found to agree with experimental measurements, indicating that the proposed mechanisms are probably the principal forces behind the motion of the discharge. In line with this conclusion, the arc cathode regime was further studied. A physical model, based on the principles of glow discharges, is presented and the predicted cathode fall voltages are found to agree with the measured ones both for metallic and water electrodes.

For the two-dimensional case, a flat-plate is used. It is first coated with a slurry of predetermined composition and then tested under fog. The threshold voltages for various surface resistivities are measured through an extensive series of testing. A theoretical model is then constructed, which accounts for the fact that the surface resistance of the flat plate changes as the arc root propagates towards the outer electrode. The theory is found to compare favorably with experimental observations.

For the three-dimensional case, an IEEE standard insulator was tested, with and without metallic bands acting as arc stoppers. The propagation of the arc discharges over the skirts are recorded on high-speed films. However, since insufficient data was taken, it will not be reported here.

The effects of surface conditions on flashover were studied next. It is found in practice that a contaminated surface, being much more wettable than a clean one, also flashes over more readily. The fact that the drops bead up rather than spread out on a clean surface is partly the cause. The role played by the presence of moisture in flashover was examined. Numerous experiments were performed to determine the flashover process both in the presence of a single drop and under fog. Different regimes of operation of the electric breakdown process were observed. In line with these observations, physical theories are offered as explanations and in particular, a mechanism known as "motion via contact angle hysteresis" is proposed. An important phenomenon - filamentation of fog drops - is observed to effectively lower the flashover voltage significantly. The tests are performed under different surface conditions so that their respective effects can be determined.

High-speed motion pictures were taken throughout the course of the above studies. Some of the proposed theories are based on the observations thus recorded.

BIBLIOGRAPHY - CHAPTER I

1. "A Survey of the Problem of Insulator Contamination in the U.S. and Canada - Part I," IEEE Trans. on Power Apparatus and Systems, PAS-90, pp. 2577-2585 (1971).

2. A. Tominaga, "Moisture Absorption and Leakage Resistance on Contaminated Surfaces," Elec. Eng. in Japan, 85, No. 1, p. 33-42 (1965).

3. P.J. Lambeth, "Effect of Pollution on High-Voltage Outdoor Insulators," Proc. IEE, IEE Reviews, Vol. 118 #9R, Sept. 1971, pp. 1107-1130.

4. F. Obenaus, "Contamination Flashover and Creepage Path Length," Dtsch. Elektrotechnik, Vol. 12, 135-136 (1958).

5. G. Neumarker, "Contamination State and Creepage Path," Deutsche Akad., Berlin, Vol. 1, 352-359 (1959).

6. B. Hampton, "Flashover Mechanisms of Polluted Insulation," Proc. IEE, Vol. 111, 985-990 (1964).

7. L. Alston and S. Zoledziowski, "Growth of Discharges on Polluted Insulation," Proc. IEE, Vol. 110, 1260-1266 (1963).

8. A. McElroy, "Flashover Mechanisms of Insulator with Contaminated Surfaces," Ph.D. Thesis, Dept. of E.E., MIT, (1969).

9. B. Macchiaroli and F.J. Turner, "A New Contamination Test Method," IEEE PAS, PAS-88, pp. 1400-1411, Sept. 1969.

10. M. Kawai, "Research at Project UHV on the Performance of Contaminated Insulators - Part I: Basic Problems," IEEE, PAS, May/June 1973, pp. 1102-1110.

11. M. Kawai, "Research at Project UHV on the Performance of Contaminated Insulators - Part II: Application to Practical Design," IEEE, PAS May/June 1973, pp. 1111-1120.

12. A. Baker, and M. Kawai, "A Study on Dynamic Voltage Distribution on Contaminated Insulator Surface," IEEE PAS Sept./Oct. 1973, pp. 1517-1524.

13. D. Jolly, "Physical Processes in the Flashover of Insulators with Contaminated Surfaces," Ph.D. Thesis, Dept. of E.E., MIT, 1971.

14. R. Wilkins and A. Al-Baghdadi, "Arc Propagation Along an Electrolyte Surface," Proc. IEE, Vol. 118, #12, 1971.

15. J.E. Toms and A.B. Suttie, "Insulator Surface Treatments Prevention of Flashover due to Pollution: Results of Test on Greases," Electrical Review, 17, p. 412, (1965).

16. T. Seta, "Combatting the Contamination Problem by Applying Grease-like Water-Repellent Substance," ETJ of Japan, 7, No. 2, p. 73 (1962).

17. J.E. Conner and A.D. Lantz, "The Insulator Contamination Problem as Influenced by Silicone Surface Coatings," AIEE, 77, Part III, pp. 1101-1106, 1958.

CHAPTER II

ONE DIMENSIONAL SIMULATION OF A CONTAMINATED INSULATOR - LINEAR MODEL

2.1 Introduction

The reasons for analyzing a one-dimensional geometry are two-fold. First, the variables are more controllable and can be assumed to depend on distance and time alone. This assumption greatly simplifies the mathematics. Secondly, with the simplified experimental set-up, data-taking is more efficient and far more consistent. In real insulator testing cases, because of the complex geometries, it is difficult to interpret experimental results, whereas in simplified geometries, the results are more easily interpretable, indicating that a deterministic, rather than probabilistic, theoretical approach can be taken. The one-dimensional channel model used in this work has been used by other researchers (e.g. Wilkins). However, their flashover theories are based on static arc models, as shown below. The nature of a static model necessarily precludes the explicit use of time as an independent variable in terms of which all the other variables can be expressed. In addition, since the elongation mechanism is not understood, it is usually neglected. The resultant theories are thus incapable of predicting insulator performance under a time-varying situation, such as during a switching surge. Further, none of the theories up to date has been able to account for the observed differences in arc propagation[1-3] when different polarities are used. This chapter will attempt a brief review of the better known theories and then present a dynamic theory of arc growth based on a dynamic arc model as well as a proposed growth rate equation. Two theories will actually be presented, the second one using a more refined arc model. The chapter concludes with a theoretical model of cathode fall voltage.

2.2 Previous Theories

Even though contamination flashover has been studied for over sixty years, it was only until sixteen years ago that any theoretical study was attempted. The first quantitate theory was proposed by Obenaus in 1958, who outlined the derivational steps involved.[4] It was fully spelled out by his associates, Neumarker.[5] The theory models the flashover process as an arc discharge in series with a resistance as shown in Figure 2.1. The arc discharge represents the partial flashover on the insulator surface and the resistance the remaining portion of the surface. Since the surface is contaminated, resistances of different values, depending on degrees of contamination and wetness can be used. Hence, Obenaus assumes that a flashover would occur if the partial discharge is able to bridge the resistance without extinguishing. Since for the kind of discharges that are prevalent, the maximum current range is around an ampere or so, the discharge should have a falling V-I characteristic. The total characteristic for the whole channel is obtained by the addition of the two curves, as depicted in Figure 2.2.

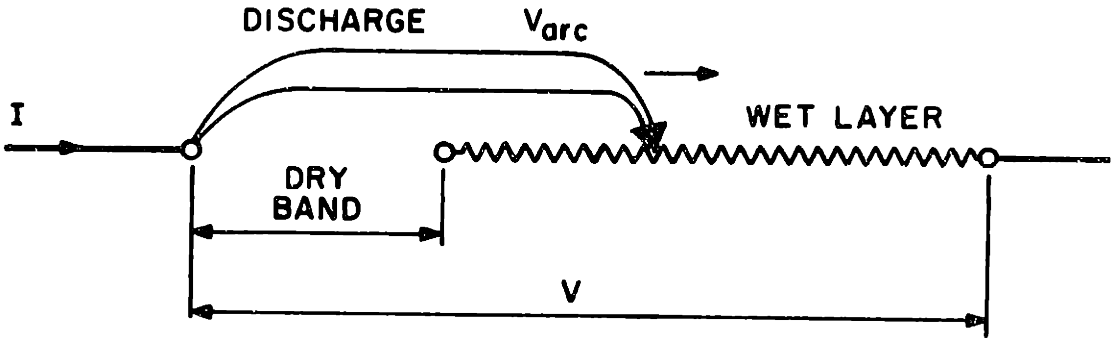

Figure 2.1 Obenaus Model

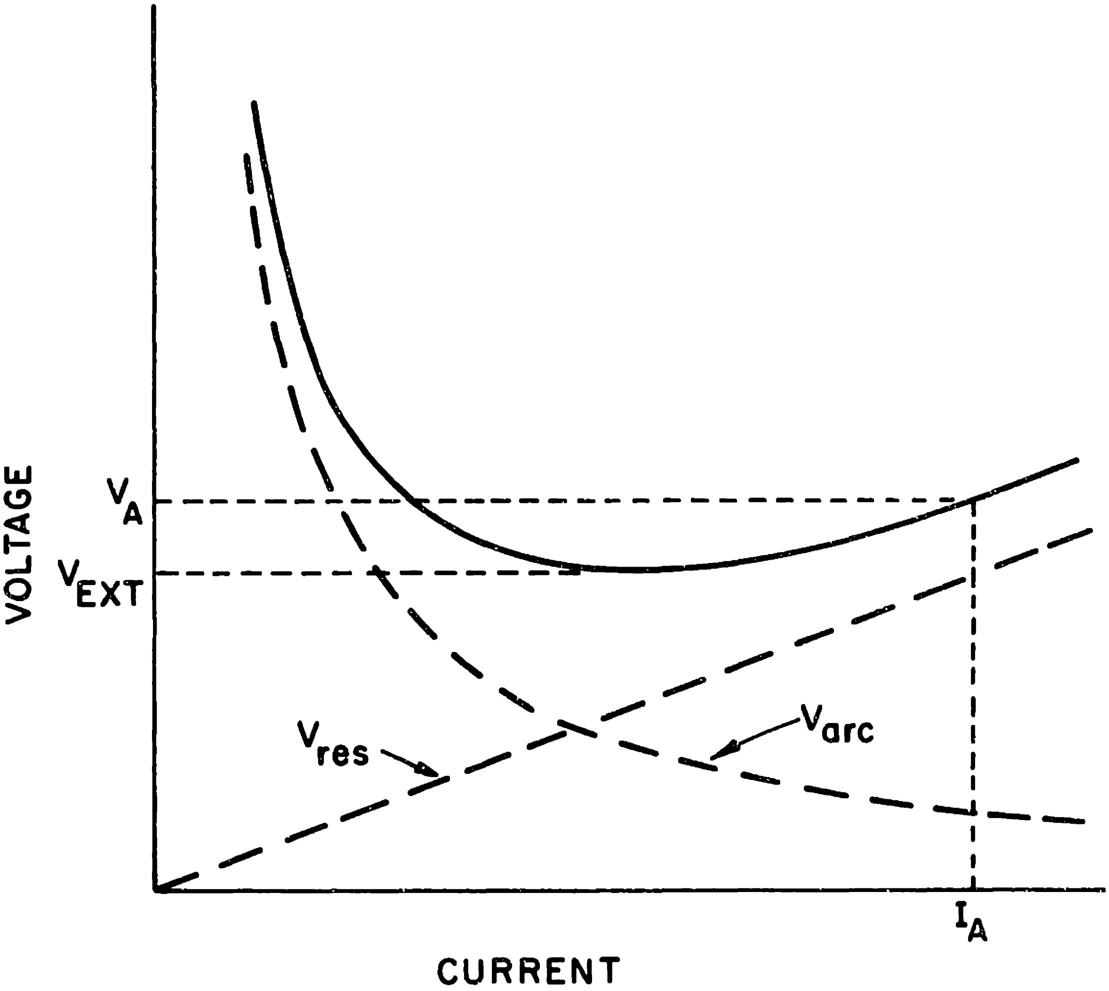

Figure 2.2 Graphical Solution for Obenaus Model

Theoretically, no solutions can exist below V_{ext}. Above V_{ext}, the operating point will be on the positively sloping portion of the curve, for the negatively sloping portion is unstable. Thus for example, with a voltage of V_a applied, a current of I_a could flow. The series resistance serves the following purpose. If the resistance is high enough, the slope of the straight line in Figure 2.2 will be very steep. Thus, when the arc V-I characteristic curve and the V_{res} curve are added, the resultant curve will have a higher V_{ext} than it would otherwise. Consequently, a higher flashover voltage is now needed. Thus, the higher the series resistance, the harder it is to flashover.

As previously mentioned, the actual calculations were done by Neumarker. The algebraic derivation for the long rod case is also given by Alston and Zoledziowski.[6] Jolly[7] carried the calculations further, deriving the critical resistivity and critical current for both the long rod case and the flat-plate case, as shown in Table 2.1. A long-rod insulator is shown in Figure 2.3 and a flat-plate in the following chapter. The critical resistivity is the limit above which flashover cannot occur. The critical current, on the other hand, has quite different meanings for the long rod and the flat-plate cases. In the former, it is the minimum current for a critical discharge length necessary for flashover. A critical discharge length is that distance discharge must bridge in order to ensure a flashover. It is

TABLE 2.1

CRITICAL DISCHARGE QUANTITIES(7)

	Idealized Flat-Plate (m=0)	Idealized Long Rod (m=1)
X_{crit}	ℓ	$\frac{\ell}{n+1}$
V_{crit}	$(n+1)\,[A\ell\,(\frac{\Omega B}{n})^{n}\,]^{\frac{1}{n+1}}$	$\frac{1}{A^{n+1}}\ \ell\,(\Omega B)^{\frac{n}{n+1}}$
Ω_{crit}	$\frac{n}{B\,(A\ell)^{1/n}}\ [\frac{V}{n+1}]^{\frac{n+1}{n}}$	$\frac{1}{BA^{1/n}}\ (\frac{V}{\ell})^{\frac{n+1}{n}}$
I_{crit}	$[\frac{nA\ell}{\Omega B}]^{1/n+1}$	$[\frac{A}{\Omega B}]^{1/n+1}$

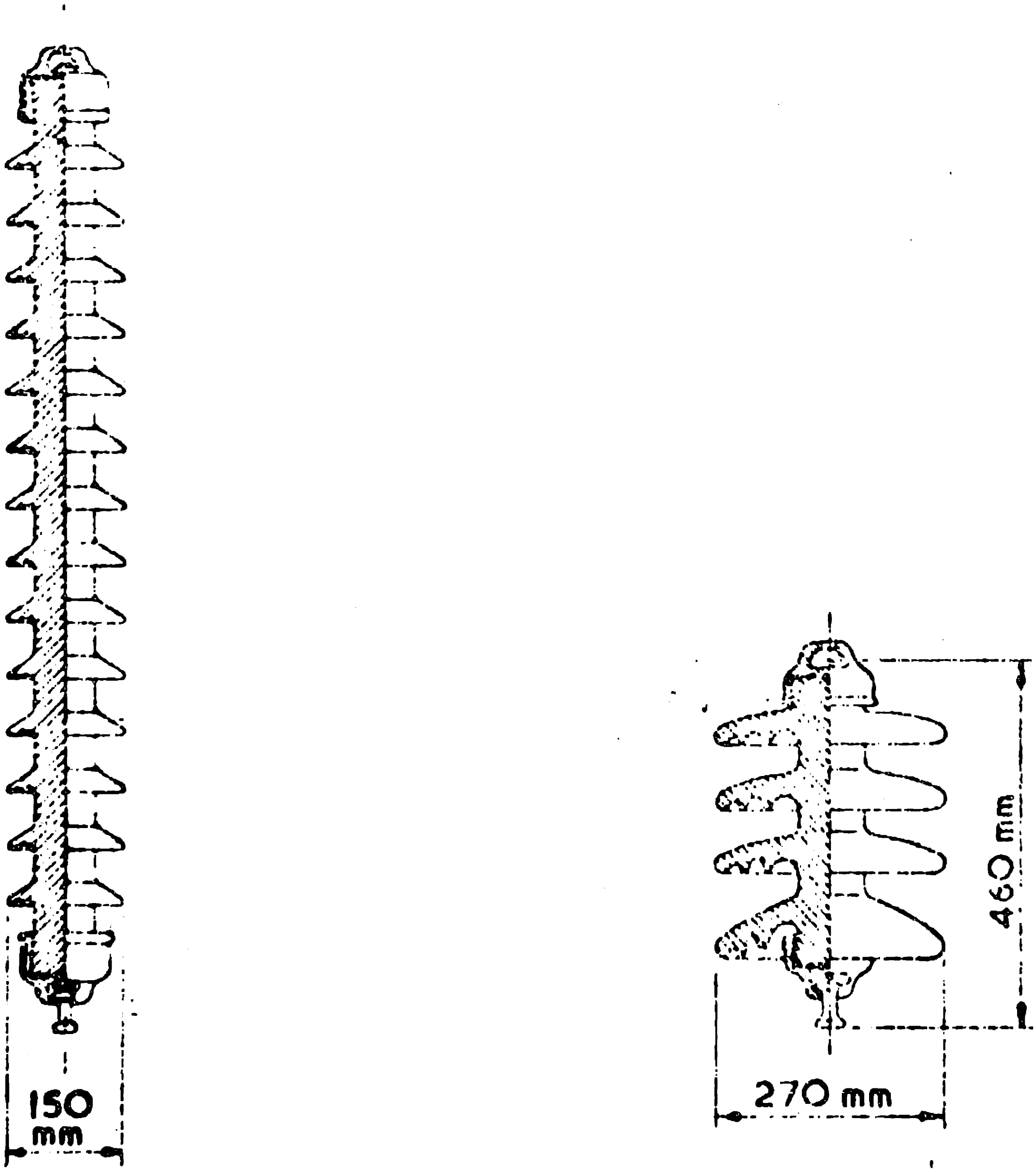

(a)

(b)

Figure 2.3 Rod Insulators

(a) Standard Long-rod (type VKL 75/14)

(b) Antifog Rod

shorter than the actual physical length of the channel for the long rod case and is close to it for the flat-plate case, as will be shown in the following chapter. For the flat-plate case, the critical current is the minimum current that can flow on an insulation which flashes over. These cases will be examined in more detail in the next chapter.

It must be realized that Obenaus' criterion is a necessary one but not a sufficient one. Thus not only must the applied voltage be above the extinction voltage, but the actual physical conditions necessary for discharge motion, such as various means of ionization, must also be present. In addition, the above theory avoids consideration of the actual physical processes involved altogether. Some of the other theories since proposed have attempted to inject some physics into the model.

Another approach is taken by Hampton[8] who used a water jet to simulate a contaminated rod insulator. He treated flashover as a stability problem. As the discharge lengthens, the current will increase and the discharge root will move rapidly across the surface. He thus proposed that the arc will elongate if the arc-voltage gradient is less than the voltage gradient in the pollution layer in series. He was able to obtain good agreement between this model and his flashover data on the water column.

Shkuropat[9] claimed that the arc will elongate if, by doing so, the current increases. Rumeli[10] and Hesketh[11] had ideas along similar lines. Hesketh was able to prove mathematically that Hampton's two criteria of voltage gradient and current increase are identical only in the case of a long rod insulator.

Nacke[12] and Wilkins[13] have suggested that the arc move to a position where the rate of energy expenditure is a maximum. Wilkins goes even a little further, invoking Steenbeck's minimum principle[14] which states that a static arc adjusts itself in such a way that its voltage gradient is a minimum. Since the principle only applies in an enclosed system with a static arc, it is not clear that the analogy can be made here.

Claverie and Rizk[15] have both developed a.c. theories of flashover. They take into consideration effects of reignition which occur every half-cycle.

McElroy[16] attempted to apply a modified form of Obenaus' theory to the flat-plate case. He postulated a value for the series resistance in the form:

$$R = \Omega B(\ell - x_{arc})^m \tag{2.1}$$

where Ω is the surface resistivity, B and m are geometric constants, ℓ the total distance the discharge must extend to bridge the insulation and x_{arc} the length of the arc. This form of resistance modeling is also used by Jolly.[7] More of this two-dimensional modeling will be covered in the following chapter.

As far as the motion of the arc is concerned, Frishmann[17] observed that for a.c. arcs in horizontal plates, propagation was along the surface, with the arc later lifting from the surface. Boylett and Maclean[1] have shown that a d.c. discharge over a water surface is in electrical contact with it. This observation means that current could be entering the solution not only at the arc tip but also underneath the body of the arc. Most theories so far have assumed only one entry point of arc into the solution. Nevertheless, they have found an empirical relationship between arc voltage and length, from which it can be inferred that the conductance per unit arc length decreases linearly with the distance from the point of origin. This observation seems to indicate that the actual situation is not as complicated as at first suspected. To take into account this multiple discharge/layer contact, our model proposes that an electrical breakdown in fact exists directly below the high-voltage electrode about one microsecond after the application of voltage. This breakdown affords an alternate current path so that some of it can indeed flow beneath the main body of the arc, as shown in Figure 2.4.

The velocity data taken by Nasser[18] showed values up to about 40 m/sec. However, far higher velocities have also been measured. Obenaus[19] has reported measurements of up to 4200 meters/sec and Hesketh[20] has observed velocities up to 600 meters/sec. Japanese workers have published[2,3] velocity

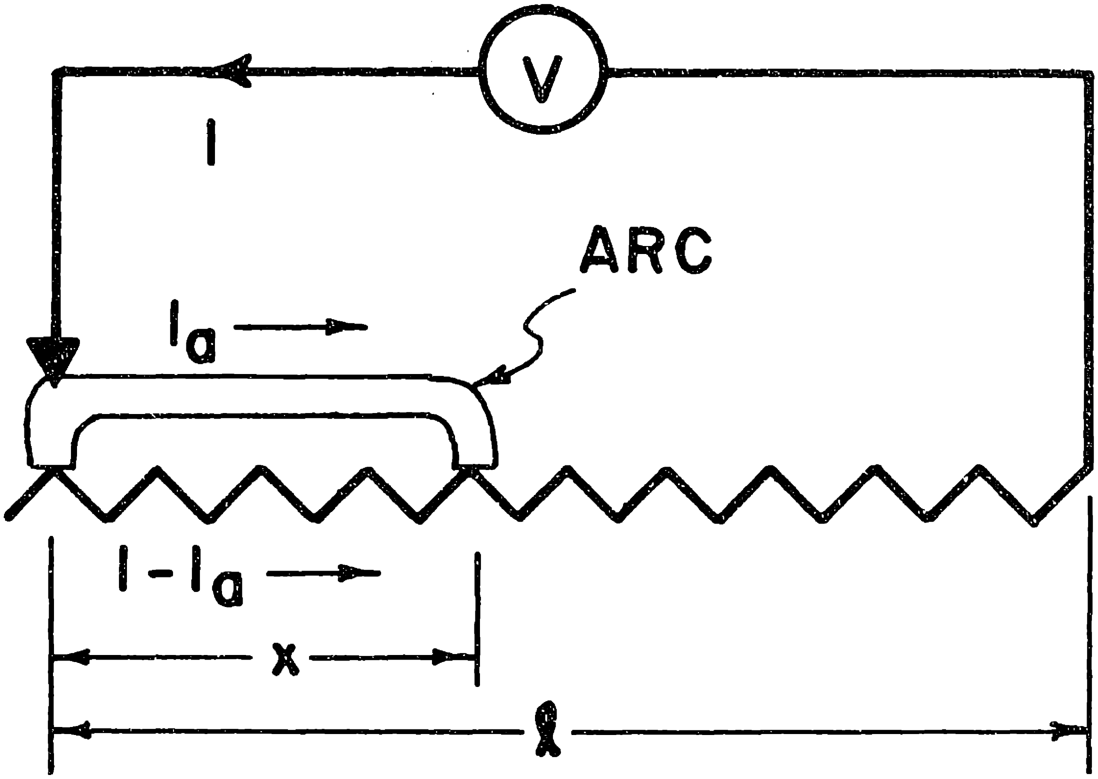

Figure 2.4 Equivalent Circuit Diagram for Dynamic Theories

data with an upper range of around 50 km/sec. Velocity measurements made at our laboratory have confirmed some of the high values observed by others. One way to account for those high velocities is to assume that contamination flashover involves an electric breakdown process. All the above theories have one thing in common, they all involve terminal conditions with little attempt to consider the actual physical mechanisms involved. Such an approach is quite understandable in view of the fact that discharge propagation is such a complex physical process. It is only recently that some attempts have been made in this direction. Wilkins[21] proposed a mechanism called "elongation by ionization and successive root formation". The theory proposes that elongation is produced by new ionization paths created at the tip of the discharge.

2.3 Recent Developments

Jolly[22] proposes that the field intensification at the discharge root will lead to the creation of new ionization, extending the discharge. Ionization by electron impact, photo-ionization and thermal ionization may all be involved. He derived a mathematical model[23] which gives the critical voltage if it is assumed that the discharge root will move forward whenever the field strength at the root exceeds some constant value E_o. In a recent paper,[24] co-authored with D. Otten and this writer, this concept of discharge growth is explored further. The idea is to calculate the threshold current above which an arc can no longer be stationary. The Townsend's breakdown criteria[25] is used:

$$\int_{R_o}^{R_1} \alpha dR \geq \ell n(1 + \frac{1}{\gamma}) \tag{2.2}$$

where α is the first ionization coefficient and γ is the secondary emission coefficient. The lower limit R_o is set equal to the arc root radius and upper limit set to maximize the integral. For a small arc root, the electric field near the arc root can be approximated to have a 1/R dependence as

$$E = \frac{I\Omega}{2\pi R} \tag{2.3}$$

where E is the radial field along the surface, I is the arc current, Ω is the surface resistivity, and R is the distance from the arc root center. The root itself is regarded as a glow discharge so that the current density remains constant.[26] The current is thus related to current density as

$$I = \pi R_o^2 J \tag{2.4}$$

The objective here is to relate I to Ω so that a critical current can be determined for a given Ω. This can be accomplished by combining eqs. (2.2), (2.3) and (2.4) and assuming a linear dependence of α on E/P. The resulting transcendental equation can be solved on a programmable calculator. In order to compare this theory with some typical observations, current densities will have to be supplied. High-speed motion pictures taken here have shown that the arc tips are usually pointed and cathode spots may even be present, which renders the accurate determination of arc root radius difficult. Wilkins[27] has reported a typical value of 1.45 A/cm^2. For glow discharges, at atmospheric pressure, an upper value of 330 A/cm^2 is usually expected.[28] Thus values can be anticipated to vary from 1.45 to 330 A/cm^2. These upper and lower bounds are thus used in the above theory to compare with some of the observations already reported,[24] as shown in Figure 2.5. The currents shown are the minimum peak currents observed during withstand tests and correspond to the maximum length advanced by the arc. They are not necessarily the critical currents, but since the current varies by only about a factor of two during a test, the currents can be regarded as typical.

The fact that the observed currents lie between the theoretical limits is significant, since it demonstrates that electrical breakdown may indeed be responsible for discharge activities particularly when Ω is high. Other physical mechanisms might also be operating, but it is plausible that at some stage a transition to electrical breakdown will occur. The high surface resistivity will cause the transition to occur even more readily.

2.4 Linear Model Experiments

As already outlined in Chapter I, the purpose of this section is to present a series of one-dimensional experiments where the variables are easily controllable and measurable so

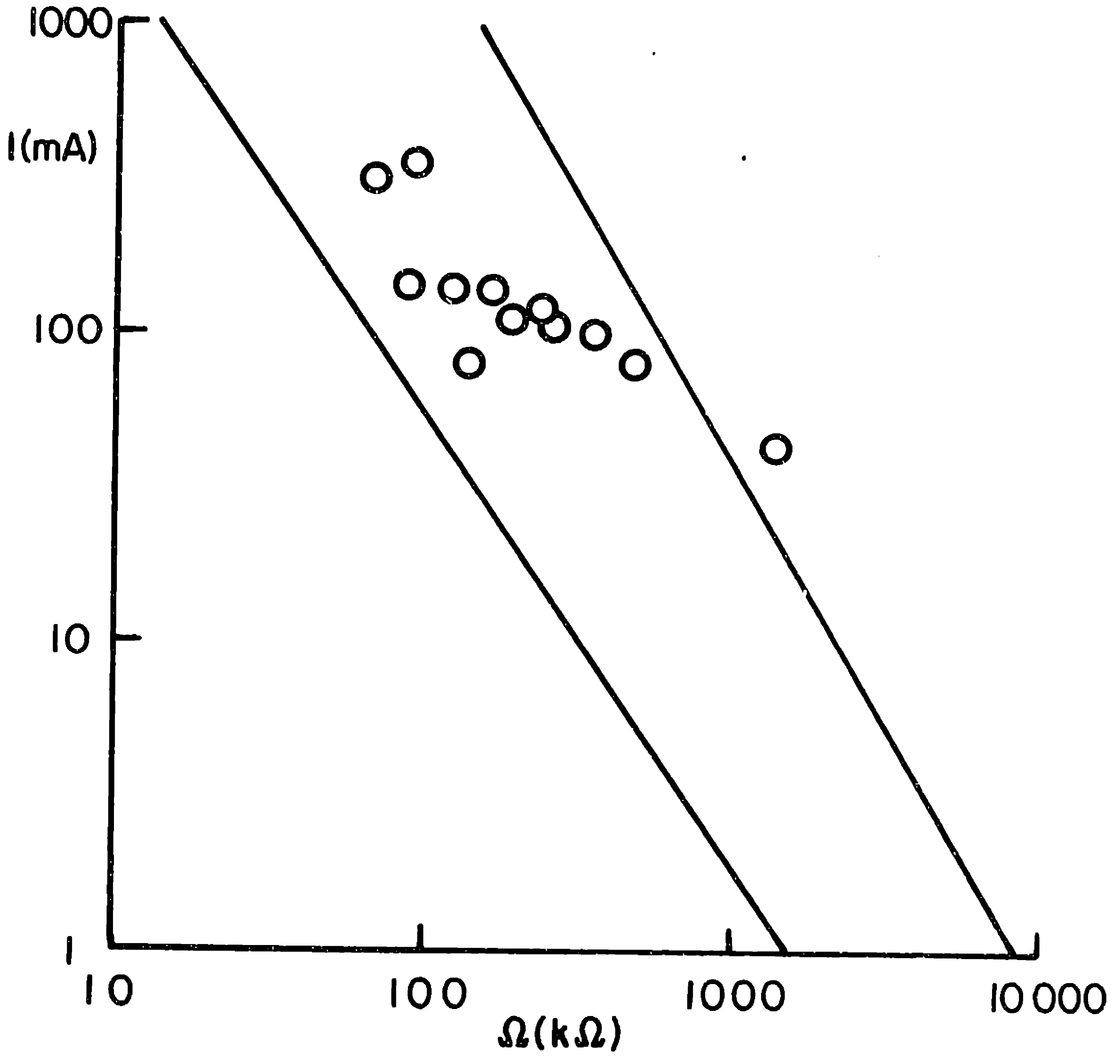

Figure 2.5 Critical Breakdown Theory Compared with Experimental Data Points. (The upper curve assumes the current density at the arc root to be 1.45 A/cm^2, while the lower curve assumes 330 A/cm^2.)

that a theory can be developed. This one-dimensional configuration has previously been used by others,[1] but never analyzed in a rigorous manner. However, because of the simplified geometry involved as well as some recent work completed in the arc discharge studies,[41,29] such an analysis can now be attempted and will be presented in the following sections.

Most of the experimental work to be described here constituted the subject matter of a recent bachelor's thesis.[30] Only the salient features will be recapitulated here; the rest of the details can be found in the thesis itself. The actual set-up as well as a sketch are shown in Figure 2.6 and Figure 2.7 respectively. The high voltage electrode represents either the cap or pin of an insulator. The trough in the middle of the plexiglas channel is filled with a solution of known quantities of salt. The conductivity of the solution can thus be controlled. The small air gap between the tip of the electrode and the surface of the solution simulates the dry zone, already mentioned in Chapter I. The far end of the channel is grounded. When the voltage is suddenly applied, a small arc is almost instantaneously ignited in the small air gap (about 1 μsec) and if conditions are fulfilled, it will travel towards the grounding electrode along the surface of the solution. The purpose of the extensive series of experiments performed is to determine, for a fixed channel length and conductivity,

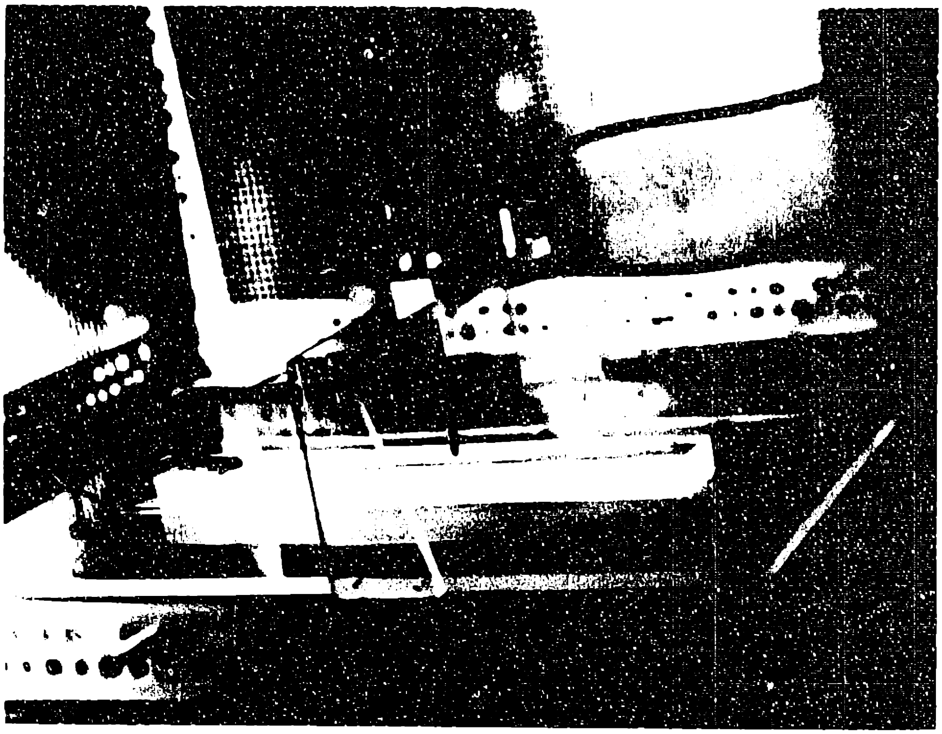

[illegible]

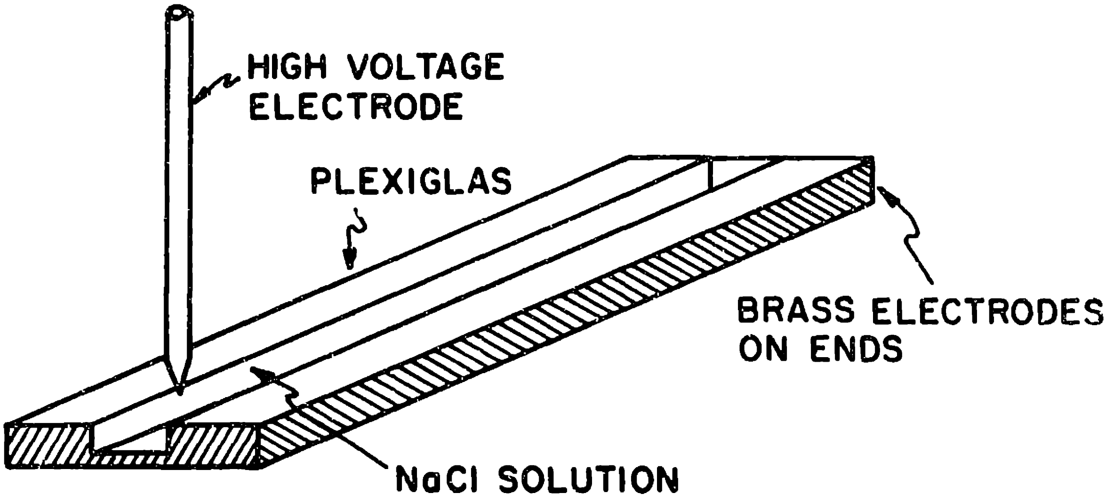

Figure 2.7 A Sketch of the Linear Model

the threshold voltage for flashover, the instantaneous current and the rate of propagation. These quantities are recorded and later compared with theoretical predictions.

A schematic diagram of the set-up is shown in Figure 2.8 and a photograph of the actual set-up in Figure 2.9. Basically, three quantities had to be measured and later compared with theory. The applied voltage and current were monitored on a Tektronix 554 Storage Scope. The growth record was measured by two different methods - a streak camera and a photo-cell array - so that the results could be checked against each other. For the streak camera, light from the arc was focused via an adjustable lens onto a rotatable mirror surface. The mirror reflected the image onto a Polaroid film placed vertically above it. The rotation of the mirror was synchronized with the application of voltage so that the time it took the arc to travel the length of the channel was about the same as it took the image to sweep across the length of the film. A sample picture of the streak camera record is shown in Figure 2.10. Time is along the horizontal axis, and x, the vertical. Each picture appears as a direct x-t plot. Note the dimness of the arc as it started out. Later, as the current started to increase, light intensity increased as well. Near the end of the channel, the velocity increased up drastically. Under examination, some pictures showed a breakpoint in velocity, indicating that a new propagation mechanism (such as a streamer) probably came into

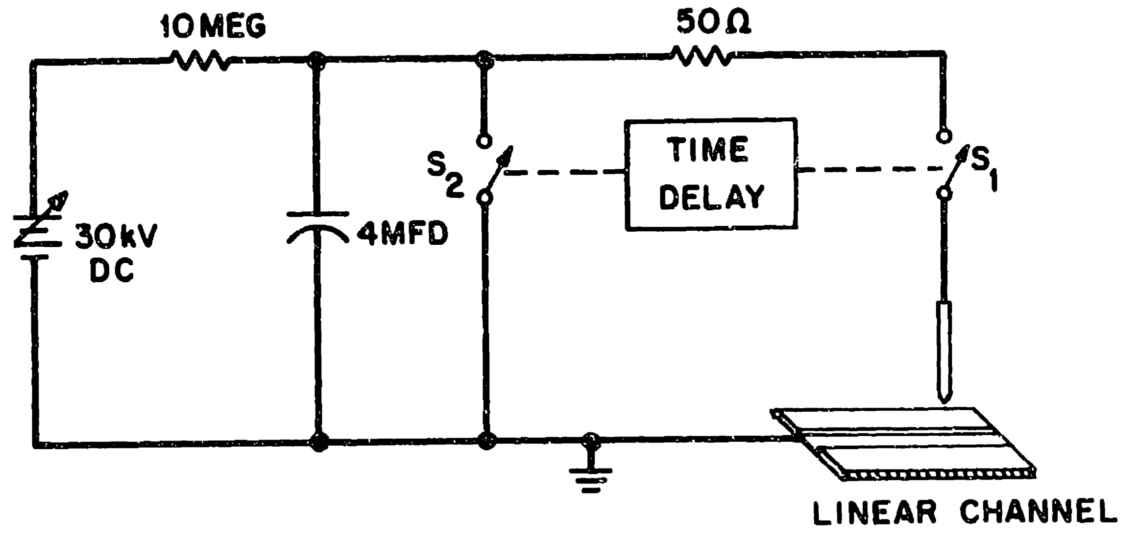

Figure 2.8 Simplified Circuit Diagram for Experimental Set-up

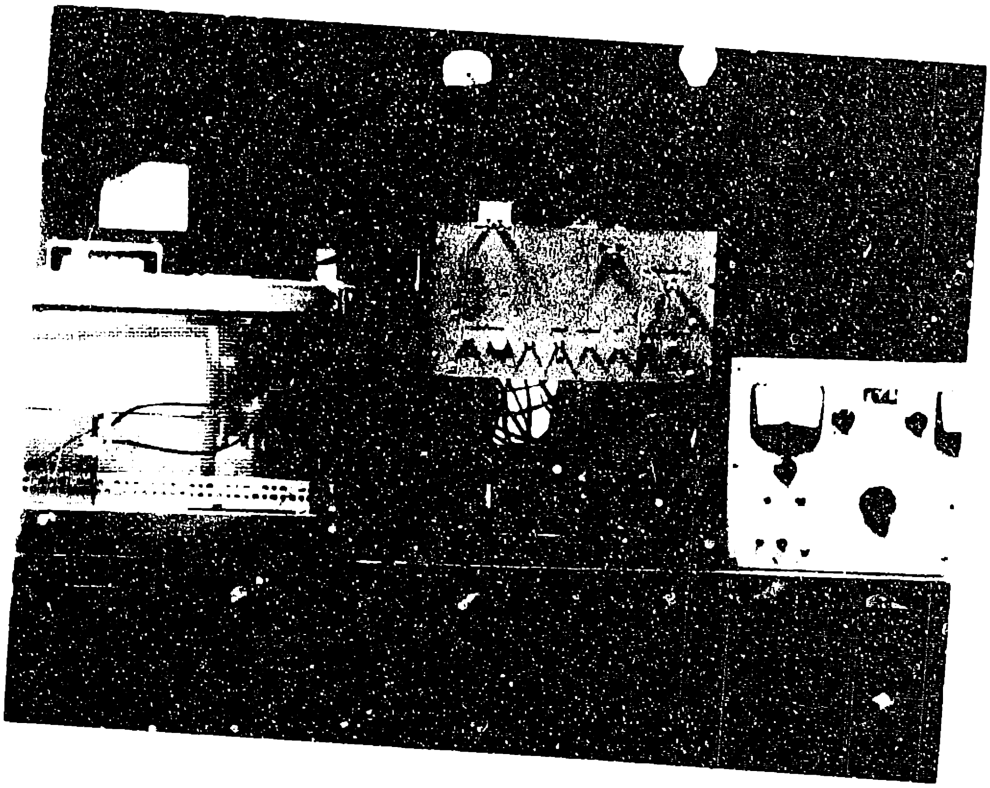

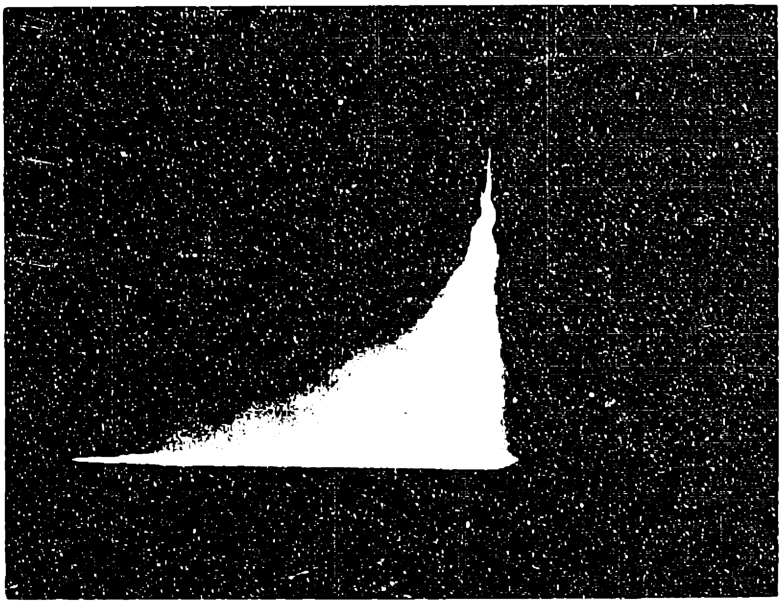

[illegible]

[illegible]

play at that point. All the experimental data thus collected will be presented in the following sections when they are compared with the theories.

The second growth measuring device was a photo-electric detector array. The device consisted of ten equally spaced photo-transistors mounted beneath the bottom of the water channel. These photo-transistors were individually triggered in succession as the arc propagated directly above them. The output of the detectors was fed into a threshold detection circuit which generated a single 1 μs pulse when the input from the photo-cell exceeded a certain level. The pulse height associated with each photo-transistor was calibrated to correspond roughly proportional to its distance from the high-voltage electrode. Thus, when the arc had completed its propagation, the ten triggered points registered on the scope would essentially be an arc length vs. time plot. Figure 2.11 illustrates a typical picture, showing current, applied voltage and the output pulses from the photo-cell circuit. The two methods were compared by using them simultaneously on one test. It was determined that at any given time, they recorded the arc tip position to within 10% of each other. Thus both methods were considered pretty reliable and data taking could now be completed fairly easily and quickly.

2.5 Dynamic Theory of Contamination Flashover I

2.5.1 Introduction

Contamination flashover research up to date has suffered from two major deficiencies. First, most theories are based on static arc models which necessarily exclude all the dynamic effects as the arc length, current and other properties change. Secondly, there has been no theories which quantify the elongation mechanism, so that it can be utilized in a comprehensive model of contamination flashover. It is the purpose of this section and the next to present two dynamic arc models which can be used to describe the low-current arcs known to occur in contamination flashovers. In addition, a growth mechanism will be proposed which, when coupled with the arc model and other physical conditions will yield a dynamic theory. This theory is capable of predicting the arc current, length and other vital properties as a function of time.

2.5.2 Dynamic Arc Model

This model is based on a simple relation derived by Mayr[31] for a conduction dominated low-current arc. The resistance of the arc is governed by the following relation:

$$r_a = \alpha e^{-Q/Q_o} \qquad (2.5)$$

where Q is the energy content/unit length of arc and α and Q_o are constants.

The conservation of energy is satisfied through the following net power balance,

$$dQ/dt = E_a I_a - N_o \qquad (2.6)$$

where E_a and I_a are the electric field and current, and N_o is the heat loss through conduction, which Mayr has shown to be roughly constant.

Taking the time derivative of (2.5) and rearranging, we have

$$\frac{dQ}{dt} = - \frac{Q_o}{r_a} \frac{dr_a}{dt} \tag{2.7}$$

Substituting (2.6) in (2.7),

$$\frac{1}{r_a} \frac{dr_a}{dt} = \frac{N_o - E_a I_a}{Q_o} \tag{2.8}$$

The net sign of the right-hand-side of eq. (2.8) is very significant. If it is positive showing net power loss, then r_a will keep on increasing and the arc will eventually extinguish. If it is negative, then the arc will continue to propagate until flashover. The direction of change of r_a can, in most cases, predict fairly early whether a flashover or a withstand will result.

The variables r_a, I_a and E_a are related through the defining relation

$$r_a = \frac{E_a}{I_a} \tag{2.9}$$

Probe measurements[32] have shown that under some conditions the longitudinal field gradient in the salt water beneath the arc is equal to the field in the arc. This observation prompted our assuming a fast (< 1μs), initial breakdown in the air gap just under the tip of the electrode.

This assumption led to the equivalent circuit already shown in Figure 2.4. Most other models neglect this parallel arc path. Two circuit equations can now be written:

$$V = r_a I_a x + V_e + I r(\ell - x) \tag{2.10}$$

$$V = V_e + (I - I_a) r x + I r(\ell - x) \tag{2.11}$$

where r is the resistance/unit length of the salt water channel and V_e is the electrode fall (either cathode or anode) at the salt water-arc interface.

Equations (2.5), (2.8), (2.9), (2.10) and (2.11) now characterize the linear model system. However, within the 5 equations, there can be counted 6 variables. An additional equation describing the growth rate of the arc must be furnished.

2.5.3 The Discharge Growth Equation

During experiments here and elsewhere[1,2], an important observation was made, namely, the arc travels anywhere from 4-10 times faster when the water electrode is acting as a cathode than an anode. The ratio of these speeds is of approximately the same magnitude as the ratio of the observed water cathode and anode falls. This suggested that the nature of the electrode falls must play a role in arc propagation. To test this hypothesis further, some preliminary experiments performed here[33], using resistive metallic surfaces instead of the normal water surface, recorded lower growth rates. It is generally known[28] that metallic electrodes usually have lower electrode falls than water. It will therefore be assumed that the energy required for the creation of a new length of arc channel comes from the electrode fall at the water surface.

The aim here is to derive an equation on the growth rate $\frac{dx}{dt}$ which can be used in conjunction with the above equations without introducing any more unknown variables. A somewhat heuristic argument will be presented below to justify reaching such an equation. Physically, it is clear that the net power fed into the arc can be expended in two ways, either extending the arc or supplying the energy that is necessary to sustain an arc in the newly created channel.

Consider the conservation of energy equation,

$$\int_v \frac{\partial}{\partial t} \rho(u+ \frac{1}{2}(v_m)^2)dv + \oint_S \rho(u+ \frac{1}{2}(v_m)^2) \frac{d\vec{x}}{dt} \cdot d\vec{a} = \text{net power input}$$

where

v = control volume

ρ = mass density within the arc

u = internal energy/unit mass

v_m = material velocity within the arc

dx/dt = arc velocity

S = surface enclosing the control volume

da = surface area element

The internal energy/unit mass, u is equivalent to the product of specific heat capacity and temperature (i.e. C_vT). For most propagating speeds of the arc, the internal energy is much greater than the kinetic energy, as can be easily verified by substituting in numbers (arc temperature $\simeq$ 5000°K). The above energy equation is then reduced to:

$$\int_V \frac{\partial}{\partial t}\,\rho(u)\,dv + \oint_S \rho u\,\frac{d\vec{x}}{dt}\cdot d\vec{a} = \text{net power input}$$

Now, consider an instant of time, t. The arc tip will have reached some position x and the main body of the arc is well-formed and has almost reached a steady-state. Let the control volume be such that it tightly encloses the volume of the arc and nothing else. At t + Δt, the arc tip will have pierced through the control surface and advanced an additional distance ΔX. The amount of energy that is needed to create this extra length (ΔX) of arc is accounted for by the second term on the left side. The first term on the left accounts for any change in internal energy (such as a temperature increase) within the control volume during Δt. Since we have assumed little temperature change in our arc model, the first term approaches zero. The energy equation thus becomes,

$$\oint_S \rho u\,\frac{d\vec{x}}{dt}\cdot d\vec{a} = \text{net power input}$$

The right side can essentially be decomposed into four terms: V_aI_a, power input through main body of arc; V_eI_a, power input through electrode falls; N_o, power loss through main body of arc; and N_{tip}, power loss at the tip of arc. Since the main body has almost reached steady-state, V_aI_a and N_o approximately cancel out (see eq. 2.6). Actually $V_a I_a$ is always a little larger than N_o in order to have a propagating arc. N_{tip} is only a small fraction N_o, since the former includes only the small tip region. Thus, the only important term left is $V_e I_a$ which is much greater in magnitude than any of the other terms.

Thus, we have

$$\rho u \frac{dx}{dt} \frac{v}{x} = V_e I_a$$

where v is the volume of the arc cylinder and x its length, at an instant in time.

But

$$Q = \rho \frac{uv}{x} = \text{heat energy of arc/unit length}$$

so that

$$\frac{dx}{dt} = \frac{V_e I_a}{Q} \tag{2.12}$$

More will be said about the electrode fall voltage V_e in section 2.7.

2.5.4 Normalization of the System Equations

Equations (2.7), (2.8), (2.9), (2.10), (2.11) and (2.12) constitute the set of governing equations for our dynamic arc model. They are recapitulated in Table 2.2 for convenience. This set of equations is clearly coupled and nonlinear and cannot be solved analytically. A numerical solution was therefore performed. However, to solve the system of equations numerically requires a prior knowledge of all the

TABLE 2.2

DYNAMIC THEORY I - SYSTEM EQUATIONS

$$r_a = \alpha e^{-Q/Q_o} \tag{2.5}$$

$$\frac{1}{r_a}\frac{dr_a}{dt} = \frac{N_o - E_a I_a}{Q_o} \tag{2.8}$$

$$r_a = E_a/I_a \tag{2.9}$$

$$V = r_a I_a x + V_e + Ir(\ell - x) \tag{2.10}$$

$$V = V_e + (I - I_a)rx + Ir(\ell - x) \tag{2.11}$$

$$\frac{dx}{dt} = \frac{V_e I_a}{Q} \tag{2.12}$$

inherent constants in the equations such as Q_o and N_o. Even though N_o can be determined via experimental means (see section 2.6), it is desirable to solve the equations in their general form. This can be achieved through a process known as normalization. Simply stated, normalization is the technique of dividing constants from both sides of an equation such that the resultant equation is rendered dimensionless.

In order to normalize the set of equations in Table 2.2, a set of constants would have to be chosen so that all quantities could be measured in ratio to them. The constants picked are the following:

V_{th} = static threshold voltage = $2\ell\sqrt{rN_o}$ (2.13)

τ = characteristic time = Q_o/N_o (2.14)

A = normalized applied voltage = $V/\ell\sqrt{rN_o}$ (2.15)

B = normalized electrode fall voltage = $V_e/\ell\sqrt{rN_o}$ (2.16)

C = normalized Mayr's constant = α/r (2.17)

The variables themselves were normalized as follows: resistance of the arc against r; voltages against $\ell\sqrt{rN_o}$; currents against $V/r\ell$; x against ℓ; t against Q_o/N_o, and Q against Q_o.

The static threshold voltage, V_{th}, is derived from static considerations and will not in general equal the dynamic threshold.

An example of normalization will now be given here. Consider eq. (2.12):

$$\frac{dx}{dt} = \frac{V_e I_a}{Q} \tag{2.12}$$

A constant $\frac{1}{\ell} Q_o/N_o$ is multiplied on both sides of the equation, yielding,

$$\frac{1}{\ell} \frac{Q_o}{N_o} \frac{dx}{dt} = \frac{V_e I_a}{Q} \frac{Q_o}{N_o} \frac{\ell r}{\ell^2 r} \tag{2.18}$$

Using the defined constants (2.15), (2.16) and (2.17), we have

$$\frac{d\tilde{x}}{d\tilde{t}} = \frac{AB\,\tilde{I}_a}{\tilde{Q}} \tag{2.19}$$

where all the "tildas" denote normalized variables. These variables are all dimensionless, being pure numbers, and they can recover their original physical meaning through denormalization.

A similar process is carried out for every one of the other five equations in the set. Equation (2.9) can be substituted in eq. (2.8) to reduce the set to a system of five equations with five unknowns. After algebraic simplifications, the set of equations are shown in Table 2.3. A, B and C are constants to be specified in accordance with each physical experiment. A determines the level of applied voltage; B controls the amount of electrode fall; C reflects the resistivity of the channel solution.

2.5.5 Initial Conditions

Since the set of equations contains two first-order differential equations, two initial conditions must be specified. $\tilde{x}(t=0)$ fixes the position of the starting arc

TABLE 2.3

NORMALIZED SYSTEM OF EQUATION

Original Equation	Normalized Equation	
2.5	$r_a = C\ e^{-\tilde{Q}}$	(2.20)
2.8	$\frac{d\tilde{r}_a}{d\tilde{t}} = \tilde{r}_a(1.0-A^2\tilde{r}_a^2\tilde{I}_a^2)$	(2.21)
2.10	$\tilde{I}_a = \frac{1}{\tilde{r}_a\tilde{x}}\ [1.0-B/A-\tilde{I}(1.0-\tilde{x})]$	(2.22)
2.11	$\tilde{I} = \frac{1.0-B/A-B/A\ 1/\tilde{r}_a + 1/\tilde{r}_a}{1.0 + \frac{1}{\tilde{r}_a}\ (1.0-\tilde{x})}$	(2.23)
2.12	$\frac{d\tilde{x}}{d\tilde{t}} = \frac{AB\tilde{I}_a}{\tilde{Q}}$	(2.19)

and is set equal to zero. $\tilde{Q}(t=0)$ represents the quantity of heat energy at the start of the simulation. This quantity can be derived in the following fashion just before the arc starts to propagate. At t = 0, we assume that the arc is already well-formed and on the verge of propagating. Its length is negligible compared to the channel length. The supply voltage is thus mainly across the liquid channel.

Writing Kirchoff's voltage law

$$I r \ell + V_e = V \tag{2.24}$$

and using Mayr's energy equation,

$$\frac{1}{r_a}\frac{dr_a}{dt} = \frac{N_o}{Q_o} - \frac{I_a^2 r_a}{Q_o} \tag{2.25}$$

Initially, r_a is nearly infinite and the second term on the right hand side dominates. This means $dr_a/dt < 0$ and r_a decreases rapidly until the arc becomes well-formed. At this point, r_a levels off and $dr_a/dt \simeq 0$, so that

$$I_a^2 = \frac{N_o}{r_a} \tag{2.26}$$

We have observed experimentally that the current approaches this value within about 1μs which is very short compared to Q_o/N_o.

At t = 0, the parallel paths shown in Figure 2.5 have not yet formed, and the entire current flows in the arc from the electrode point into the solution. Thus, from (2.24)

$$I_a = I = \frac{V-V_e}{r\ell} \tag{2.27}$$

Substituting (2.27) into (2.26)

$$r_a(t=0) = \frac{N_o r^2 \ell^2}{(V-V_e)^2} \tag{2.28}$$

Using the normalization technique, this equation can be reduced to

$$\tilde{r}_a(t=0) = \frac{1}{(A-B)^2} \tag{2.29}$$

Now, combined with the normalized Mayr's equation,

$$\tilde{r}_a(t=0) = C\ e^{-Q(t=0)} \tag{2.20}$$

we have,

$$\tilde{Q}(t=0) = \ell n[C(A-B)^2] \tag{2.30}$$

The initial condition $\tilde{Q}(t=0)$ is thus completely determined once A, B and C are specified. This conclusion is entirely reasonable, since together A, B and C define the experimental conditions.

2.5.6 Computer Simulation

The system of equations was solved on an IBM 370/165 using the IBM Continuous System Modeling Program. Details of programming techniques can be found in Appendix A. During insulator flashovers across the country, different conditions such as degrees of contamination, voltage surges, electrical stress level etc. necessarily prevail. In order to encompass most of these diverging circumstances under which flashoversoccur, the simulation has taken into account the following range of parameters as shown in Table 2.4.

TABLE 2.4

RANGE OF INPUT PARAMETERS

Applied Voltage	6-20 kV
Resistivity of Solution	153-6400 Ω/cm
Cathode Falls	500-800 volts
Anode Falls	80-250 volts

These input parameters were fed into the program in the form of A's, B's and C's, as mentioned before. Since any combination of the above variables will wholly determine a distinct field condition all by itself, the simulation endeavors to cover as wide a range as possible - simulations were carried out during the course of this work. For the sake of brevity, however, only representative samples will be presented in the next section.

In a typical test, the quantities monitored are arc voltage, arc current and distance of arc propagation. A flashover occurs when the arc bridges the entire length of the channel. A withstand is a case when the arc only partially bridges the channel. Experimentally during a withstand, the arc reaches a certain point of the channel, burns there for a while and then goes out when the energy storage capacitor used to supply the voltage discharges. In the computer simulation, it simply stops propagating since the arc can never extinguish and some of the variables, including velocity become negative, clearly indicating that forward propagation is no longer possible, at which point the simulation is stopped. The simulation is also capable of distinguishing between propagation and withstand cases fairly early in the arc propagation. During a flashover, the arc voltage decreases while the current increases. For a withstand case, the opposite is observed.

2.5.7 Comparison Between Theory and Experiment

In the previous sections, we have discussed the experimental techniques used in data collection. We have also presented a comprehensive flashover model that is capable of predicting all the arc variables vs. time. In this section, theory and experiment will be compared. In order to have meaningful comparisons, however, the dimensionless quantities from simulation must be "denormalized" to their respective actual values for voltage, current, time etc. This process is completed as follows.

Using the computer model the threshold voltage for a particular polarity and resistivity is determined by varying the normalized voltage, A, until at a certain value, the arc is barely capable of propagating. This represents the dynamic threshold values as compared with $\ell\sqrt{rN_o}$, used earlier as a normalizing constant. The latter, derived on a purely static basis, is actually quite close to the dynamic predictions (i.e. $A \simeq 2.0$).

To clarify further, an example is used here. For a certain set of conditions the program yielded $A = 1.90$ as the threshold voltage. Experimentally, we found that the threshold voltage corresponded to 8.0 kV. Hence, $A = 1.90$ would correspond physically to 8.0 kV. If 16 kV is now applied to the same set-up, a corresponding computer simulation can be run with $A = 3.80$. In this fashion, A can be readily transformed into actual kilovolts. The constant B denotes either the cathode fall or anode fall, depending on the polarity of the channel solution. Probe measurements showed that the cathode fall on water surface was on the order of 800 volts,[32] while the anode fall was approximately on the order of 200 volts. These values compare reasonably well with Baghdadi's measurements of 725 and 225 volts, respectively. These are the values that were used in our simulations. The constant C is the Mayr's constant α divided by resistivity of the solution, r. α is about 10^4 Ω/cm for an 1-amp arc.[31,24] Thus, for r = 1 kV/cm, C=10.0. A, B and C form the only input parameters to our program.

As far as the output parameters are concerned, $\tilde{x} = 1.0$ is equivalent to the actual length of the channel in cm. The simulation gives a theoretical time to flashover in terms of τ and can be recovered by equating with the experimental value (in μs). The value of τ can thus be calculated. The current is recovered by multiplication of the factor $V/r\ell$. With these correspondences, all the output variables can be converted into physical numbers which can then be compared with experimental findings.

Figures 2.12 and 2.13 illustrate a typical comparison between theory and experiments. The continuous curves (both solid and dashed) are from the simulation and the crosses and dots are experimental observations. The physical setup for both cases is as follows: $\ell = 10$ cm and $r = 490$ Ω/cm. For the positive polarity case, the applied voltage was 8.0 kV, approximately the threshold level. For the negative polarity case, the applied voltage was again near threshold,

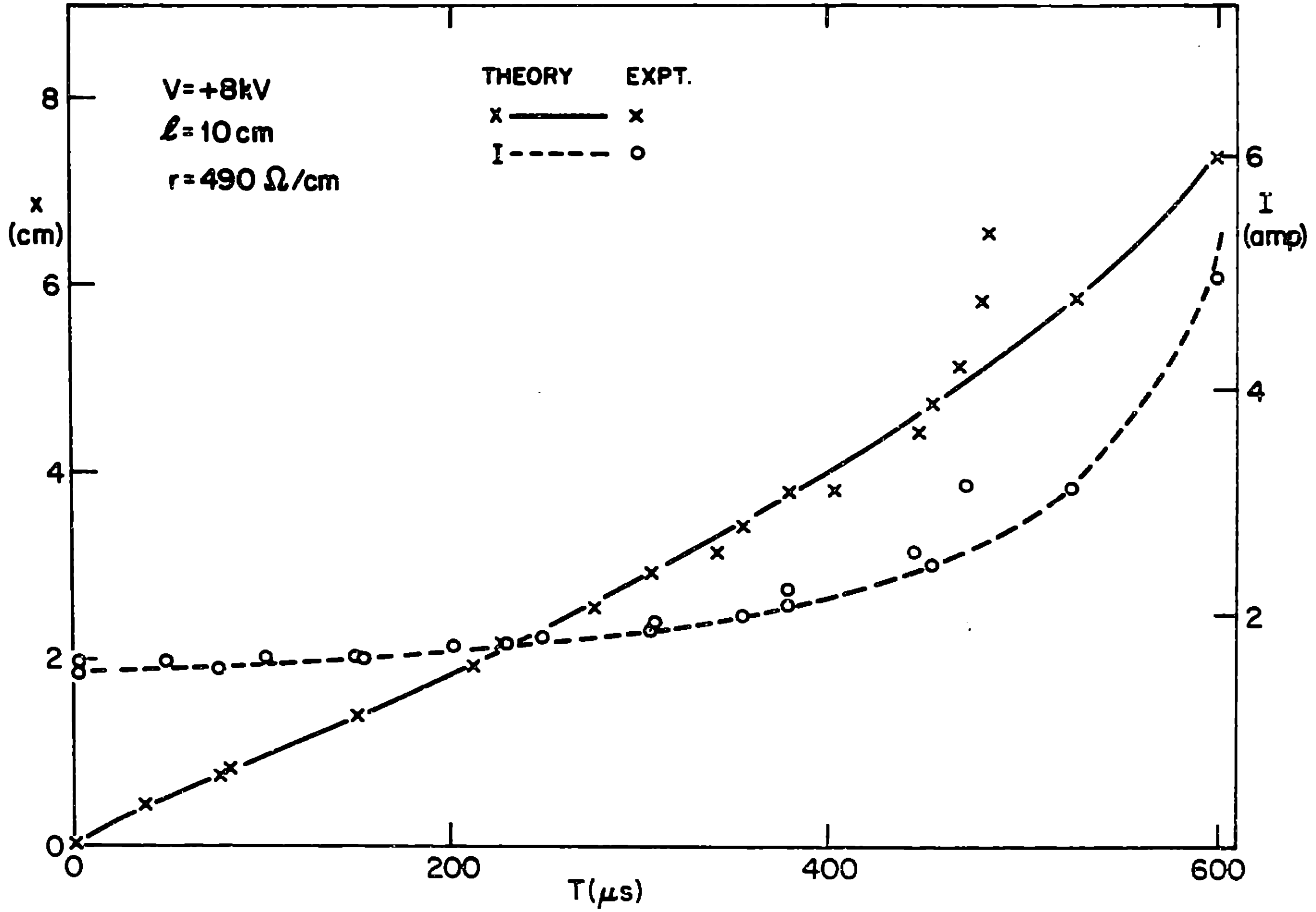

Figure 2.12 Comparison between Dynamic Theory I and Experiments

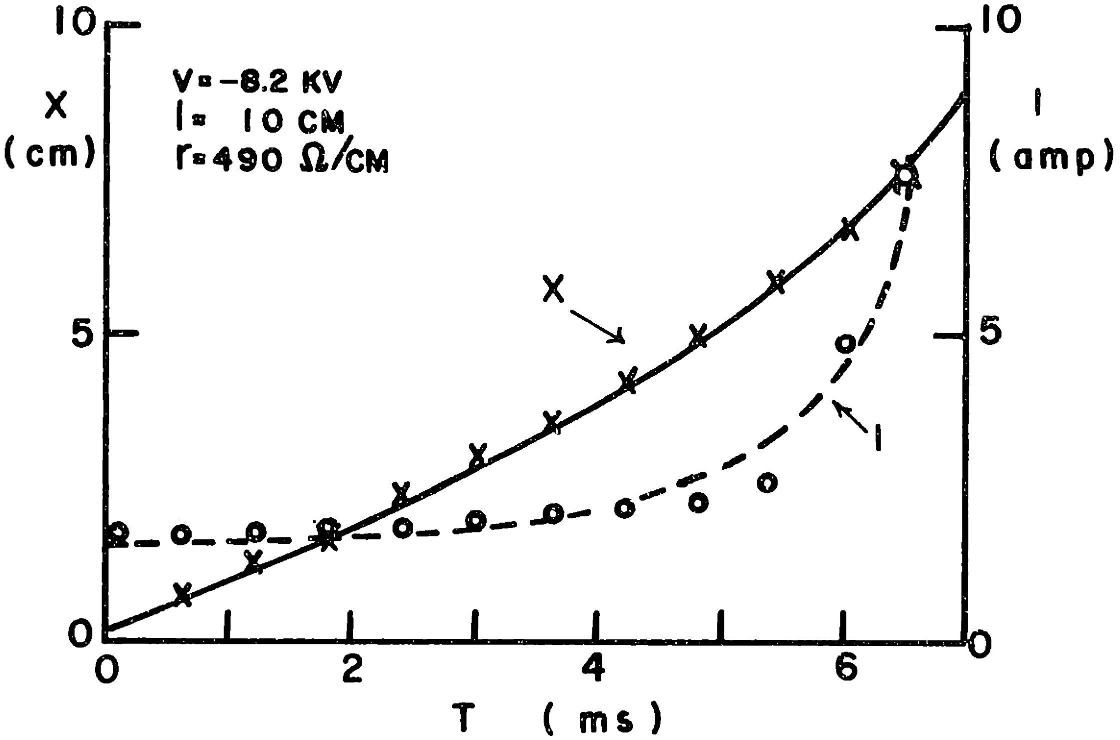

Figure 2.13 Comparison between Dynamic Theory I and Experiments

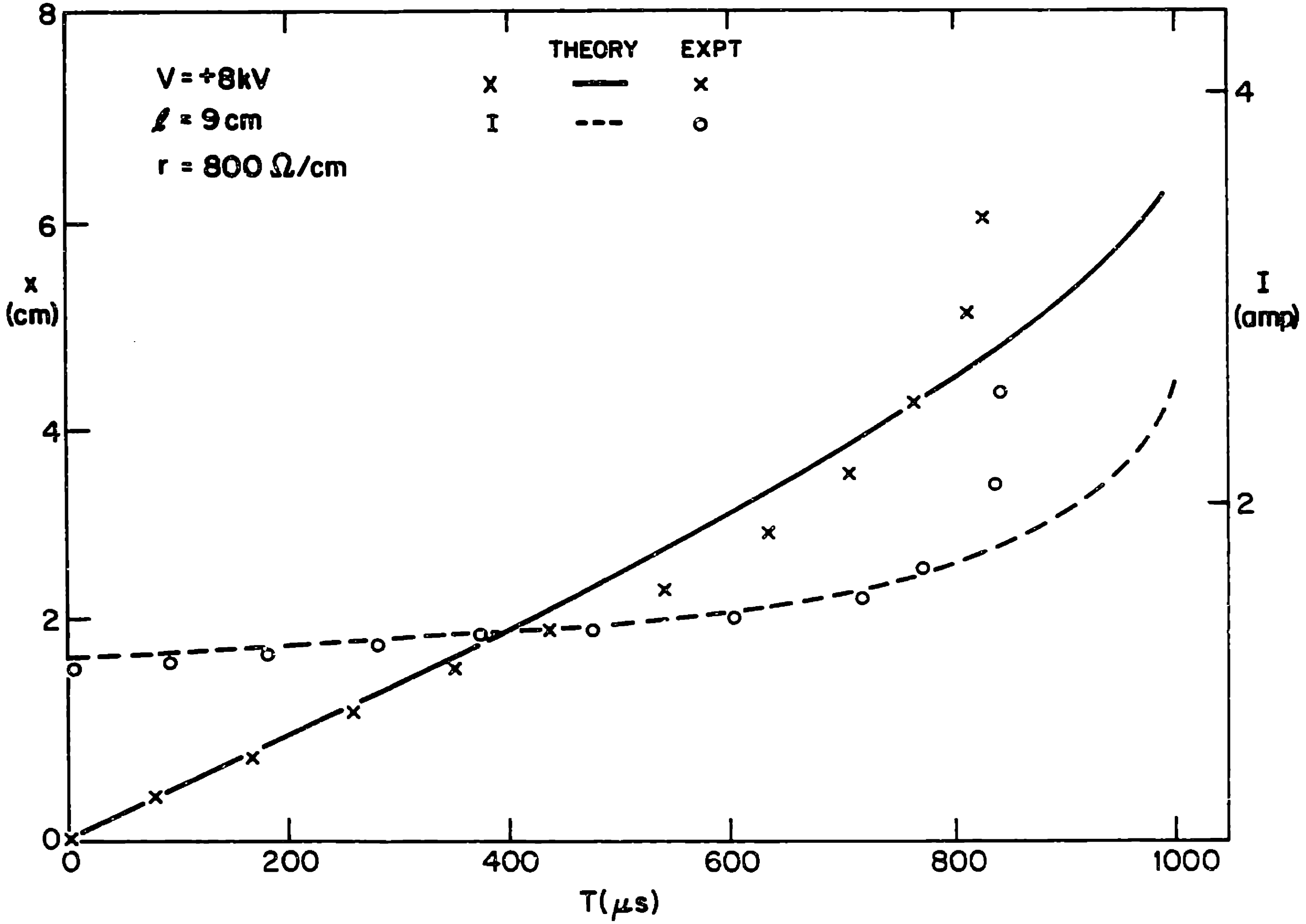

Figure 2.14 Comparison between Dynamic Theory I and Experiments

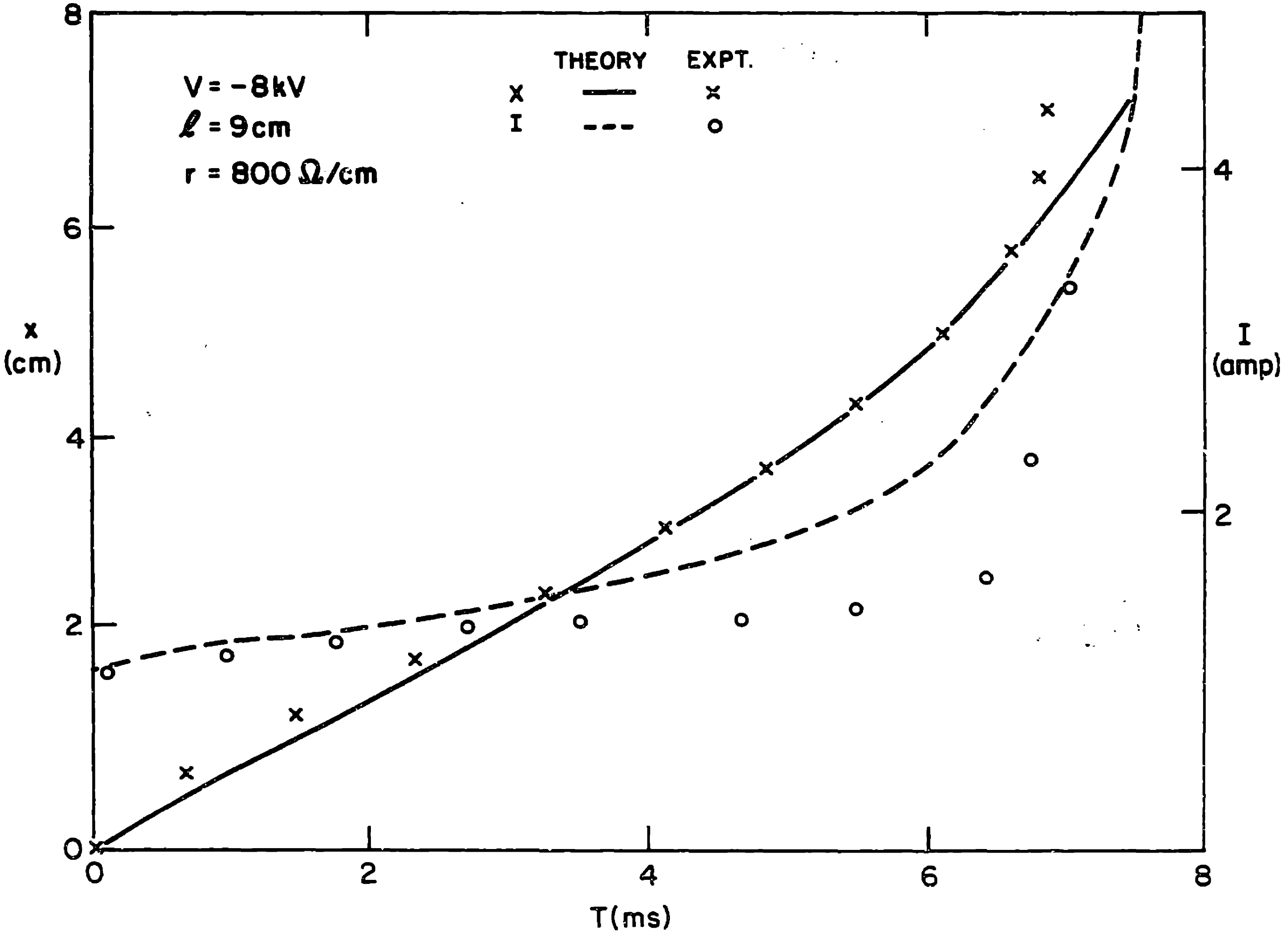

Figure 2.15 Comparison between Dynamic Theory I and Experiments

8.2 kV. Note the difference in propagation times. During the simulation, a cathode fall of 800 volts, and an anode fall of 200 volts were assumed respectively. These values were used in determining the B's for the two cases. The resistivity of solution (490 Ω/cm) was used in calculating C. Since both cases corresponded in reality to threshold flashovers, in simulation the A for each case was found by varying it till at a certain value, the simulated arc was barely capable of propagating.

The agreement between the theory and experiment is encouraging, as can be seen from the figures. Figures 2.14 and 2.15 depict another two cases for comparison. Nearly all of the cases performed experimentally as described in 2.5.4 have been simulated on the computer. Despite the good agreements, however, there are limitations to the model, which will be discussed in a following section.

2.5.8 Discussion

The theory presented above represent a departure from the traditional research done in the field of contamination flashover. The arc is treated here as a dynamic propagating entity. Traditionally, a static theory is invoked to arrive at some threshold value for flashover or withstand, without including the motion of the arc. This approach, though mathematically simpler, is not appropriate, for a propagating arc with velocities of up to thousands of meters per second[34] is necessarily a dynamic phenomenon. Any static description of the arc such as $V = A \times i^{-n}$ is not valid for all times as the arc grows faster and faster. To illustrate this point, Figure 2.16 shows the E_a-I_a characteristic of the arc in the computer simulation compared to the static characteristic, derived by setting $dr_a/dt = 0$ in eq. (2.8). The static curve is close to what others have assumed as E_a-I_a characteristics. At low currents (i.e. near the beginning of the arc propagation), these characteristics approach each other closely, as the arc still travels very slowly. But, as the arc velocity increases, the characteristics deviate further and further apart, indicating that the static approximation is no longer valid. Hence, time must inevitably enter as a variable, justifying our using a dynamic rather than static model.

Furthermore, there is an independent test that provides a means of checking the reasonableness of the theory. From our derivation, it is clear that N_o and Q_o are a set of constants which characterize a particular type of arc. Other researchers[35-37] in arc physics have measured τ, the characteristic time constant for arcs burning in cylindrical tubes and E. Los at our laboratory has also performed experiments designed to ascertain its value for low current arcs on water surfaces. From our theory and experiment, it is possible to derive N_o, Q_o and their ratio τ, the last of which can then be checked against these other independent findings. Our characteristic time τ is derived by first

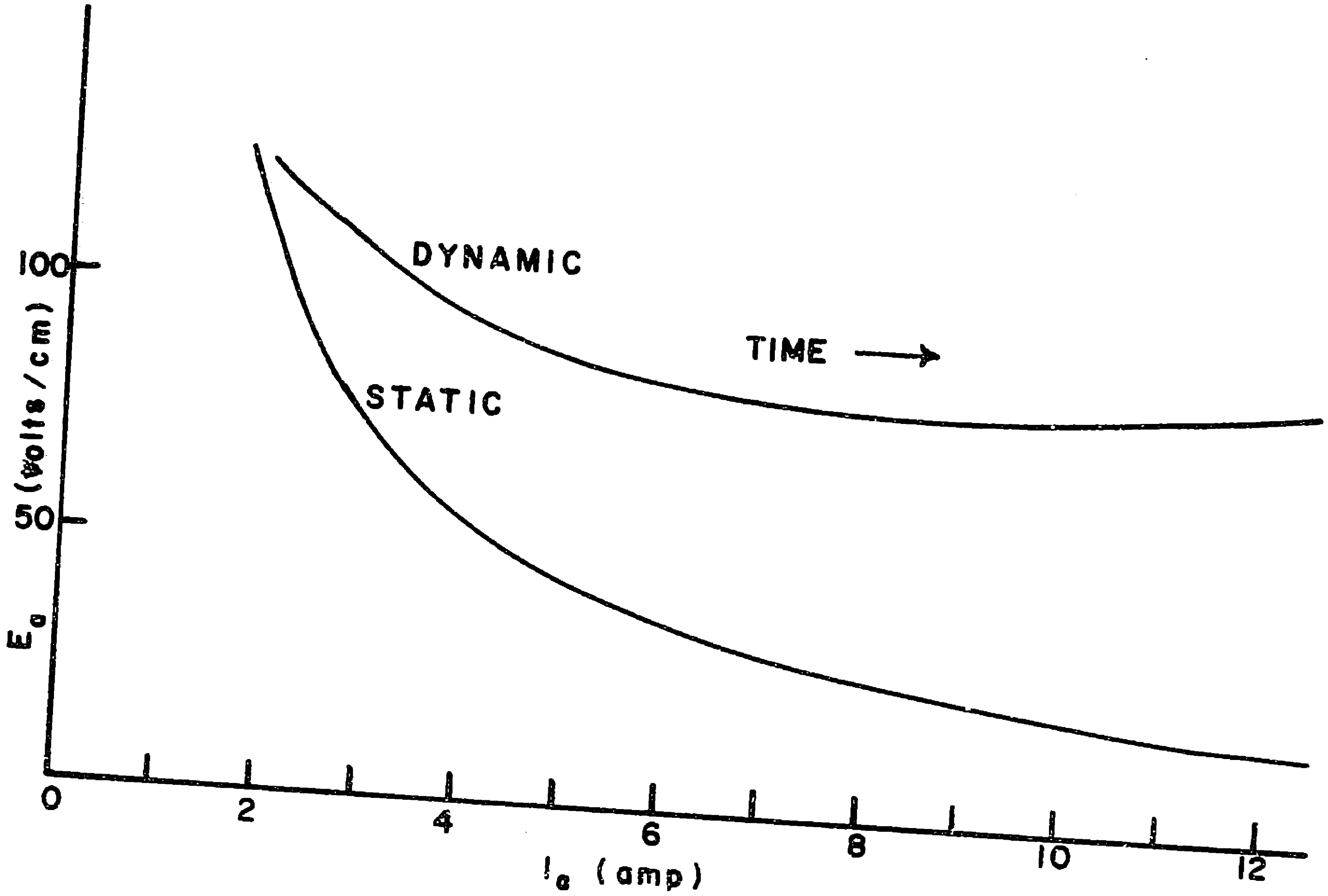

Figure 2.16 Comparison between the Static and a Dynamic E_a-I_a Characteristic for a Propagating Arc

TABLE 2.5

CHARACTERISTIC ARC TIME CONSTANTS

Researchers	Current	τ
Yoon & Spindle	1 amp	50-110 μs
T. Lee	1 amp	80 μs
Edels & Graffmann	1 amp	30-90 μs
E. Los	1-2 amps	40-120 μs
Derived from computer model	1-3 amps	30-110 μs

experimentally determining the voltage level at which flashover barely takes place. N_o is then obtained by equating this measured value to $2\ell\sqrt{rN_o}$. As already discussed, this threshold value is derived on purely static assumptions and N_o thus derived is subject to about a 10% error. In simulation, the time to flashover is normalized against τ. This time constant τ can be recovered by comparison with the experimental flashover time. These independently derived τ's are compared in Table 2.5 and it can be seen that our values are in reasonable agreement with those of others.

2.5.9 Limitations of the Model

The model discussed above is offered as a tentative explanation of the flashover process. Despite its good agreement with experimental observations, there are several limitations of the model, which will now be discussed. The main assumption of the model is that the growth rate is proportional to the cathode or anode voltage fall. For low-velocity arcs, this is a good first approximation as shown in the last section. As the arc develops, however, the velocity increases more and more drastically. At some stage of its propagation, some new physical mechanism might come into play. From the streak camera record, such a point, if it occurs, usually occurs after 60% of the channel has been traversed. In such a case, there usually appears on the film a discernible discontinuity in the slope of the x vs. t plot. The arc accelerates rapidly afterwards and there is reason to suspect that streamer or streamer-like propagations are in progress. Since photo-ionization plays an important role in streamer propagation, the velocities can increase dramatically. Since the growth model does not include any streamer formation, the model is no longer valid at this point. Fortunately, however, whenever such a stage has been reached, the arc always flashes over afterwards, so that there is little practical interest in modeling streamers.

Since the electrode falls, especially the cathode fall, play such an important role in the model, their nature should be examined in more detail. The cathode fall will be studied in section 2.7 and a theoretical analysis using the principles of glow discharge, will be presented.

Another important component of the model is the Mayr's dynamic arc equation. The equation was derived by assuming constant thermal conductivity. An important conclusion is that

$$\tau_f = Q_o/N_o \tag{2.31}$$

where τ_f is the free conductivity decay time constant mentioned earlier. N_o is the steady-state power dissipation and Q_o, a heat constant. (2.31) essentially stipulates that τ_f and N_o must be inversely proportional to each other. Recent tests by E. Los[38] at our laboratory showed that such a relation is not generally true. Even though τ_f does yield reasonable values when compared with other independent findings, (see 2.5.6) its relation with N_o is not as simple as (2.31) suggests. Because of the simplicity of this dynamic arc model, such a deficiency can be expected. It has been since remedied by the application of a refined arc model to be discussed in the following section.

Lastly, to simulate the flashover of actual insulators, the model must be modified to include other effects such as heating and evaporation of the water. These represent no problem in theory, but the actual computation can be very complex.

2.6 Dynamic Theory of Contamination Flashover II

2.6.1 Introduction

Until very recently, arc discharge research was carried out for the main purpose of understanding and improving circuit breakers as well as studying insulation breakdown. Almost nothing was done exclusively for contamination flashovers. As already mentioned, the serious application of electrical breakdown phenomenon to insulator flashover occurred only in the past few years. Fortunately, however, some of the circuit breaker research can be readily applied to our cases.

From the beginning, arc research has been hampered by the fact that many of the important properties and temperature dependent e.g. thermal conductivity, $K_e(T)$, are electrical conductivity, $\sigma(T)$. Any imposed changes will bring forth a finite thermal response time leading to transient arc behavior. Furthermore, such a change is usually accompanied by complicated mathematics so that no simple solution can generally be found. It has thus become necessary to define an "arc time constant" which provides a reasonable description of the rate of change of a certain arc property. Mathematically, Edels[36] has defined it as follows:

$$\tau(F) = F(t) \Big| \frac{dF}{dt} \qquad (2.31)$$

Much of the work has been directed towards finding this time constant for various physical conditions. As discussed in the last section, Mayr's simple time constant $\tau = Q_o/N_o$ has its deficiencies. The purpose of this section is to find a better justified τ, hence a more realistic description of r_a vs. t to be used in the overall flashover model. First, a brief review of the search for this time constant is in order, concluded by the recent work of E. Los[38], which eventually resulted in the formulation of "dynamic theory of contamination flashover II".

The general governing equation is sometimes known as the Elenbaas - Heller equation (expressed in cylindrical coordinates):

$$\frac{1}{R}\frac{d}{dR} RK_e(T)\frac{dT}{dR} + \sigma(T)E^2 + Q_{rad} = 0 \qquad (2.32)$$

It expresses the balance between the electrical energy dissipation and the removal of energy by conduction and radiation, radiation being frequently ignored. By using the heat flux potential, S, (attributed to Schmitz[39]), (2.32) can be simplified to

$$\nabla^2 S + \sigma E^2 = 0 \tag{2.33}$$

where

$$S = \int_{T_o}^{T} K_e \, dT \tag{2.34}$$

and Q_{rad} is set equal to zero. This equation is usually solved in conjunction with conservations of mass and momentum as well as some form of Ohm's law, (see e.g. Emmons [40]). The energy equation, by itself, is a static model. A quasistatic model can be introduced by adding a thermal diffusion term, $\frac{K_e}{\rho_a C_p} \frac{\partial S}{\partial t}$ to the right hand side of (2.33) to account for changing temperatures within the arc.[41] The solution of the equation essentially centers around the question of how to approximate σ as a function of temperature.

The earliest and most well-known cylindrical arc models belong to Cassie[42] and Mayr.[31] Both yielded simple exponential decays of column conductance/unit length for free recovery. Frind[43] discovered the same form of decay and was theoretically supported by the filled tube model of Edels and Fenlon.[44] Maecker[45] combined his assumptions of constant core temperature and constant conductivity with Steenbeck's Minimum Principle.[14] Emmons[40] improved the model by assuming a step discontinuity in $\sigma(T)$, while maintaining K_e constant. He also allowed the temperature profile to vary. Yoon and Spindle[35] made numerous arc time measurements in various gases, based on Mayr's model.

Near the end of the sixties, two pieces of significant work were published. Phillips[41] applied a Taylor series expansion in powers of time to the energy balance equation with the thermal diffusion term added. He showed that, independent of the variable nature of the transport coefficients, the instantaneous finite current step and conductance recovery time constants at the instant of disturbance are simply related through the steady-state characteristic.

Edels and Graffmann applied the results of perturbation analysis to measuring field strength responses as a result of a step current change. The arc currents ranged from 4 to 40 amps in different gases.

All the models discussed so far are based on a cylindrical geometry with wall stabilization. Such a simplification is probably appropriate for free-burning arcs in air. For our linear model, however, the physical constraint is somewhat different. A liquid surface (the salt solution) of almost constant temperature has been placed just beneath the arc. For such a geometry, the bi-cylindrical coordinate is far more descriptive and useful. This realization formed the main thesis of Los' research. He transformed all the relevant equations into bi-cylindrical coordinates and solved them numerically using Phillips' method of Taylor expansion. The principal advantage of the coordinate transformation lies in the fact that now all isotherms can be approximated to conform to the coordinate system itself.

Furthermore, he made careful measurements on the linear model set-up described in 2.4 to determine time constants and other important arc parameters to check against his theory. The details of his work can be found in his thesis and they should have important bearings on the arc discharge research in general and contamination flashover in particular. Some of the parameters thus determined will be used in the following sections. The results of his findings will also be incorporated into our refined model.

2.6.2 Theoretical Considerations

The ultimate purpose of Los' research is to improve the dynamic arc model so that, when coupled with the rest of the system equations, a more comprehensive flashover model will result. His results, however, were not in a directly usable form for our model, so that some additional derivation is necessary and will be presented below.

All the coordinate variables used here are bi-cylindrical[46] so that,

$$y = \frac{a \sinh u}{\cosh u - \cos v} \tag{2.35}$$

$$x = \frac{a \sin v}{\cosh u - \cos v} \tag{2.36}$$

Lines of constant V form circles which begin perpendicular to the x-axis and intersect each other at a central point which is at a distance, a, along the y-axis from the origin. The lines of constant u will form the isotherms of the arc model.

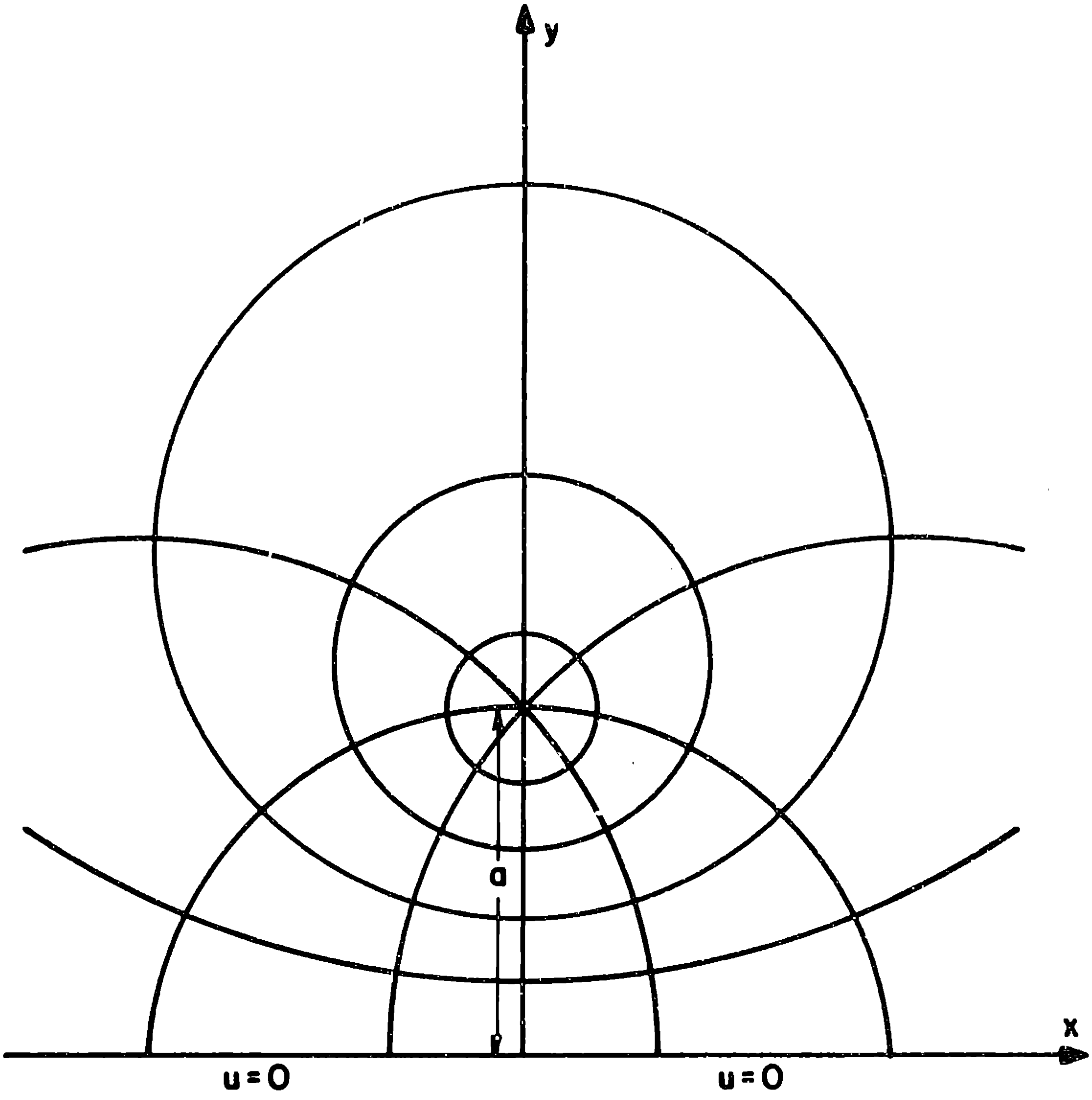

Figure 2.17   Bi-cylindrical Arc Geometry

These lines are also circles which have their centers on the y-axis at a distance (a coth u) from the origin. The radius of each of these circles is

$$R = \frac{a}{|\sinh u|} \quad \text{or} \quad \rho = \frac{1}{|\sinh u|} \tag{2.37}$$

where $\rho = R/a$ is a normalized radius. The coordinate system is shown in Figure 2.17. The governing energy eq. (2.33) can be expressed in the new coordinate system as

$$\sigma E^2 \frac{dA}{du} + 2\pi \frac{d^2S}{du^2} = \frac{1}{\lambda(S)} \frac{dS}{dt} \frac{dA}{du} \tag{2.38}$$

where

$$\lambda(S) = \frac{K_e(S)}{\rho_a C_p} \tag{2.39}$$

and

$$\frac{dA}{du} = \frac{2\pi a^2 \cosh u}{\sinh^3 u} \tag{2.40}$$

The last equation results directly from the coordinate transformation. Ohm's law is also used:

$$E \int_0^\infty \frac{dA}{du} \sigma(S) du = I \tag{2.41}$$

Note that both σ and λ can be approximated as functions of S rather than T.

The initial conditions before the current step are:

$$\sigma E_o^2 \frac{dA}{du} + 2\pi \frac{\partial^2 S_o(u)}{\partial u^2} = 0 \tag{2.42}$$

and

$$E_o \int_o^{\infty} \sigma(S_o) \frac{dA}{du} du = I_o \tag{2.43}$$

The key assumption of both Phillips and Los is that immediately after the step, the heat flux potential, S, can be expanded as a Taylor series

$$S(u,t) \simeq S_o(u) + S_1(u)t + 0(t^2) \tag{2.44}$$

The other variables may also be expressed in terms of a similar Taylor series:

$$\sigma(S) \simeq \sigma(S_o) + \left.\frac{\partial\sigma}{\partial S}\right|_{S_o} (S-S_o)$$

or

$$\sigma(S) \simeq \sigma(S_o) + \left.\frac{\partial\sigma}{\partial S}\right|_{S_o} S_1 t \tag{2.45}$$

and similarly,

$$\lambda(S) \simeq \lambda(S_o) + \left.\frac{\partial\lambda}{\partial S}\right|_{S_o} S_1 t \tag{2.46}$$

$$G(t) = \frac{1}{R(t)} \simeq G_o + G_1 t \tag{2.47}$$

Substituting (2.44), (2.45) into (2.42) and equating zero orders of t:

$$G(S_o)E^2 \frac{dA}{du} + 2\pi \frac{\partial^2 S_o(u)}{\partial u^2} = \frac{1}{\lambda(S_o)} S_1 \frac{dA}{du} \tag{2.48}$$

Using (2.42), (2.48) can be reduced to

$$\sigma(S_o)\ (E^2-E_o^2) = \frac{1}{\lambda(S_o)} S_1 \tag{2.49}$$

From Ohm's law,

$$G = \int_o^\infty \frac{dA}{du}\,\sigma(S)\;du \tag{2.50}$$

and

$$G \simeq G_o + G_1$$

$$= \int_o^\infty \frac{dA}{du}\,\sigma(S_o)\;du + \int_o^\infty \frac{dA}{du}\left(\frac{\partial\sigma}{\partial S}\right)_{S_o} S_1\;du \tag{2.51}$$

so that

$$G_1 = \int_o^\infty \frac{dA}{du}\left(\frac{\partial\sigma}{\partial S}\right)_{S_o} S_1\;du \tag{2.52}$$

Now,

$$\frac{\partial}{\partial t}\,\ell n\;G = \frac{1}{G}\frac{\partial G}{\partial t} \tag{2.53}$$

Using (2.47), and keep zero order time terms

$$\frac{1}{G}\frac{dG}{dt} \simeq \frac{G_1}{G_o}$$

$$= \frac{1}{G_o}\int_o^\infty \frac{dA}{du}\left(\frac{\partial\sigma}{\partial S}\right)_{S_o} S_1\;du \tag{2.54}$$

(2.40) and (2.49) can now be substituted into (2.54),

$$\frac{1}{G}\frac{dG}{dt} = \frac{2\pi a^2}{G_o}E_o^2\left(\frac{E^2}{E_o^2} - 1\right)\int_o^\infty \frac{\cosh u}{\sinh^3 u}\left(\frac{\partial\sigma}{\partial S}\right)_{S_o}\lambda(S_o)\sigma(S_o)du$$

$$\frac{1}{G}\frac{dG}{dt} = \left(\frac{E^2}{E_o^2} - 1\right)\frac{1}{\tau_f} \tag{2.55}$$

where

$$\frac{1}{\tau_f} = \frac{2\pi a^2E_o^2}{G_o}\int_o^\infty \frac{\cosh u}{\sinh^3 u}\,\frac{\partial\sigma}{\partial S}\,\sigma(S_o)\lambda(S_o)du = \frac{a^2E_o^2}{G_o}\,P \tag{2.56}$$

and

$$P = 2\pi \int_0^\infty \frac{\cosh u}{\sinh^3 u} \frac{\partial\sigma}{\partial S} \sigma(S_o)\lambda(S_o)du \tag{2.57}$$

Equation (2.55) is applicable under any change of power supply characteristic. This result is more general than Phillips' theory since he assumed the arc to be powered by a current source.

From (2.56), τ_f can now be found as

$$\tau_f = \frac{1}{R^3 I^2 a^2 P}$$

after an approximation has been introduced to replace I_o by I.

The integration of P was carried out numerically on a programmable calculator by Los and the integrated function expressed as a function of r' (i.e. $r_a a^2$) is reproduced here in Figure 2.18. The P function is fitted by the following relation

$$P = 0.5(r_a a^2)^{-1.27} \tag{2.58}$$

Equations (2.55), (2.57) and (2.58) now define the dynamic state of an arc at any instant of time. Before they can be incorporated into the flashover model, however, E_o must be determined. By definition, E_o is the steady-state field strength before the occurrence of a disturbance. Seventy-five experiments were performed by Los and an empirical relationship for E_o was found:

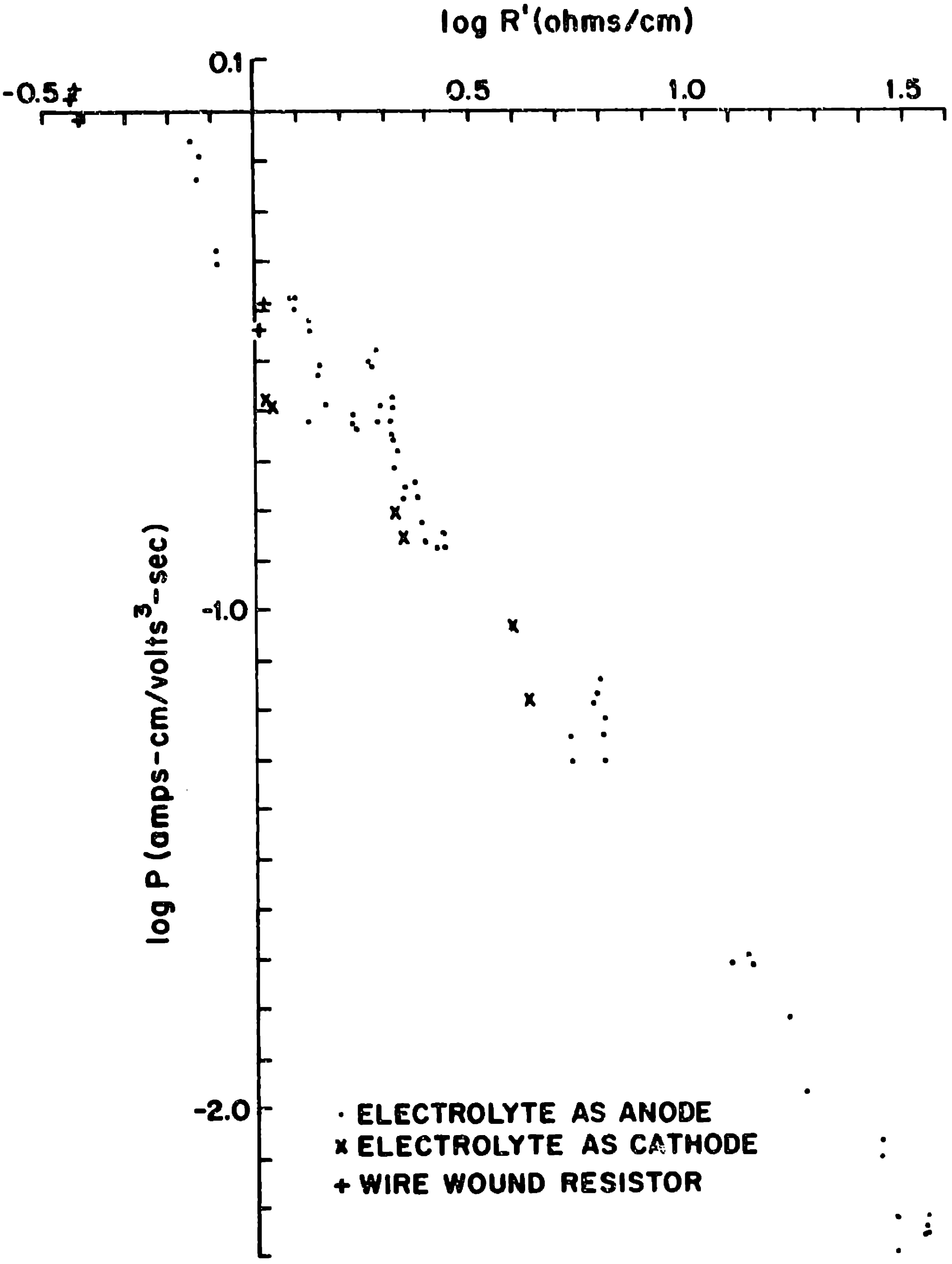

Figure 2.18 Experimental Results : Normalized Time Constant vs Normalized Resistance

$$(E_o a)^{1.42} = 52.0(a^2 r_a)^{0.42} \tag{2.59}$$

Note that both empirical equations (2.58) and (2.59) are expressed in terms of r_a purely for the sake of mathematical convenience. The purpose is to eliminate one variable E and replace it by $(r_a i_a)$ whenever possible.

Finally, the results of the 75 experiments provided us with another important empirical relation that we were incapable of getting before. In 2.5.2 the energy equation was stated as,

$$\frac{dQ}{dt} = EI - N_o$$

The loss term N_o is not known a priori and supplies the reason why the previous system of equations had to be normalized first. Now, under essentially the same experimental conditions as before, a steady-state arc was being maintained, meaning $dQ/dt \to 0$. N_o could now be equated to the product EI, and expressed as follows:

$$N_o = 52.0 \ (I/a)^{0.58} \tag{2.60}$$

The system of equations for theory II have all now been derived and are presented in Table 2.6.

Three of the equations in the system are first-order partial differential equations. Three initial conditions must be specified $x(t=0)$ is set equal to zero as before. $r_a(t=0)$ is derived along the same line of reasoning as

TABLE 2.6

DYNAMIC THEORY II - SYSTEM EQUATIONS

$$\frac{1}{r_a}\frac{dr_a}{dt} = \left(1 - \left(\frac{I_a r_a}{E_o}\right)^2\right)\frac{1}{\tau_f} \qquad (2.55)$$

$$\tau_f = \frac{1}{r_a^3 I_a^2 a^2 P} \qquad (2.56)$$

$$P = 0.5\ (r_a a^2)^{-1.27} \qquad (2.58)$$

$$(E_o a)^{1.42} = 52.0\ (a^2 r_a)^{0.42} \qquad (2.59)$$

$$N_o = 52.0\ (I_a/a)^{0.53} \qquad (2.60)$$

$$\frac{1}{r_a}\frac{dr_a}{dt} = \frac{N_o - E_a I_a}{Q_o} \qquad (2.8)$$

$$\frac{dx}{dt} = \frac{V_e I_a}{Q} \qquad (2.12)$$

$$V = r_a I_a x + V_e + Ir(\ell - x) \qquad (2.10)$$

$$V = V_e + (I - I_a) rx + Ir(\ell - x) \qquad (2.11)$$

presented in 2.5.4. An initial arc is assumed to bridge the air-gap between the electrode and the water channel. Such an arc usually takes about 1 μs to form, so that it reaches steady-state almost immediately. Equation (2.25) at steady-state yields:

$$r_a(t=0) = \frac{52.0(I_a/a)^{0.58}}{I_a^2} \tag{2.61}$$

But,

$$I_a = \frac{V-V_e}{r\ell}$$

so that

$$r_a(t=0) = 52.0\ (r\ell)^{1.42}/(a)^{0.58}(V-V_e)^{1.42} \tag{2.62}$$

The right-hand-side of eq. (2.62) are all known constants. The determination of Q(t=0), however, is not so simple. The problem essentially is determining the heat content of the initial arc discharge in the air gap. In Theory I, such a value was derived from Mayr's equation which is no longer being used in Theory II. Only a reasonable estimate of the range of Q(t=0) can be supplied here, based on Theory I as well as on experimental observations.[33] Q(t=0) is estimated to range between 0.1 - 3.0 joules/cm for most of our experimental conditions. It might seem here that the theory suffers from some arbitrariness, as far as the determination of one initial condition is concerned. Such is not really the case, however. When all the simulations had been performed for a diverse range of physical conditions (see following sections), the values of Q(t=0) that yielded the best agreement between theory and experiments for almost all of these cases were remarkably close to one another. This finding had an important physical meaning.

Another constant a, the height of the arc above the water surface, must be determined also. It was measured photographically and determined to be 0.1 cm. Values of 0.2 cm and 0.05 cm were also tried in the simulations to provide an error bound. A difference of 10% was observed in the simulation results.

2.6.3 Computer Simulation

With the determination of all the initial conditions and constants, the system of equations in Table 2.6 were solved on IBM 370/165 using IBM Continuous System Modeling Program. The details of the programming can be found in Appendix B and will not be elaborated here. Altogether 100 simulations were carried out and some of these are presented below.

2.6.4 Comparison Between Theory and Experiment

Figures 2.19-2.24 illustrate the comparison between theory and experiment for a variety of cases. For convenience sake, the important parameters are listed in Table 2.7.

2.6.5 Discussion

Most of the comments in sec.(2.5.6) about the theory are still valid, except for the part on dynamic arc modeling. This section will, therefore, be mainly concerned with the

TABLE 2.7

COMPARISON BETWEEN THEORY AND EXPERIMENT

Fig. #	Voltage (V) kV	Resistivity (r) Ω/cm	Length (ℓ) cm	Q(t=0)
2.19	+10	158	15	1.80
2.20	+9	490	10	0.13
2.21	-9	490	10	0.12
2.22	+8	800	9	0.14
2.23	-8	800	9	0.30
2.24	-12	6400	9	0.06

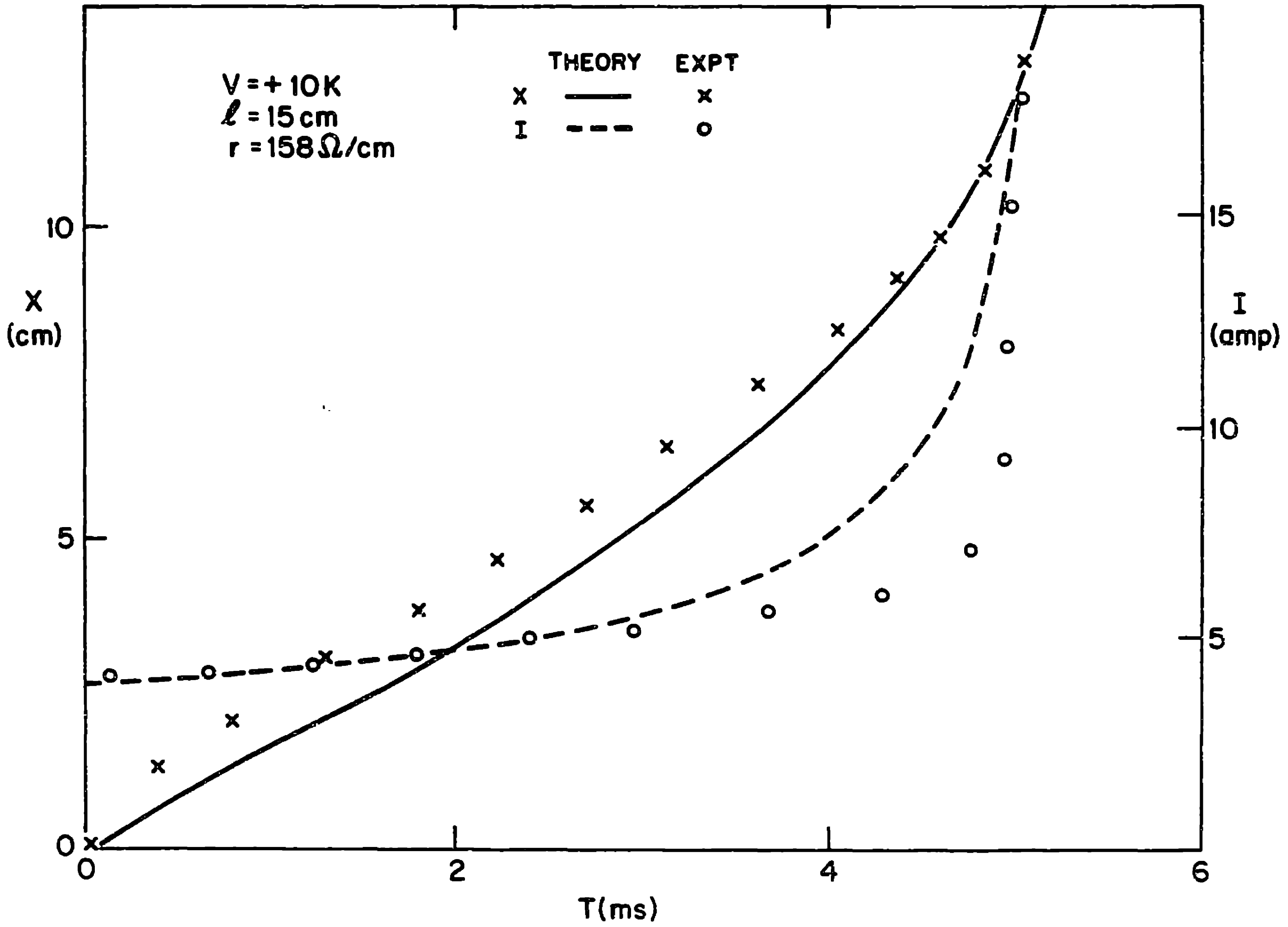

Figure 2.19 Comparison between Dynamic Theory II and Experiments

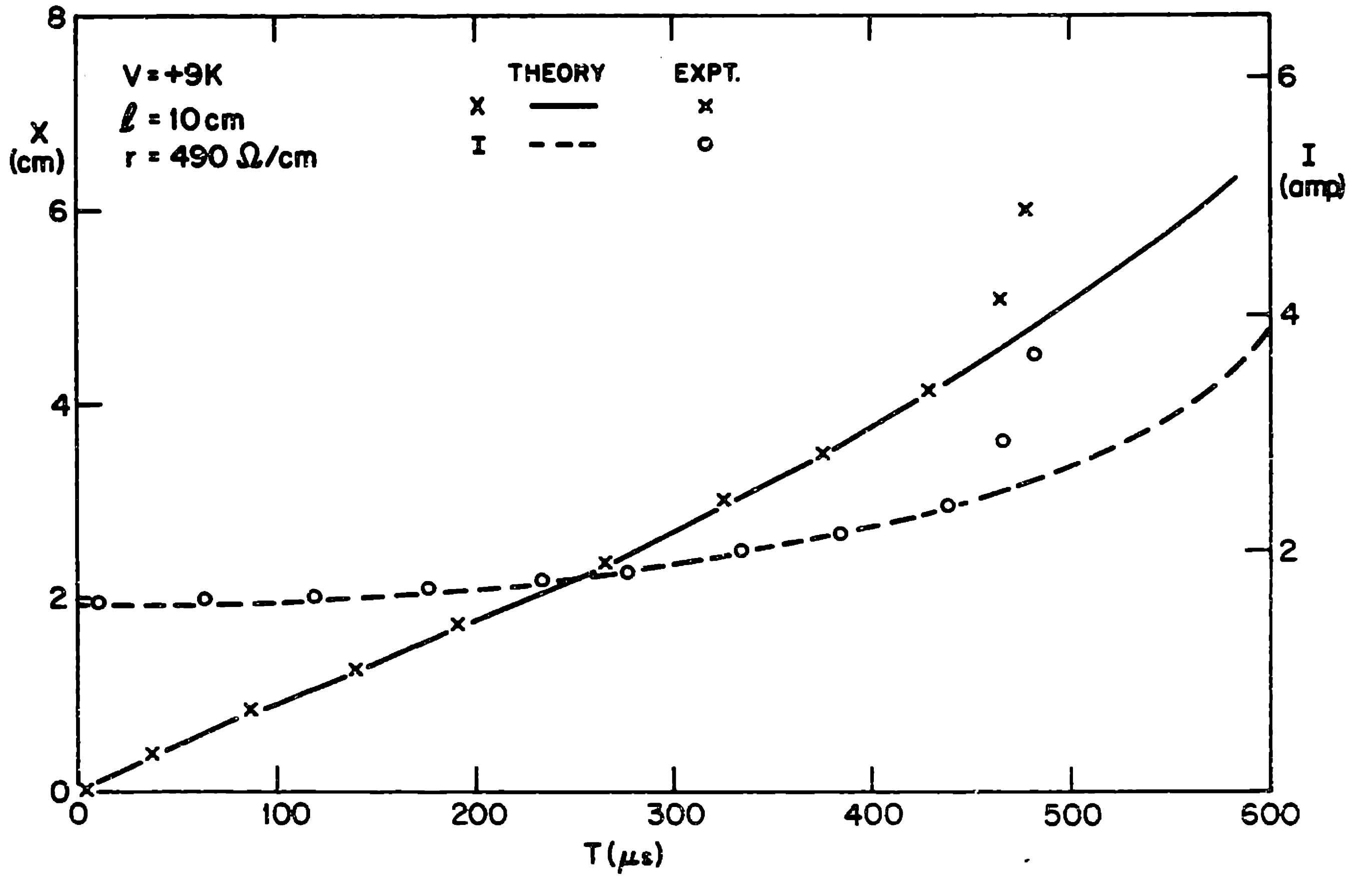

Figure 2.20 Comparison between Dynamic Theory II and Experiments

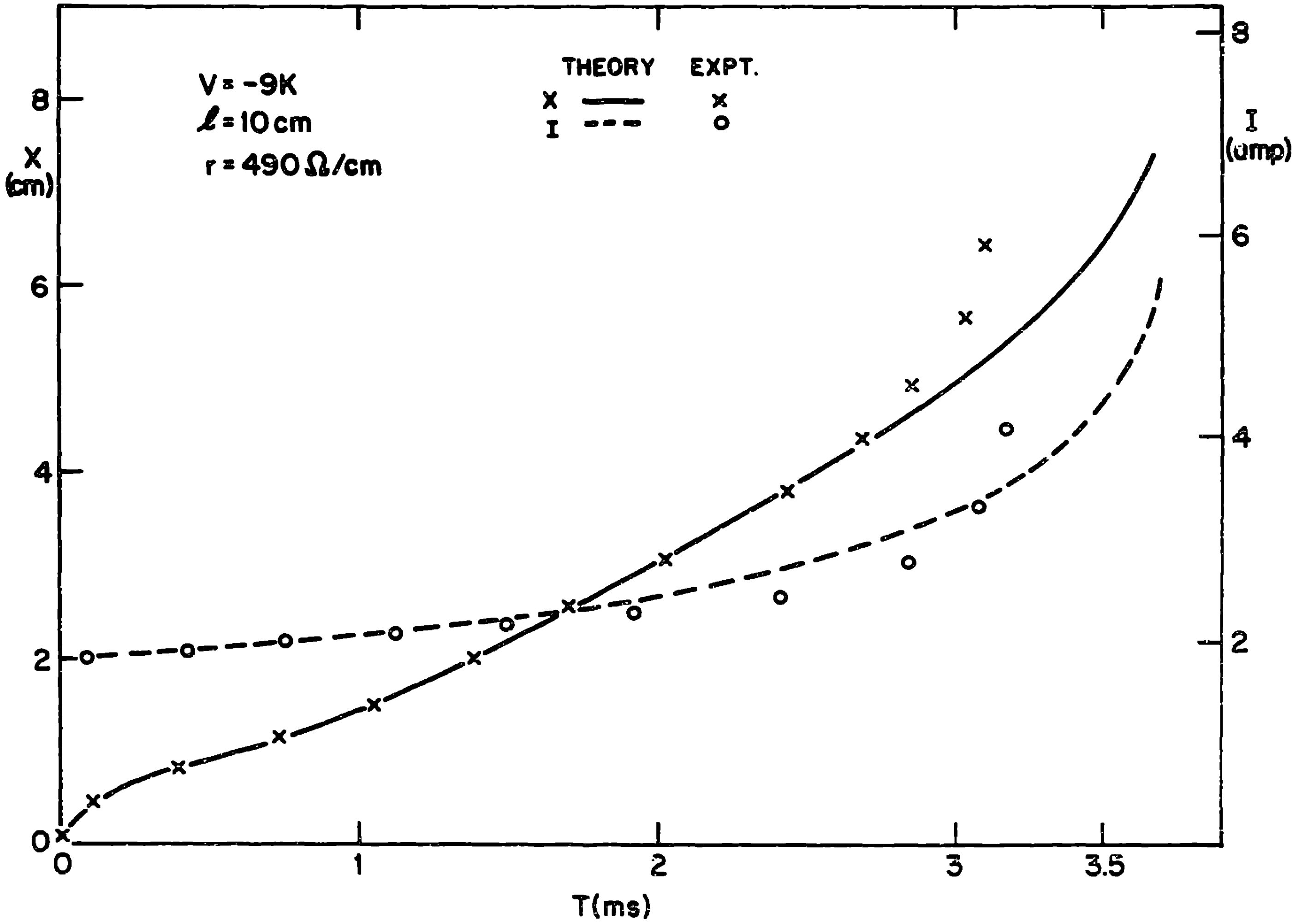

Figure 2.21 Comparison between Dynamic Theory II and Experiments

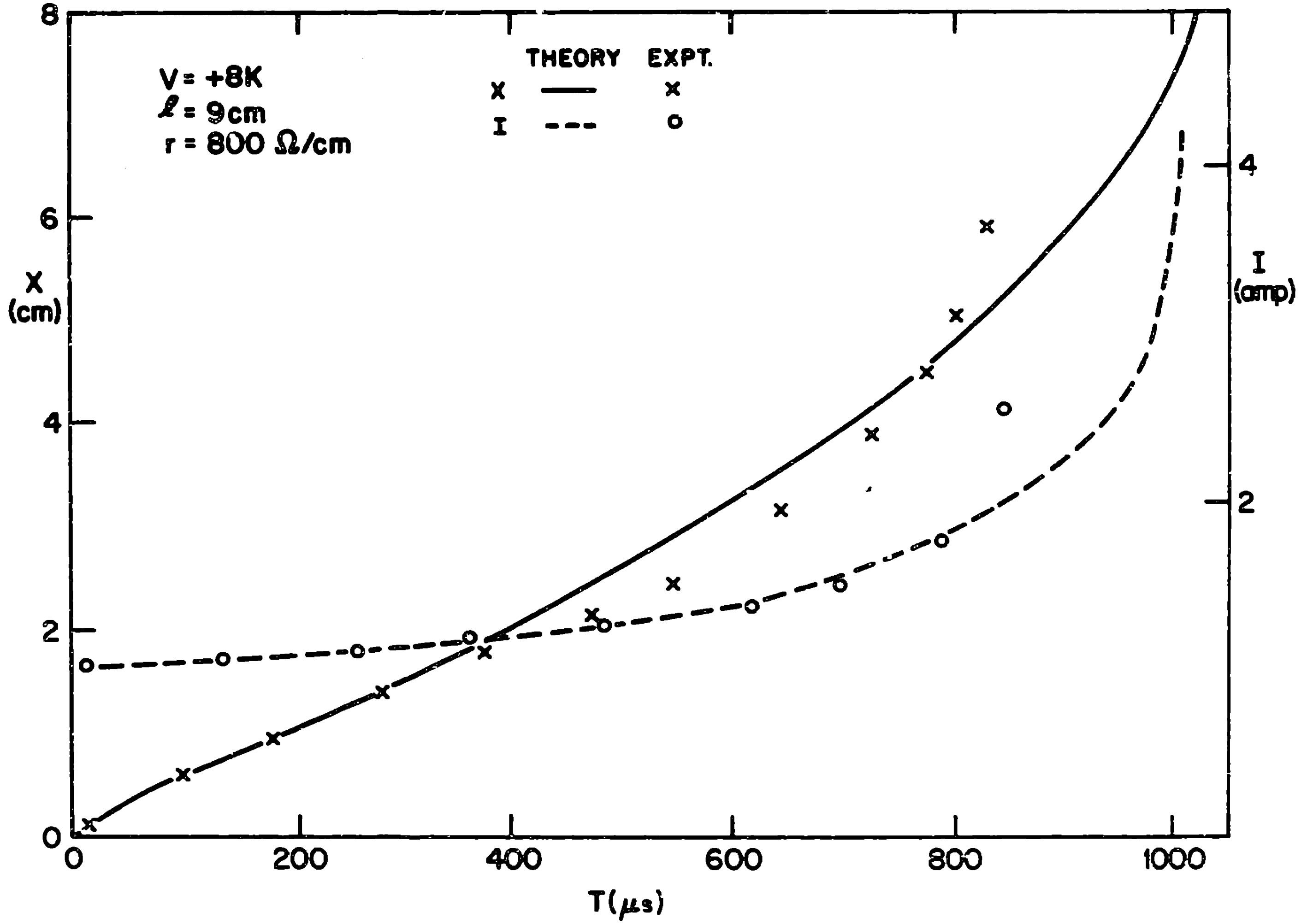

Figure 2.22 Comparison between Dynamic Theory II and Experiments

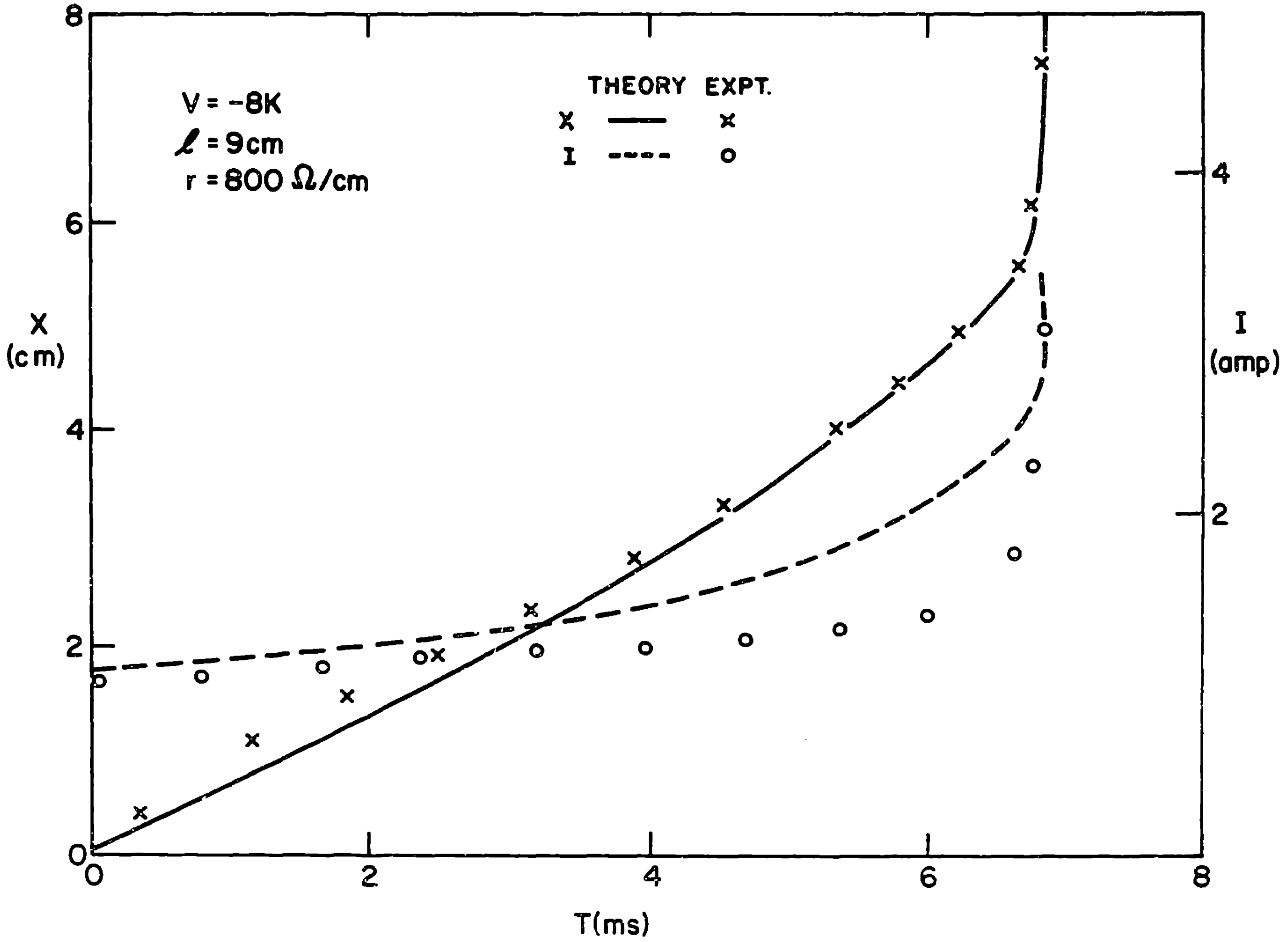

Figure 2.23 Comparison between Dynamic Theory II and Experiments

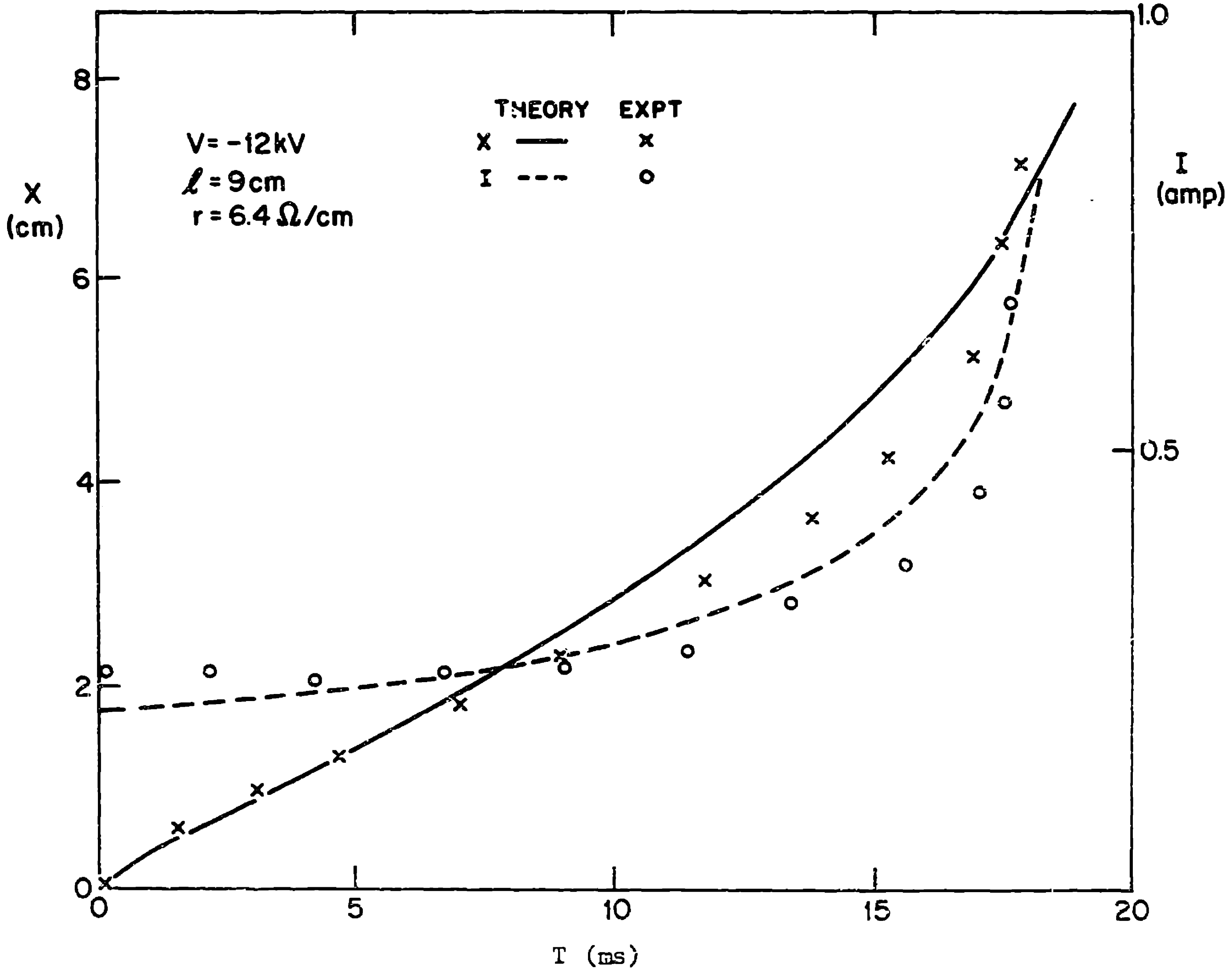

Figure 2.24 Comparison between Dynamic Theory II and Experiments

improvements rendered possible by the new arc model. Note that the agreement between theory and experiment is far better in the beginning of the propagation than near the end. The reason has already been stated, namely, that some other growth mechanisms, particularly streamers, were possibly triggered at the tip of the accelerating arc.

Mayr's equations, in order to be numerically solvable, had to be normalized. Then, in order to be practically usable, the solutions had to be denormalized by comparing with experimental data. The theoretical prediction is thus a posteri rather than a priori. This can be a limiting factor in its practical usage. Theory II, on the other hand, have all of the constants predetermined except one, i.e. Q(t=0). Even that parameter can be easily determined by comparing one simulation with one experimental test. Q(t=0) is found by the best fit between the two and once determined can be applied to all the other cases. Therein lies the usefulness of the theory.

Fundamentally, the time constant in Mayr's equation is derived on the assumption of free decay, namely, the current is interrupted instantaneously. Such a value is at best an approximation. The time constant in Theory II is derived on the basis of a perturbation analysis and hence is dependent, at every instant in time, on the current state of the arc. Such a value is therefore far more realistic.

Finally, there has been a long-standing controversy in contamination flashover research on the question whether the arc burns in atmosphere of steam or dry air (all e.g. Hampton[8] and Wilkins[21]). Both pros and cons seem to have proofs to support their contention. Mayr's equation is based on the assumption that the arc is burning in dry air. Theory II, however, circumvented the issue by using actual experimental data so that the question of steam or dry air never arose.

2.7 Studies of Cathode Fall Phenomenon

2.7.1 Introduction

In all the one-dimensional modeling, electrode falls played a very important role, particularly the cathodic voltage drop. From the high-speed movies taken during the course of this research (see Chapter V), it can be clearly seen that for all cases of interest, the discharge growth is most evident when the water surface is acting as a cathode. This observation is true for linear, two dimensional flat-plate and real insulators. Therefore, it is clear that a closer investigation at the nature of the cathode drop is warranted, with the objective of theoretically predicting such a voltage drop for an aqueous surface. Furthermore, cathode falls on a water surface have been scarcely measured before and never analyzed theoretically.

Some exploratory tests were first carried out. A piece of #13 copper wire was suspended vertically a few mm's above the surface of a pool of tap water which was grounded along the walls through a current-limiting resistor. High voltage (a.c.) was applied to the wire and above a threshold value, a greenish discharge, sometimes tinged with sodium yellow, formed in the air gap. The discharge could usually burn stably for a few minutes until the tip of the wire melted off, lengthening the gap and extinguishing the discharge. If the voltage applied was too high, on the other hand, a flashover might result. Still pictures were taken and a typical one is shown in Figure 2.25.

Because the voltage used was a.c., it was impossible to tell whether the water was acting as a cathode or anode at any instant by the naked eye. Other efforts to differentiate the two (e.g. sampling through a rotating slit) were generally not successful. Regardless of the polarity, however, it was clear that the discharge was not that of a corona nor was it likely full fledged arc discharge. The latter would tend to be rather unstable and would flashover from time to time. The most plausible dsscription would seem to be a glow discharge. This type of discharge is of relatively low current density and high voltage (as observed) when compared to the relatively high current density and low voltage of the arc. Transitions between the two modes, however, are possible and do occur readily. In fact, in our modeling, we assume only the tip portion of the arc to be a glow discharge, the rest being a normal arc. The discharge was usually confined to an area much smaller than the whole available area of the water electrode. Thus in our experimental set up, the glow could

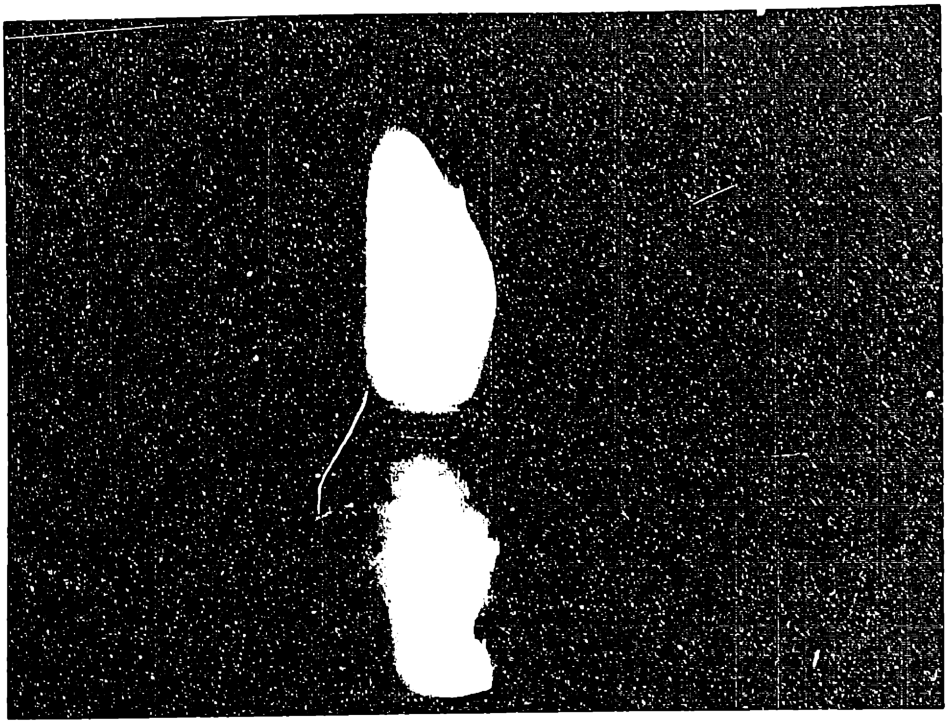

[illegible]

[illegible]

be classified as a normal glow (as opposed to abnormal). A normal glow is one where the discharge area is smaller than the available area of the electrode. An abnormal glow, on the other hand, covers the whole electrode surface.

2.7.2 Previous Research on Glow Discharges

Reference 26 gives a rather thorough survey of the literature on this subject. Only a few of the relevant features will be mentioned here. The easiest way to obtain a glow discharge is probably by energyzing a glow tube of a few centimeters in diameter and about 50 cm leng, filled with low pressure gas. A sketch is shown in Figure 2.26 and Figure 2.27 together with some typical parameters such as voltage, field strength charge densities, and etc. The diagrams are only schematic, actual values being dependent upon the physical constraints used in each particular set-up. Because these parameters can be monitored, they constitute a ready check against any proposed theory. A few of the better known theories will be briefly discussed.

Most authors use Townsend's avalanche formula

$$e^{\int_0^d \alpha dx}$$

as a means of electron and ion multiplication, where α is the rate of ionization. They differ, however, in their assumptions about v^+ and v^-, velocities for ions and electrons, and also in the forms f(E), they use for α. Others have ignored some of the physical equations, such as Poisson's, and used in-

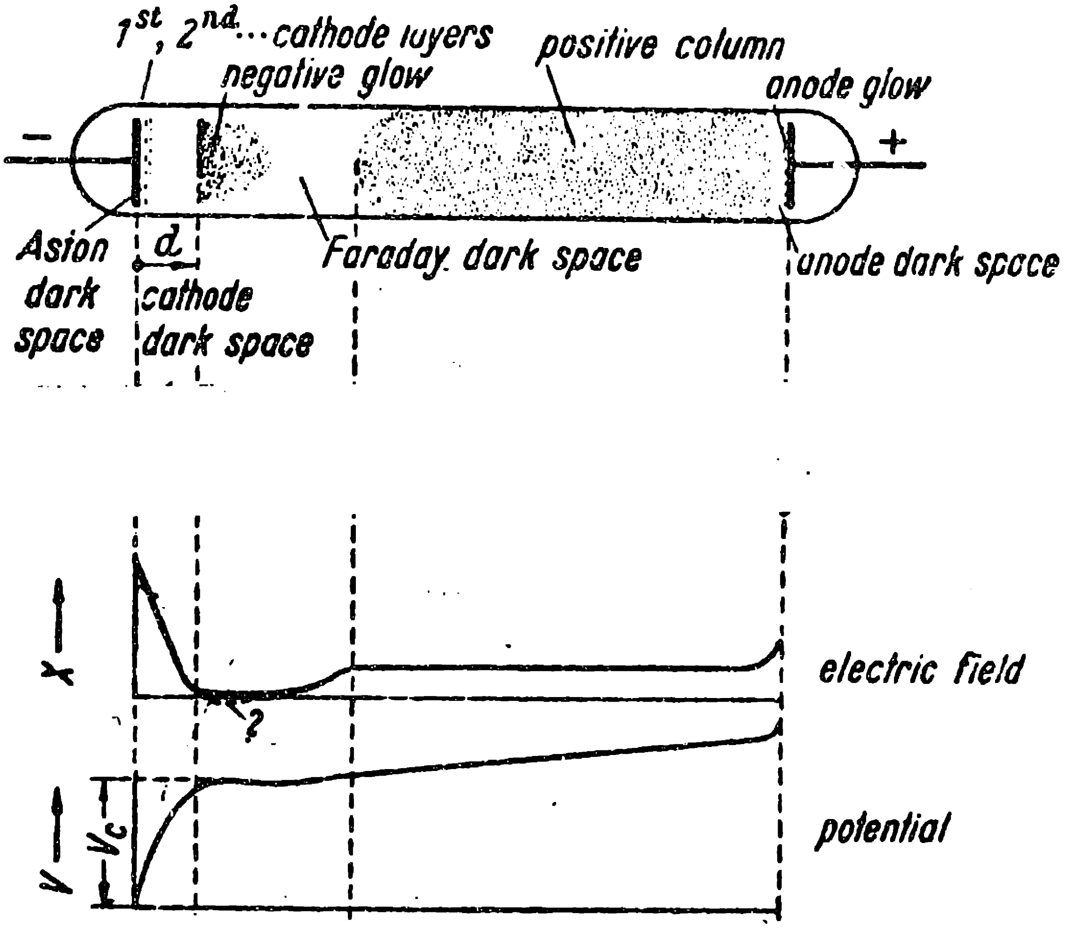

Figure 2.26 Glow Discharge Parameters

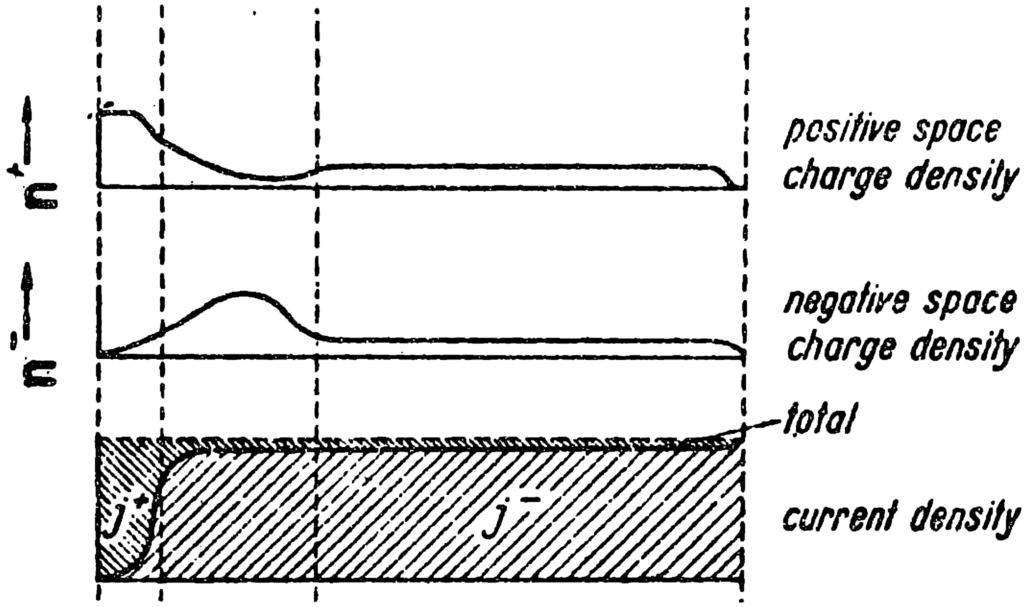

Figure 2.27 Glow Discharge Parameters

stead experimentally measured quantities. All of the theories had to make compromises in order to compare favorably with the experimental findings.

Compton and Morse[47] invoked a minimum principle which states that the potential distribution must be such that most currents would flow, subject to the limitations of Poisson's equation.[48] They assumed α to be

$$\alpha/P = A\ e^{-BP/E} \tag{2.63}$$

as given by Townsend, where A and B are constants. They defined d_n, the distance from the cathode to the end of the cathode drop region, somewhat arbitrarily and did not yield good agreement with experiment.

Morse[49] abandoned the minimum principle and assumed equal ion and electron temperatures. He further assumed $v^+ \sim \sqrt{E}$ and derived $E = C_1\ e^{-A'PX} + C_o$, where A' depends on gas properties. This form of the E-field did not conform to the measured variation with respect to x.

Rogowski[50], Weizel, Rompe and Schon[51] neglected diffusion and took α to be constant, equal to its maximum value at the cathode and assume v^+ and v^- both $\alpha\ \sqrt{E}$. They further assumed a small ion current to flow into the glow from the positive column; which is a valid assumption which has been used by others.[52] Their solutions, however, were too complicated to be of general use and comparisons with experiments were difficult. Despite some rather shaky approximations, such as making α constant, their general approach was correctly formulated.

One of the best accepted theories is that of Von Engel and Steenbeck.[53] They made one important observation, both in theory and in experiment, which eliminated the need for an additional physical law. Their finding is reproduced in Figure 2.28. As the current density j is varied, v_c (cathode fall voltage in general) passes through a minimum, which corresponds to the normal cathode fall V_{cn}; at this point j is denoted by j_n and d by d_n to indicate that they are in the normal glow regime. Experimentally this means that the current density will remain constant at j_n when this point is reached even though total current may decrease further. This is accomplished, by the discharge contracting to ccver a smaller area of the cathode. V_c too remains roughly constant at this point and does not follow the dotted curve of Figure 2.28. This observation pinpoints the regimes of operation of a normal glow and theoretically helps to define a unique cathode fall voltage V_{cn} as well as a cathode distance d_n. Like others before them, however, they had to compromise accuracy for mathematical simplicity in order to arrive at an analytically interpretable solution. They disregarded the equation of continity and imposed a linear distribution of field (as experimentally observed) thus ignoring Poisson's equation. They used Townsend's formula for α and set $J_+=0$ at x = d. The last two were at best approximations. Despite this inadequacies, their results compared reasonably well with

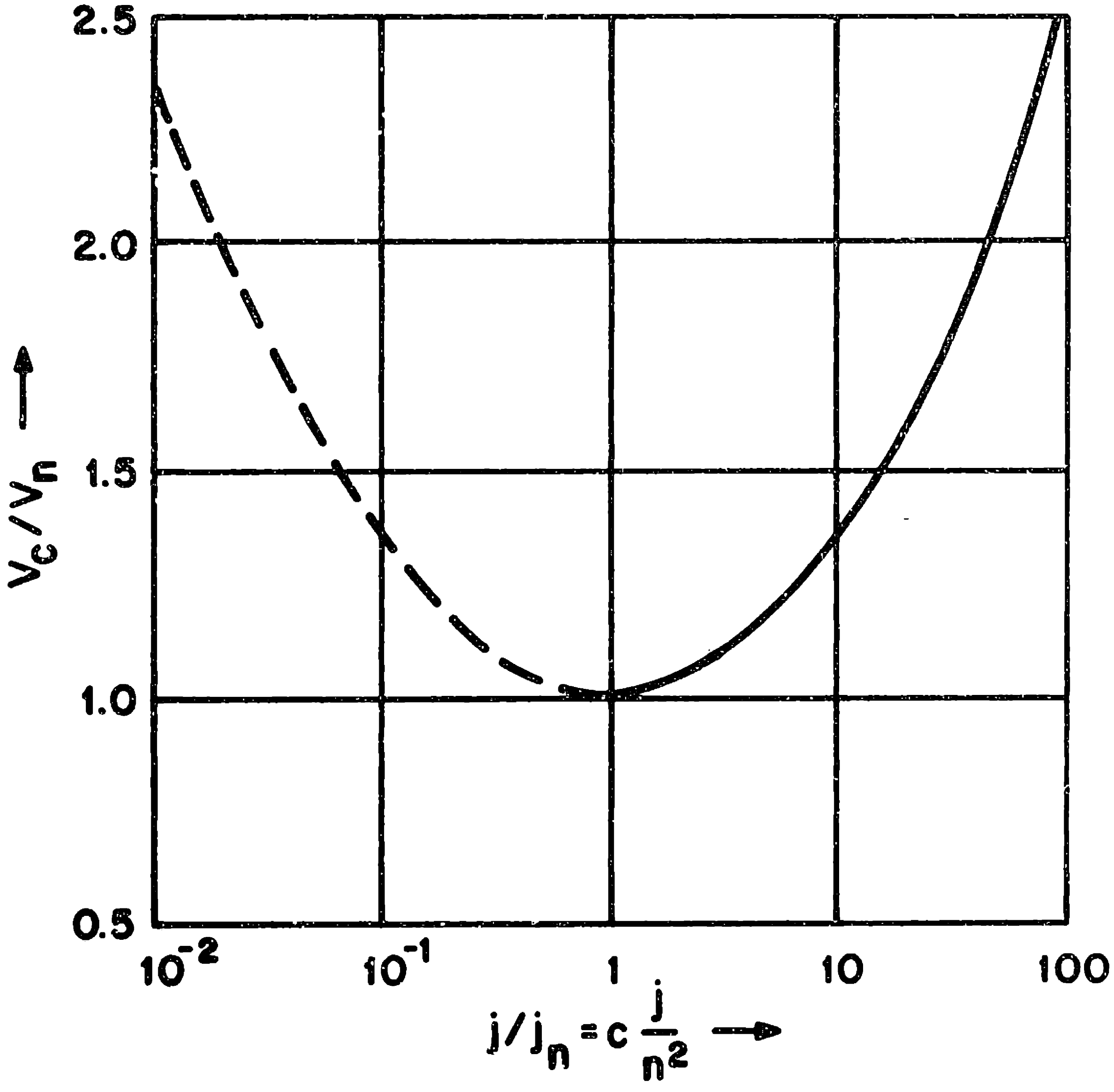

Figure 2.28 Steenbeck's Theory of Cathodic Voltage

experiments, chiefly due to the success of their minimum theory.

As already noted, to a large extent the need for approximations arose in the above theories as a result of the mathematical complexity of the problem. With the advent of computers and numerical calculations, analytical solutions were no longer a necessity. Below will be presented a theory that attempts to encompass most of the fundamental equations with a minimum of the approximations.

2.7.3 A Model for Cathode Fall Region

The basic physical equations that govern a cathode region are as follows:

(1) Poisson's eqaation

$$\frac{\partial E(x)}{\partial x} = \frac{q(n_+(x) - n_-(x))}{\varepsilon_o} \tag{2.64}$$

where q is the electronic charge; n_+, the ion density; n_-, the electron density and ε_o, permittivity.

(2) Mobility:

for ions, $v^+ = \mu_+ E(x)$

and for electrons, $v^- = \mu_- E(x)$

where μ_+ and μ_- are the mobility coefficients for ions and electrons respectively so that

$$J_+(x) = q\, n_+(x)\mu_+ E(x) \tag{2.65}$$

$$J_-(x) = -\, q\, n_-(x)\mu_- E(x) \tag{2.66}$$

The total current is $J(x) = J_+(x) - J_-(x)$

(3) Continuity of Current:

Ions and electrons are created in equal numbers through Townsend's ionization:

$$\frac{\partial J_-(x)}{\partial x} = \alpha J_-(x) \tag{2.67}$$

In a steady-state, since there is no net production or loss of charges, the total current is constant or

$$J(x) = J_+(0) - J_-(0) = J_o \tag{2.68}$$

Note that the ionization equation for $J_+(x)$ is thus automatically taken care of. The above equations constitute the governing equations for the region. Some boundary conditions must be considered. At the cathode surface (x=0), a secondary emission coefficient γ is assumed, so that

$$J_-(0) = -\gamma J_+(0) \tag{2.69}$$

Combining (2.68) and (2.69) yields

$$J(x) = J_o = J_+(0)(1+\gamma)$$

or

$$J_+(x) - J_-(x) = J_+(0)(1+\gamma) \tag{2.70}$$

At the other end of the cathode region i.e. $x = d$, the boundary conditions are far less well-defined. For one thing, there is no definite physical boundary at $x = d$. Most researchers have assumed that at such an imaginary plane, $E \to 0$ and $J_+ \to 0$. A recent study[52] (1972) showed that

$$J_+(x=d) \approx \delta J_o \tag{2.71}$$

where $\delta \cong 0.1$. Such an assumption will be used in our model.

The condition $E(x=d) \rightarrow 0$ is a vague one, because it is not clear if E even reaches zero. A more usable condition is $E(x=d) = \xi\, E(x=0)$ where $\xi << 1$. In our actual simulation runs, a sensitivity test was carried out for $E(x=d)$ to determine its effect on the cathode drop. For $\xi < 0.01$, a change of $E(x=d)$ by two orders of magnitude produces a difference of only 5% in the predicted V_c's.

Lastly, we have the defining equation,

$$v_c = - \int_o^d E(x)dx \qquad (2.72)$$

which contains two unknowns v_c and d, both of which must be determined. The values of α used are given by Meek and Craig[54] and reproduced in Table 2.8. The system of equations are recapitulated in Table 2.9.

The above set of equations contain the following seven unknowns: $E(x)$, $n_+(x)$, $n_-(x)$, $J_+(x)$, $J_-(x)$, v_c and d. Yet, only six equations have been written; where is, or rather, what is the missing equation? It is clear that this additional piece of information must be physical in nature and probably a characteristic of the glow cathode only so that it cannot be quantified into a general law. Researchers were confronted by this question for quite some time until Von Engel and Steenbeck proposed the minimum theory, as discussed earlier. Their theory was backed by experimental observations and will therefore, be used here. The normal cathode fall voltage is thus found by solving the above set of equations for v_c as a

TABLE 2.8

TABULATION OF α/P VS. $E/P^{(54)}$

E/P volts/cm/mm	α/P
20	3.4×10^{-5}
22	5.2×10^{-5}
24	1.34×10^{-4}
26	2.34×10^{-4}
28	4.30×10^{-4}
30	9.10×10^{-4}
35	6.05×10^{-3}
40	1.67×10^{-2}
50	5.54×10^{-2}
60	1.27×10^{-1}
70	2.24×10^{-1}
80	3.40×10^{-1}
90	4.91×10^{-1}
100	6.37×10^{-1}
120	1.02
140	1.48
160	1.76
200	2.50
400	6.00
600	8.00
800	9.40
1000	10.40

TABLE 2.9

GLOW CATHODE MODEL - SYSTEM EQUATIONS

Poisson's equation:

$$\frac{\partial E}{\partial x} = \frac{q((n_+(x) - n_-(x))}{\varepsilon_o} \tag{2.64}$$

Mobility:

$$J_+(x) = qn_+(x)\mu_+ E(x) \tag{2.65}$$

$$J_-(x) = - qn_-(x)\mu_- E(x) \tag{2.66}$$

Ionization:

$$\frac{\partial J_-(x)}{\partial x} = \alpha J_-(x) \tag{2.67}$$

Continuity:

$$J_+(x) - J_-(x) = J_+(0)(1+\gamma)$$

$$= J_o \tag{2.70}$$

Definition:

$$V_c = - \int_o^{\alpha} E(x)dx \tag{2.72}$$

Boundary Conditions:

$$J_+(x=d) = \delta J_o, \ \delta \simeq 0.1$$

$$E(x=d) = \xi E(x=0), \ \xi < 0.01$$

$$J_-(x=0) = - \gamma J_+(x=0)$$

function of J(x), i.e. the total current. A range of J(x) will be used and a minimum v_c can be found, which corresponds to the true normal cathode fall voltage.

2.7.4 Numerical Solution

The system of equations was simulated on IBM 370/165 using IBM Continuous System Modeling Program. One distinctive feature of the simulation must be noted. Conventionally, all integrations start from the cathode surface (i.e. x=0) and progress towards x=d, at which point some pre-specified boundary conditions must be satisfied. This approach requires the knowledge of the field strength at the starting point, x=0. Such a field strength has never been accurately measured, but only estimated at around 5 x 10^5 volts/cm.[55] Since any approximation in E(x=0) will cause a considerable error in yielding values for v_c, it is dangerous to have a theory on pure guesses. Furthermore, unlike most metallic surfaces, water's secondary emission coefficient, γ, is not known with any precision. To start integrating from the cathode would naturally need just such a number. For these reasons, it is decided to start integrating from x=d towards x=0. The boundary conditions at x=d are more easily determined. Sensitivity tests, already mentioned, indicated that an error of a factor of 100 in the magnitude of E at x=d will produce only a difference of 5% in v_c, certainly not a significant difference. The exact value of field strength assumed at x=d is thus no longer a critical issue, as long as it is much smaller than E(x=0). In addition, this reverse integration affords more flexibility to assuming a value for γ. Estimates of γ for various surfaces range from 10^{-5} to 1. For a water surface, it is probably near the lower limit, water being a relatively poor secondary emitter.[56] By integrating from x=d towards the cathode surface, the values of γ are continuously monitored by the ratio, $\gamma = J_-(x)/J_+(x)$. Thus, v_c is determined as a function of γ.

The programming details are included in Appendix C. In order to determine the normal cathode drop, v_{cn}, a set of v_c's is simulated corresponding to a range of current densities. The minimum thus found is the required value. There is a unique minimum for each γ.

2.7.5 Discussion

As always, the success of a theory depends on its capability of describing a system as realistically as possible. Even though the prediction of a cathode fall voltage has been our final aim, other physical parameters are also generated, whose trends of behavior can also be compared with previous observations (see Figures 2.26 and 2.27). In Figures 2.29 and 2.30 are shown the variables E, n_+, n_-, J_+, and J_- vs. x. Though the exact values will depend on the external constraints, nevertheless, their respective functional dependences on x are found to be quite similar. Note especially the E-field's almost linear dependence on x, which has been assumed by many in their theories (thus deriving a

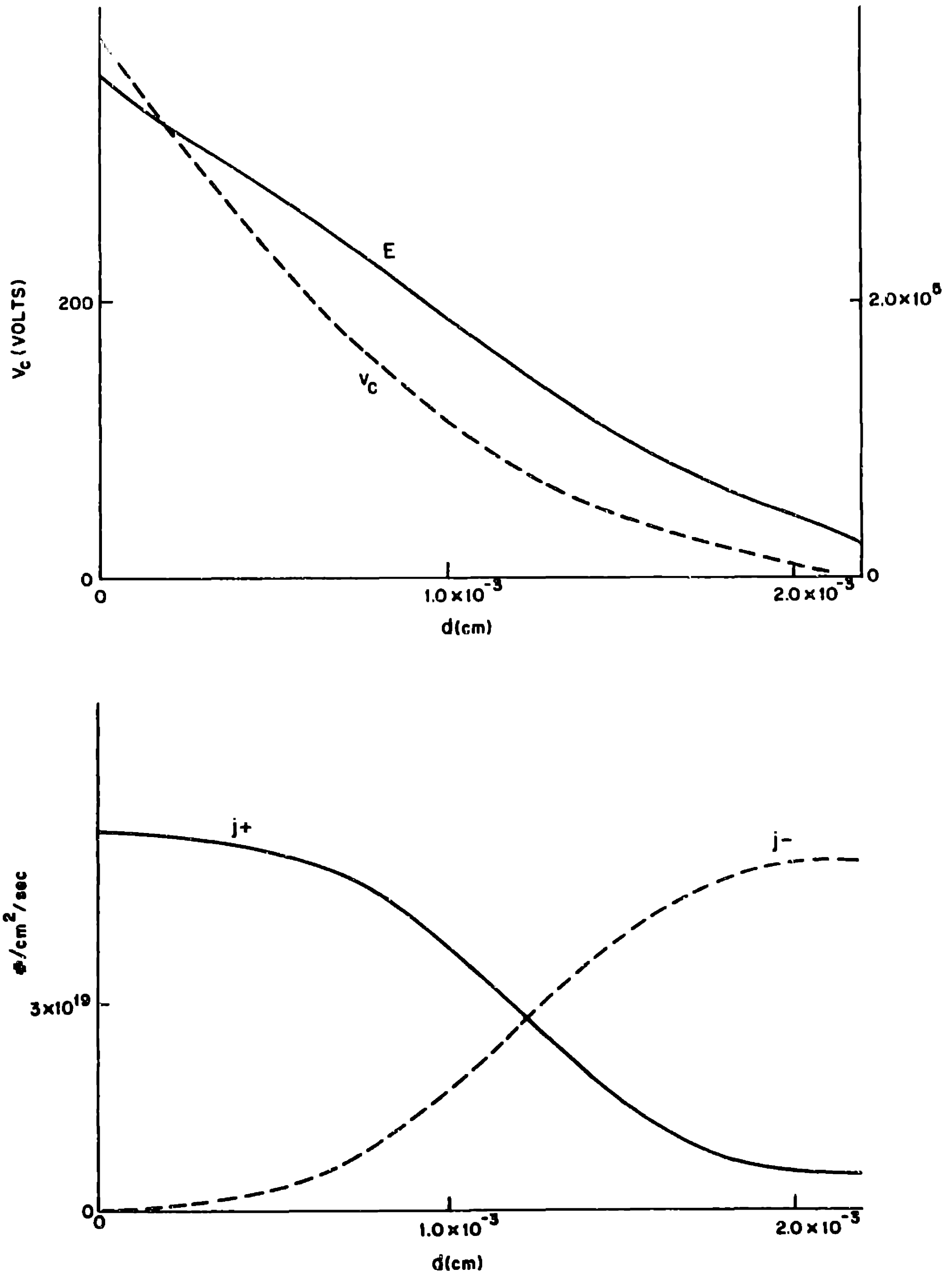

Figure 2.29 Calculated Discharge Parameters

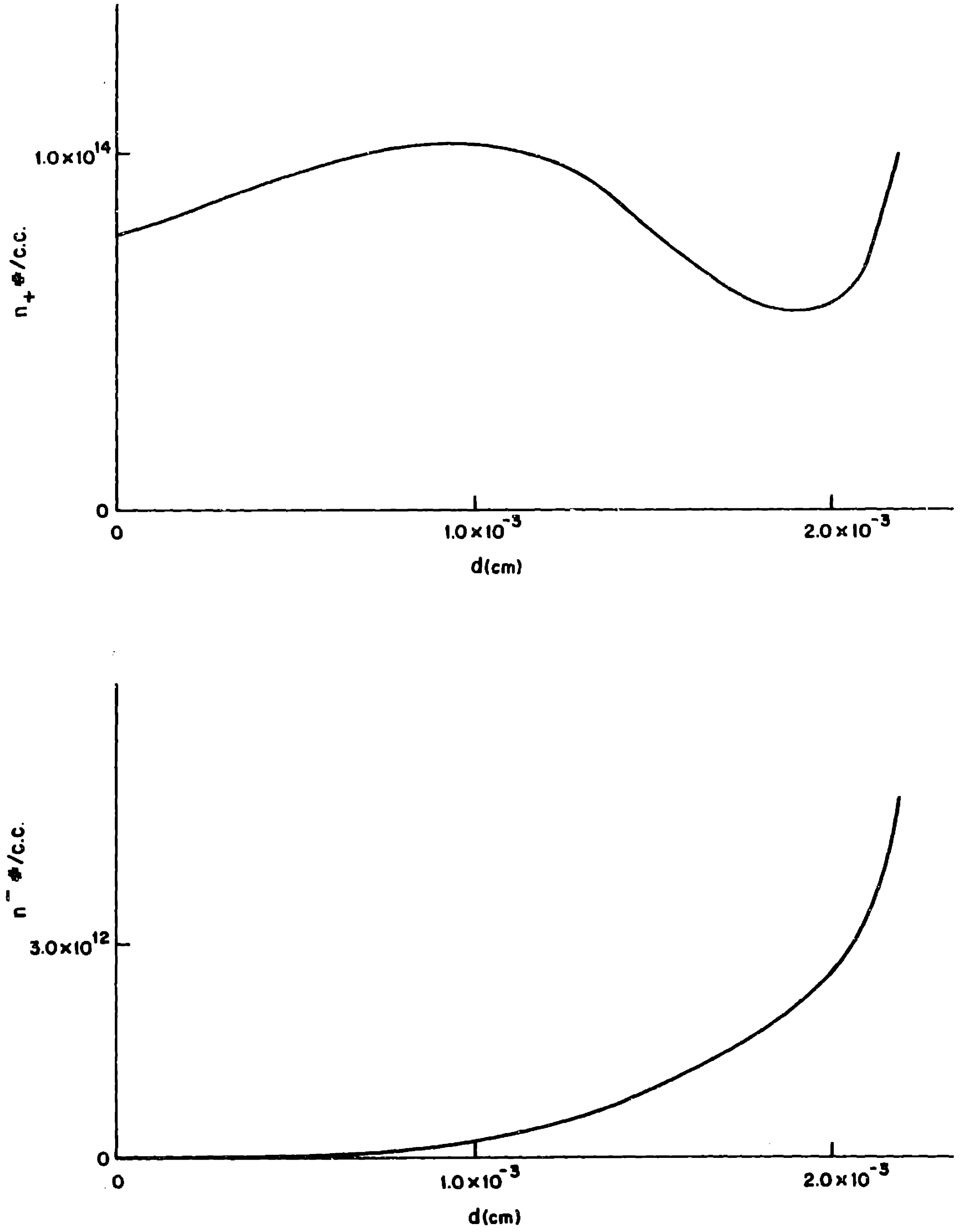

Figure 2.30 Calculated Discharge Parameters

boundary condition at E(x=0), but which is nevertheless an unnecessarily restrictive imposition on Poisson's equation. The fact that all of the above variables are "behaving correctly" adds further plausibility to the theory just proposed.

A final test for the theory, before its application, lies in its ability to predict cathode drop voltages for some surfaces other than water, whose measurements have been extensively recorded.[28] Table 2.10 gives some sample predictions. Except for copper which seems to have an exceptionally high cathode fall voltage, out of line with the other metals, the other predictions are generally good (some are not reported here because their values are close to Al and Fe).

Using the simulation method described, Table 2.11 gives a list of normal cathode fall voltages vs. γ, since the exact value for γ is unavailable at this time. However, γ is generally known to be very small for a water electrode. The assumption that V_c = 800 volts in our Dynamic Theories is, therefore, quite reasonable. Heat loss at the arc tip is considered negligible.

TABLE 2.10

COMPARISON BETWEEN THEORY AND EXPERIMENT FOR SOME METALLIC SURFACES

Metal Cathode	Measured γ	Measured V_c (volts)	Predicted V_c (volts)
Al	0.035	229	240
Fe	0.02	269	280
Cu	0.025	370	270

TABLE 2.11

WATER CATHODE FALL VOLTAGES FOR VARIOUS γ

γ	V_c (volts)
10^{-2}	331
3×10^{-3}	381
10^{-3}	490
5×10^{-4}	549
10^{-4}	664
5×10^{-5}	735
10^{-5}	831

BIBLIOGRAPHY - CHAPTER II

1. F. Boylett and L. MacLean, "The Propagation of Electric Discharges Across of the Surface of an Electrolyte," Proc. Roy. Soc., Vol. 324A, p. 1559, 1971.

2. M. Akazaki and L. Tsuneyasu, "Flashover on Electrolyte Surface at Impulse Voltage Application," Elect. Eng., Japan, Vol. 88 (11), p. 46-54, 1968.

3. H. Matsuo, Y. Yunoki, T. Oshige, and N. Mita, "Impulse Discharge on Contaminated Surface," ibid, Vol. 89, p. 26-34, 1969.

4. F. Obenaus, "Contamination Flashover and Creepage Path Length," Dtsch. Elektrotechnik, Vol. 12, 135-136 (1958).

5. G. Neumarker, "Contamination State and Creepage Path," Deutsche Akad., Berlin, Vol. 1, 352-359 (1959).

6. L. Alston and S. Zoledziowski, " Growth of Discharges on Polluted Insulation," Proc. IEE, Vol. 110, 1260-1266 (1963).

7. D. Jolly, "physical Processes in the Flashover of Insulators with Contaminated Surfaces," Ph.D. thesis, Dept. of E.E., MIT, 1971.

8. B. Hampton, "Flashover Mechanisms of Polluted Insulation," Proc. IEE, Vol. 111, 985-990 (1964).

9. P. Shkuropat, "Development of a Discharge on a Wet Insulator Surface with D.C." N-Tekh. Inf. Byull. Leningrad Polytechnic Inst., Vol. 1, 41-51 (1957).

10. A. Rumeli, "The Mechanism of Flashover of Polluted Insulation," Ph.D. thesis, University of Strathelyde, 1967.

11. S. Hesketh, "General Criterion for the Prediction of Pollution Flashover," Proc. IEE., Vol. 114, 531-532 (1967).

12. H. Nacke, "Lichtbagentestigkeit und Kriechstromfestigkeit von Isolierstoffen," Dissertation, University of Berlin - Charlottenburg, 1962.

13. R. Wilkins, "Flashover Voltage of High-Voltage Insulators with Uniform Surface-Pollution Films," Proc. IEE, 116 (3), pp. 457-465 (1969).

14. M.F. Hoyaux, "Arc Physics," Springer-Verlag, 1968, p. 299.

15. P. Claverie, "Predetermination of the Behaviour of Polluted Insulators," Paper 70 TP 609-PWR, presented at the IEEE Summer Power Meeting and EHV Conference, Los Angeles, Cal., July 12-17, 1970.

16. A. McElroy, "Flashover Mechanisms of Insulator with Contaminated Surfaces," Ph.D. thesis, Dept. of E.E., MIT, (1969).

17. W. Frischmann, "Fremdschichtuberschlag und Fusspunktwanderung," Deutsche Electrotech., Vol. II, pp. 290-295, 1957.

18. E. Nasser, "The Problem of Contamination Flashover on Insulators," ETZ-A, Vol. 83, 376-365 (1962).

19. F. Obenaus and H. Bohme, "Laboratory and System Tests on Contaminated Shed Insulators and the Model Concept of Creepage Flashover," Elektrie, Vol. 10, 417-422 (1966).

20. S. Hesketh, "The Propagation of Arcs over a Water Surface," Proc. of the 8th International Conference on Phenomena in Ionized Gases, Vienna, p. 255, 1967.

21. R. Wilkins and A. Al-Baghdadi, "Arc Propagation Along an Electrolyte Surface," Proc. IEE, Vol. 118, #12, 1971.

22. D. Jolly, "Contamination Flashover Theory and Insulator Design," Journal of Franklin Institute, Vol. 294, No. 6, December 1972, pp 483-500.

23. D. Jolly, A Preliminary Theoretical Interpretation of Wet Containment Testing of Suspension Insulators," EPSEL Report No. 24, July 21, 1970.

24. D. Jolly, T.C. Cheng, and D. Otten, "Dynamic Theory of Discharge Growth over Contaminated Insulator Surfaces," Paper C 74 068-3, presented at the IEEE Winter Power Meeting, N.Y., January 1974.

25. E. Nasser, "Fundamentals of Gaseous Ionization and Plasma Electronics," Wiley-Interscience, J. Wiley and Sons, Inc., N.Y., 1971.

26. G. Francis, "The Glow Discharge at Low Pressure," Encyclopedia of Physics, Edited by S. Flugge, Vol. XXII, Gas Discharges II, 1957.

27. R. Wilkins, "Characteristics of Low-Current Arcs Relevant to Pollution Flashover," 2nd International Conference on Gas Discharges, 1972.

28. J. Cobine, "Gaseous Conductors," Dover Publications Inc., 1958.

29. E.J. Los, "Time Constants of Low Current Arcs Near Flat Surfaces," S.M. Thesis, School of Engineering, MIT, 1974.

30. D.M. Otten, "Measurement of Arc Growth Velocity Along an Electrolyte Surface," S.B. Thesis, School of Engineering, MIT, 1973.

31. O. Mayr, "Beitrage zur Theorie des statischen und des dynamischen Lishtbogens," Archiv fur Elektrotechnik, 37 Band, Heft 12, p. 588-608 (1943).

32. E.J. Los, private communication.

33. E.J. Los, private communication.

34. F. Obenaus and H. Bohme, "Laboratory and System Tests on Contaminated Shed Insulators and the Model Concept of Creepage Flashover," Elektrie, Vol. 10, 417-422 (1966).

35. K.H. Yoon and H.E. Spindle, "A Study of the Dynamic Response of Arcs in Various Gases," Trans. Amer. Inst. Elect. Engrs. 77, Part III, p. 1634, 1959.

36. H. Edels and E. Graffmann, "Time Constant Measurements of High Pressure Arc Columns, Z. Physik, 228, 396-415, 1969.

37. T.H. Lee, "Plasma Physics and Interruption of an Electric Circuit," Proc. of the IEEE, 57, No. 3, p. 307, 1969.

38. E.J. Los, "Time Constants of Low Current Arcs Near Flat Surfaces," S.M. Thesis, School of Engineering, MIT, 1974.

39. G. Schmitz, "Zur Theorie der Wandstabilisierten Bogensaule," Z. Naturforsch, 5a, 571, (1950).

40. H.W. Emmons and R.I. Land, "Poiseville Plasma Experiments," Physics of Fluids, 5, pp. 1489-1500, (1962).

41. R. Phillips, "Time Constants for Non-stationary Arcs," Z. Physik, 211, pp. 113-131, (1968).

42. A.M. Cassie, Conf. Int. des Grands Res. Elect. and Haute Tension, 102, 1 (1939).

43. G. Frind, "Uber das Ablingen Vol Lichtbogen I," Zeitschrift fur angewandte Physik, 12, pp. 231-236, (1960).

44. H. Edels and F.H. Fenlon, "Theory of a Filled-Tube Thermal Arc Column," Brit. J. Apll. Phys. 16, p. 219 (1964).

45. H. Maecker, "Uber die Charakteristiken Zylindrischer Bogen," Zeitschrift fur Physik, 157, pp 1-29, (1959).

46. P. Moon and D. Spencer, "Field Theory for Engineers," D. Van Nostrand Co., Princeton, 1961.

47. K.T. Compton and P.M. Morse, Phys. Rev. 30, p. 305, (1927).

48. A.V. Hippel, Z. Physik, 76, p. 1, (1932).

49. P.M. Morse, Phys. Rev. 31, p. 1003, (1928).

50. W. Rogowski, Arch. Elektrotechn. 26, p. 643, Z. Physik, (1932), Z. Physik, 114, p. 1 (1939).

51. Weizel, Rompe and Schon, Z. Physik, 112, p. 339, (1939), Z. Physik, 113, p. 87, p. 730 (1939).

52. K.N. Ul'yanov, translated from Teplofizika Vysokikh Temperatur, Vol. 10, No. 5, pp. 931-938, (1972).

53. A.V. Engel and M. Steenbeck, Elektrische Gasentladungen, Berlin, Springer (1932).

54. J. Meek and J. Craggs, "Electrical Breakdown of Gases," Clarendon Press, Oxford, 1953.

55. J. Slepian, "Theory of Current Transference at the Cathode of an Arc," Phys. Rev., 27, pp. 407-412 (1926).

56. L.B. Loeb, "Electrical Corona, Their Basic Physical Mechanisms," University of California Press, Berkeley, 1965.

CHAPTER III

TWO DIMENSIONAL SIMULATION OF A CONTAMINATED INSULATOR - THE FLAT-PLATE

3.1 Introduction

This chapter describes an effort to simulate a contaminated insulator on a two-dimensional basis. The simulation is carried out both experimentally and theoretically. The previously described linear model experimentally simulates the rod insulator best, while the flat-plate, best resembles a suspension insulator, although both are decidedly simplified versions of their prototypes. Theoretically, it is far easier to derive a mathematical model for the linear case, since all the variables must necessarily depend, at most, on only one spatial coordinate. The flat-plate is geometrically more complex. It is for this reason that the theories presented in this chapter appear less "sophisticated" than the previous chapter. Here, we are not overly concerned with propagation mechanisms and times (see Chapter IV for a closer look at times to flashover). Instead, the questions being asked are more basic: what is the effect of the contaminants, and hence surface conductivities, on flashover voltages? For a particular conductance, what is the threshold voltage for flashover? Our aim is thus clear: for a particular level of contamination on a flat-plate, we wish to determine its conductance and hence its surface conductivity. For that surface conductivity a threshold voltage for flashover is determined. In the first half of this chapter, a series of tests performed under different contamination levels will be described. The surface conductivity for each case as well as the threshold voltage will be determined. In the second half of the chapter, a theoretical derivation will be proposed to explain the experimental findings.

3.2 Description of Experimental Apparatus

The flat-plate was first designed and experimented on by McElroy[1] and later extensively tested by Jolly.[2] As shown in Figure 3.1, it is a twelve inch square, 1/4 inch thick plate of pyrex glass. Six holes have been drilled through it so that two circular, concentric brass electrodes can be screwed onto it on both sides. The outer electrode is one inch wide and the radius of its inner edge five inches. The inner electrode has been recently modified, as shown in Figure 3.2, to achieve better contact with the surface.

Testing is performed in a fog chamber described in Ref. 1. A high voltage lead enters the chamber through its roof and is shielded inside a conduit on its way from a General Electric testing transformer (Type#195C4010), capable of supply 50 kV (A.C.), with a short circuit current of about 10 amps. The voltage is applied to the test specimen by the use of a high-voltage vacuum switch (ITT # N400), immersed in a tank of transformer oil for insulating purposes. The discharge current is monitored by a visicorder as well as a Tektronix type 554 Storage Scope. During the fogging period, it is also necessary to continuously monitor the resistance (or conductance) of the flat-plate. This is achieved by

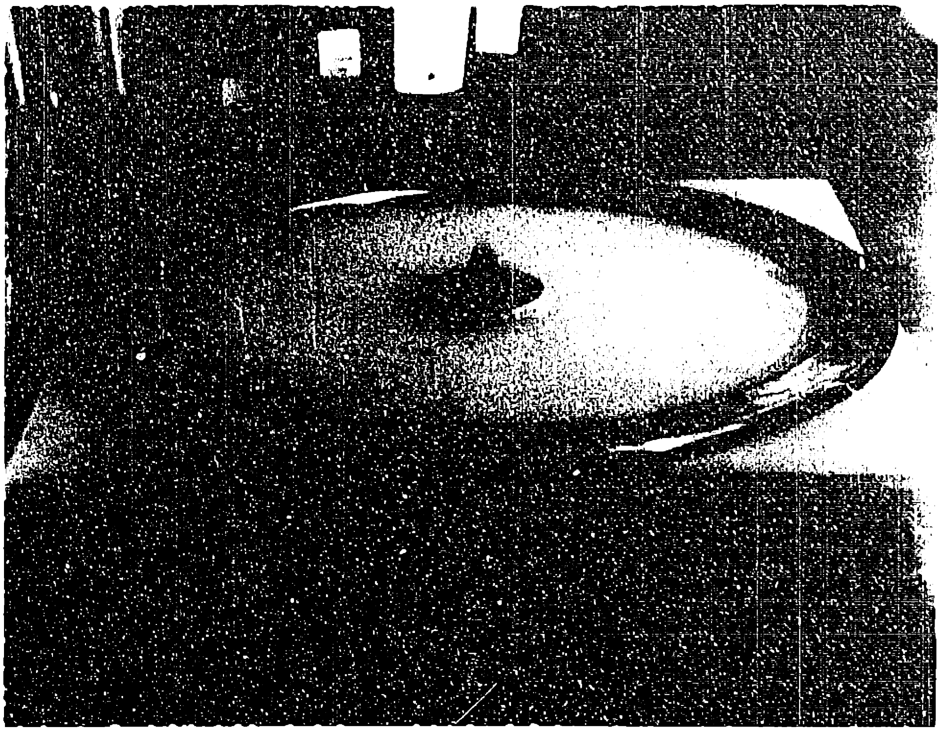

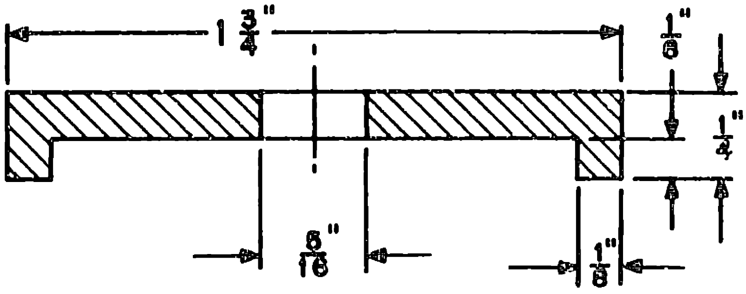

(a) Side View

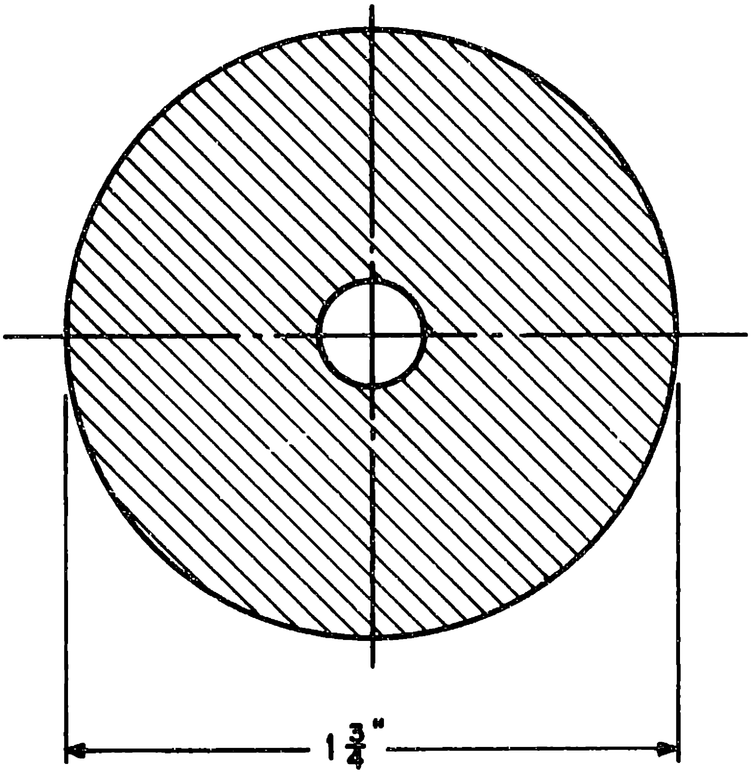

(b) Top View

Figure 3.2 Inner Electrode

applying 100 volts a.c. across the surface and balancing its resistance against a Precision Decade Box via a Wheatstone bridge. The device measures resistances accurately to within 1%.

3.3 Experimental Testing Procedure

To complete a flat-plate text, three steps must be executed in sequence as follows:

(a) preparation of the plate

(b) testing in the fog chamber

and (c) washing of the plate.

Each step will be described below.

Step (a) involves the coating of the plate. In artificial testing, a contaminant is usually substituted by a dissolved mixture of an inert binder - bentonite, for our case - and salt (NaCl). The inert binder is supposedly non-conducting (for a discussion, see Ref. 2) and the quantity of salt used represents the level of contamination. The mixture, usually dissolved in tap or distilled water, is known as a slurry and is thoroughly mixed in an electric blender. The compositions of various slurries used are summarized in Table 3.1.

Before coating, the plate is first washed with detergent and wiped dry with Kimwipes. It is then mounted on the rotor, as shown in Figure 3.3. The motor is then started and adjusted to an appropriate speed of about 5 rev./min. The slurry is poured into a squeezable bottle and sprayed, in a

TABLE 3.1

COMPOSITION OF SLURRY

Constituent	Quantity
Tap or distilled water	1 liter
Bentonite	40 gm → 50 gm
Salt	40 gm → 0.2 gm

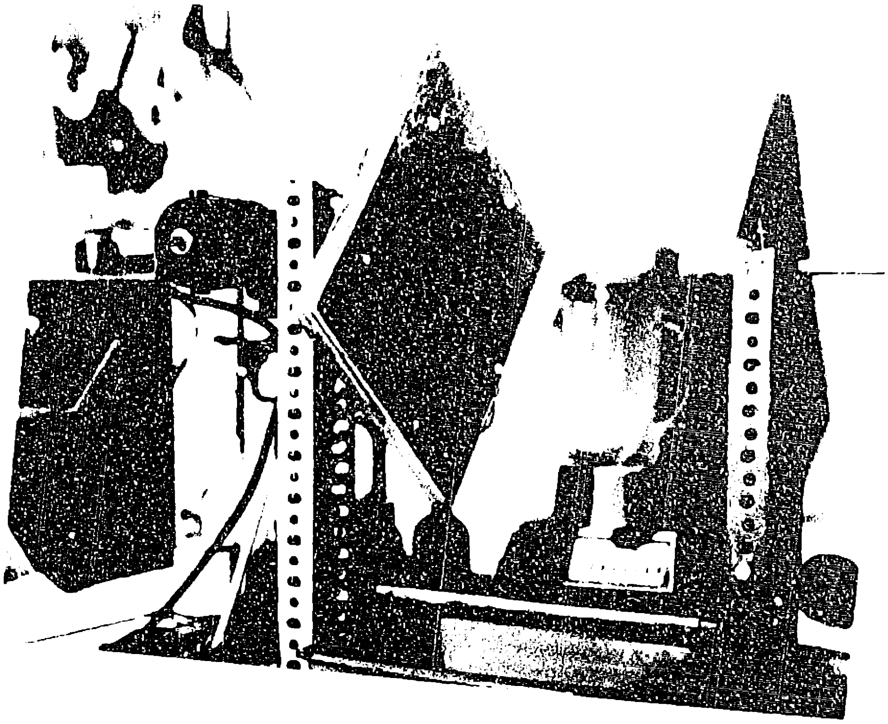

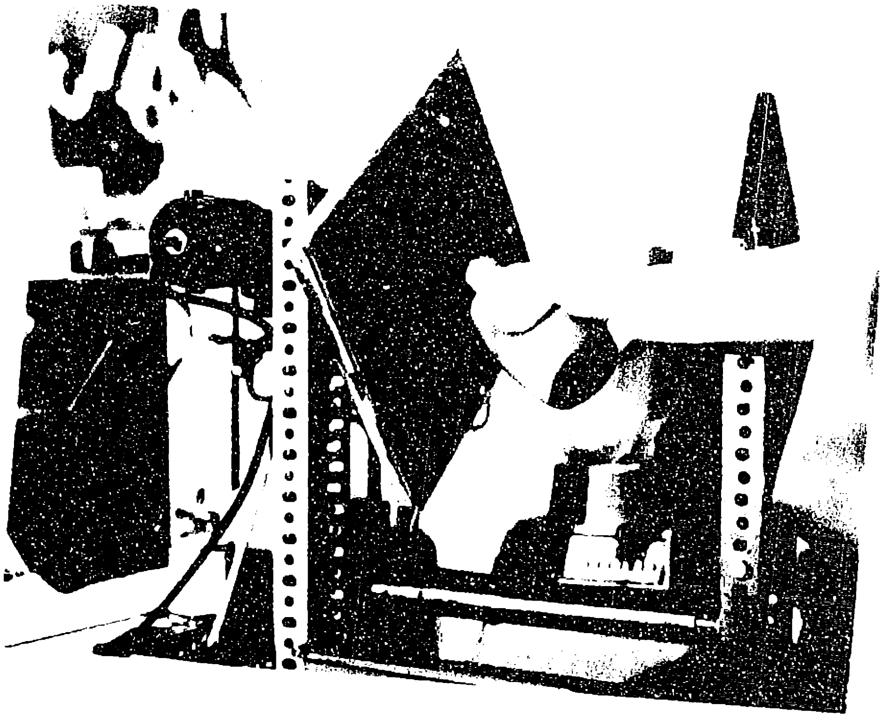

jet form, onto the plate as the latter rotates by; as shown in Figure 3.4. Enough slurry is applied so that the liquid readily rolls off from the surface to the collecting tray placed below. The coating process is stopped when it is clear that the surface has been saturated with slurry and no more will stick. At this point, six heat lamps which are placed at a distance of about 3 ft. away are switched on to dry the plate as it continues to rotate, as shown in Figure 3.5. Ten minutes later, a small fan is used to cool off the surface. This procedure is found to be necessary after plates have cracked because of over-heating by the heat lamps. The process is continued until the surface is completely dry. This plate is now ready for testing. This coating method[3] is different from the one used by Jolly. It is found that this method yields even surfaces.

Step (b) is the actual testing. The electrodes are bolted onto the plate which is then placed on top of a leveled support inside the fog chamber, as shown in Figure 3.6. Leads are attached to the center disc as well as to the outer ring to monitor the resistance. One lead goes to the Wheatstone bridge, while the other is grounded through the vacuum switch. The door to the chamber is then closed.

Tap/distilled water fog is turned on. The resistance is continuously monitored and a typical record is shown in Figure 3.7. When the desired resistance level has been reached, the fog is shut off. The chamber door is opened,

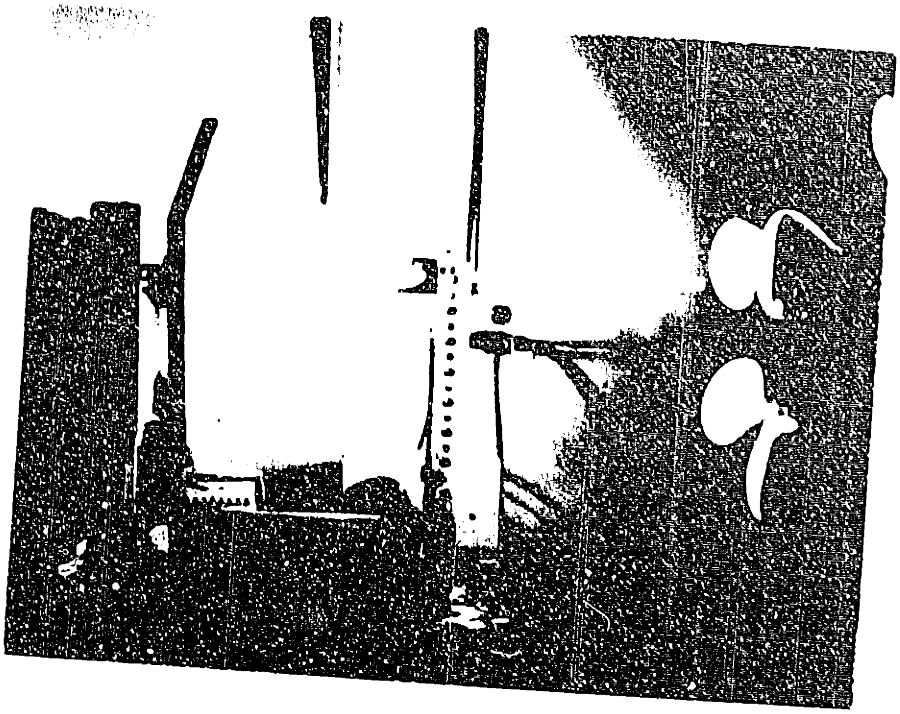

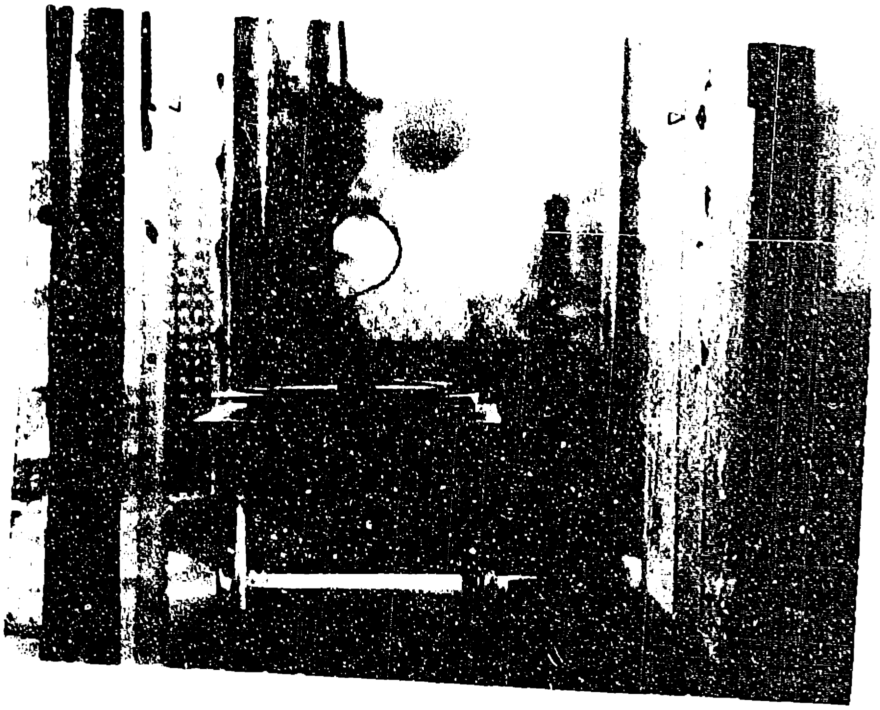

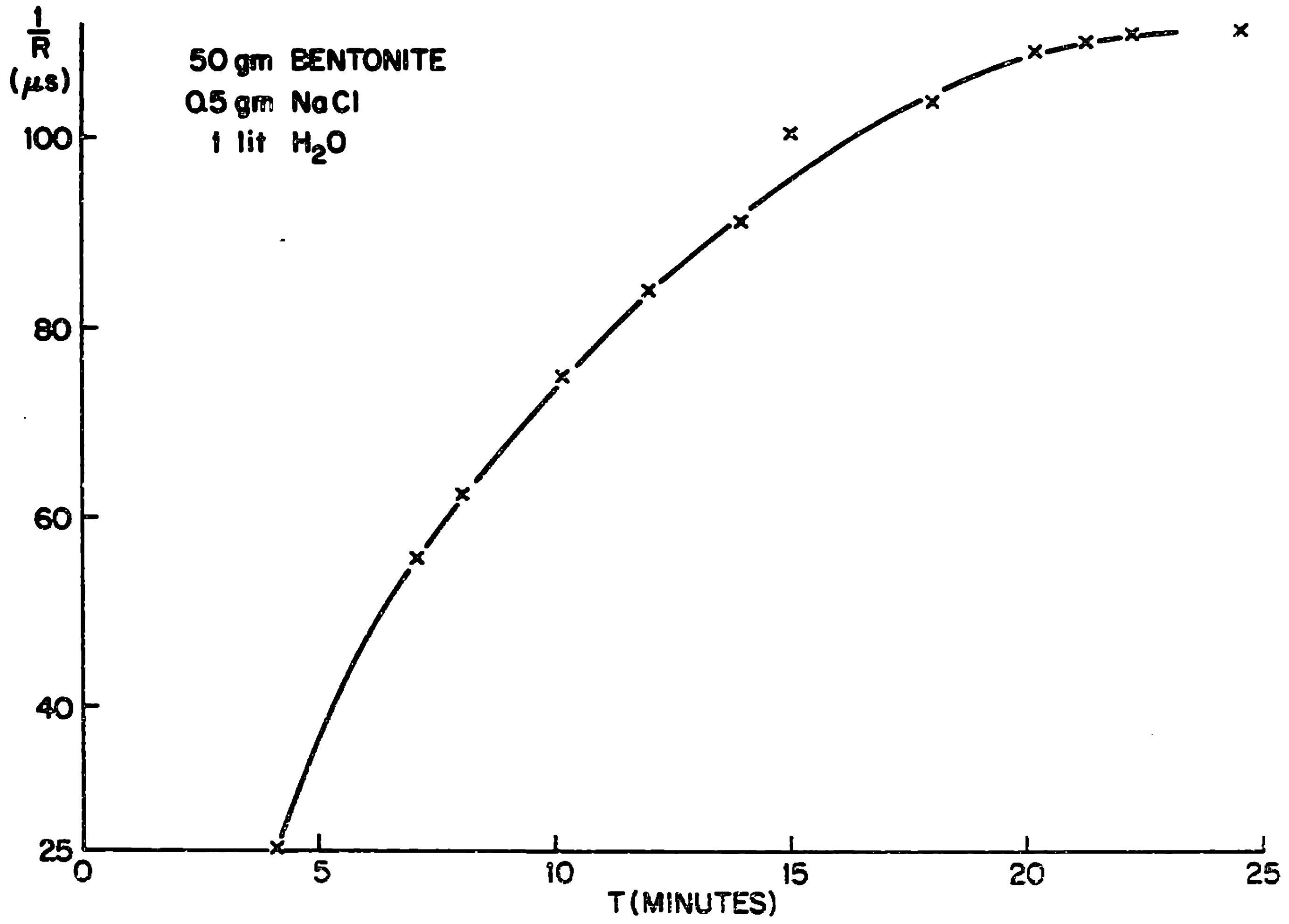

Figure 3.7 Conductance of Flat-Plate as Function of Fogging Time

the lead attached to the center disc is replaced by the high voltage terminal and the door closed again. The visicorder and the scope are both readied, while the vacuum switch is turned off. The power supply is then raised to the desired level and the voltage applied by activating the switch. The test results either in a flashover or a withstand. After all activity has ceased, the visicorder is stopped and the voltage turned off, ending the test. The maximum and the minimum radii of the dry zone are then immediately measured and recorded. A standard test sheet is included in the following page to illustrate the data taking process. Figures 3.9 and 3.10 illustrate a sample of visicorder record and a scope picture record.

Step (c) is carried out after the test has been completed. Its purpose is to determine how much salt and bentonite were deposited on the surface of the plate during coating and possibly during fogging (for tap water fog). The deposits are first thoroughly washed from the surface with a brush and distilled water, into a developing tray. The solution is then emptied into a beaker, care being taken that all the remnants are included. The liquid portion of the mixture is then completely evaporated. The beaker with its solid contents is carefully weighed. This weight, with the empty beaker's weight subtracted, will be the total weight of both the bentonite and the salt. This solid mixture is then dissolved in 500 ml. of distilled water. The conductivity of

FLAT PLATE TEST FORM

Test number 1

Plate number 8

Date 3 / 5 /1974

Test voltage: 5.0 kV

A.C. ☑

D.C. positive ☐

D.C. negative ☐

Test result:

Flashover ☑

Withstand ☐

Coating data:

Bentonite 50 gm

NaCl 0.3 gm

Water 1000 ml

Coloring Blue

Dry zone radii:

Maximum 4.5 cm

Minimum 2.5 cm

Area 22.5 cm²

Fog (tap water unless otherwise indicated) distilled % NaCl

Duration of fog 35 minutes

Resistance 8.0 ohms

Washing data:

Amount of water (one liter unless indicated) 500 ml

Conductivity of test water (distilled) S

total NaCl = 0.0265 gm

Conductivity of wash water 1/9100 S/cm

Resultant conductivity ______ S

Temperature of wash water 24° C

100 volt A.C. resistance 8.0 K

Resistivity ______ K

Discharge resistance
(1st half cycle) 7.0 K

Resistivity ______ K

(2nd half cycle) ______ K

Resistivity ______ K

Discharge Current
(1st half cycle) ______ mA
(2nd half cycle) 710 mA

Scope Current 720 mA

(last half cycle) ______ mA

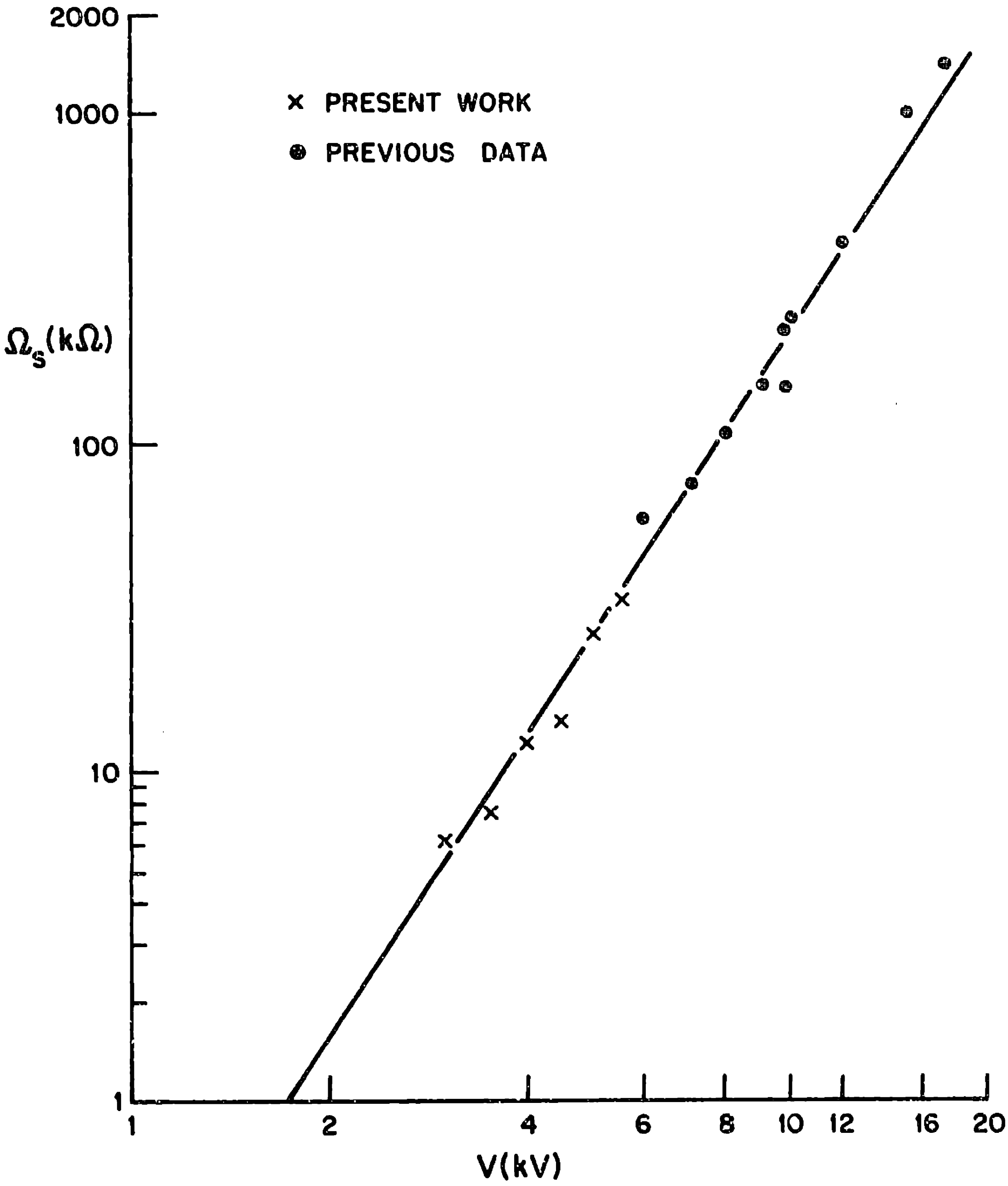

Figure 3.8 Critical Resistivity vs Voltage

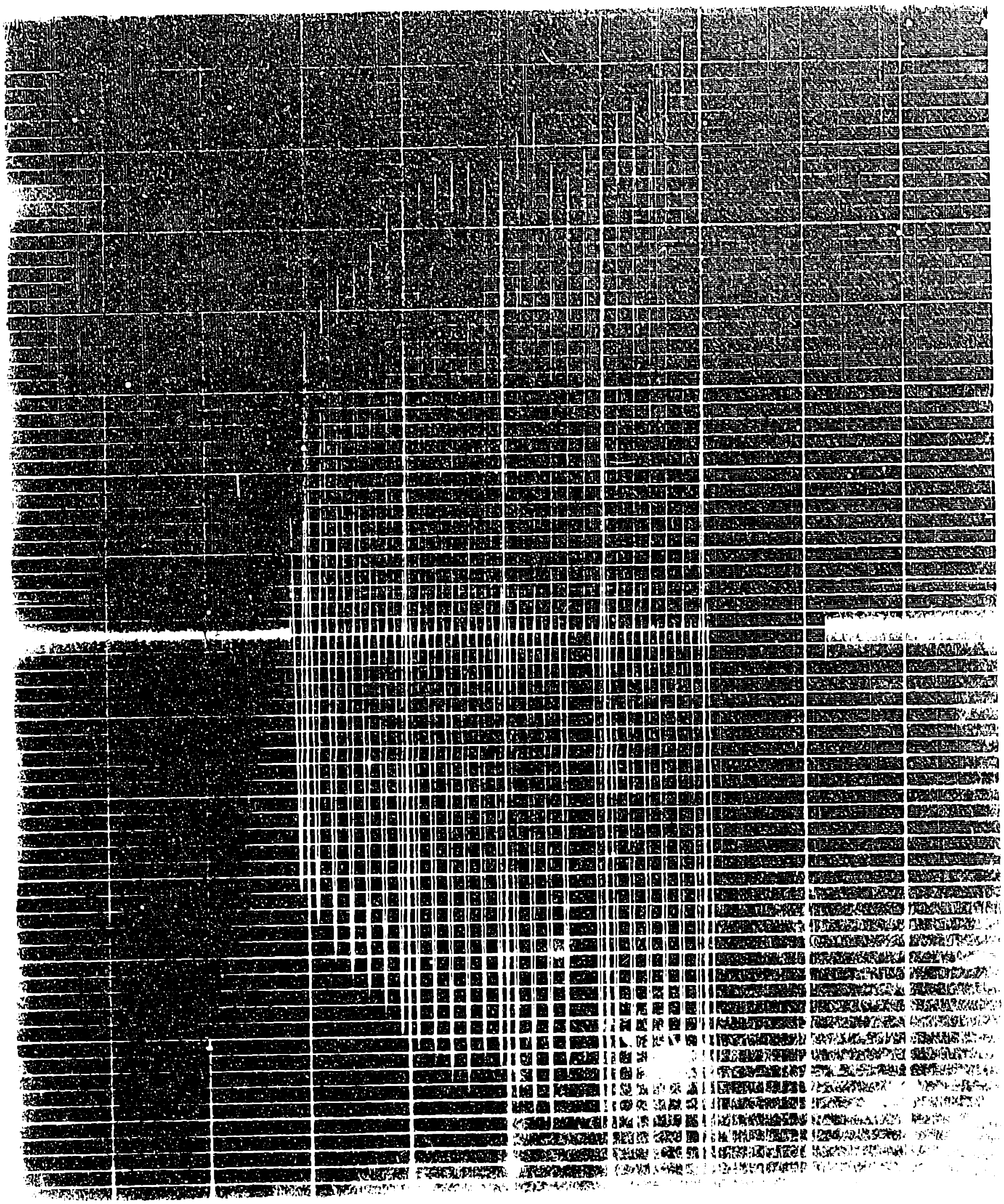

Figure 3.9 A sample Visicorder Record (vertical scale: 0.1 Amp./div.)

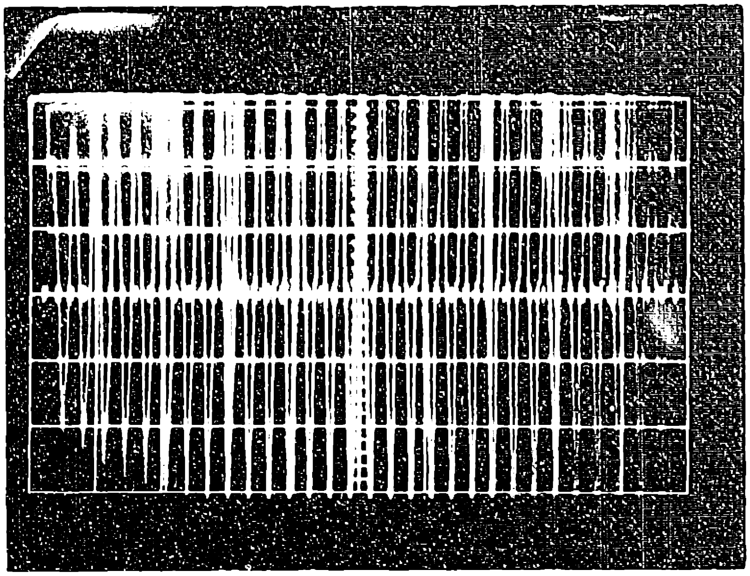

this solution is then measured using a conductance meter (Beckman). From the conductivity tables[4], it is possible to determine the amount of salt (assuming mainly NaCl) in the solution and hence originally on the plate. The amount of bentonite is then deduced by subtracting from the total weight of the mixture the known amount of salt. The contamination can thus be classified as light, medium or heavy according to the washing data. Out of a set of identically coated plates, usually only one plate was selected to be washed and its composition of deposits determined.

3.4 Discussion of Experimental Results

Altogether about 60 flat-plate tests were performed and the results are summarized in Table 3.2. Some explanations are needed to explain the results here. Under the heading, Fog (min.), is recorded the time interval during which either tap water or distilled water (D) fog is being applied. The resistance is being continuously monitored, as described above, until it reaches a stable value at which point the fog is turned off. The resistance can then be converted into resistivities (KΩ per square) by simply noting the following relation:

$$\Omega_{LV} = \frac{2\pi R}{\ln(R_o/R_i)} = 3.62\ R_s \qquad (3.1)$$

where R_s = measured resistance

R_o = inner radius of outer electrode

R_i = outer radius of inner electrode

TABLE 3.2

FLAT-PLATE TEST DATA

Test #	Voltage (kV)	Bentonite (gm)	NaCl (gm)	Fog (min)	Ω_{HV} (kΩ/sq)	Result	Dried Area (cm^2)
1	3.0	60	40	14	5.23	F	-
2	4.0	"	"	20	5.66	F	-
3	3.0	"	"	22	6.24	F	-
4	2.5	"	"	14	6.63	W	-
5	5.0	60	5	17	9.79	F	-
6	4.0	"	"	18	7.25	F	-
7	3.5	"	"	20	7.41	F	-
8	3.5	"	"	18	8.19	W	-
9	4.0	"	"	16	12.10	F	-
10	4.5	50	2	23	13.65	F	69
11	4.5	"	"	25	13.26	F	86
12	4.5	"	"	25	13.65	F	67
13	4.0	"	"	15	13.65	W	47
14	4.5	"	"	11	9.75	W	69
15	4.5	"	"	23	14.43	F	67
16	4.5	"	"	14	17.55	F	93
17	4.5	"	"	25	15.60	F	69
18	4.0	"	"	18	10.53	F	80
19	3.5	"	"	17	6.63	F	54
20	4.0	"	"	28	13.65	F	54
21	3.5	"	"	27	13.65	W	47
22	5.0	50	1	29	18.33	F	42
23	4.5	"	"	22	23.40	W	-
24	5.0	"	"	27	16.38	F	54
25	5.0	"	"	25	18.33	F	54
26	5.0	"	2	25	17.16	F	54
27	5.0	"	"	18	17.16	F	54

Test #	Voltage (kV)	Bentonite (gm)	NaCl (gm)	Fog (min)	Ω_{HV} (kΩ/sq)	Result	Dried Area (cm^2)
28	7.0	50	0.5	25	25.55	F	31
29	6.0	"	"	30	30.66	F	27
30	5.5	"	"	27	23.73	F	45
31	5.0	"	"	22	21.54	W	86
32	5.0	"	"	28	21.54	F	102
33	5.0	"	"	24	23.36	W	78
34	5.5	"	"	28	21.90	F	47
35	5.5	"	"	21	21.90	F	95
36	5.5	"	"	21	23.73	F	80
37	5.0	"	"	19	25.55	F	74
38	5.0	"	"	22	23.36	W	78
39	5.0	"	"	24	21.17	F	80
40	6.0	50	0.3	24	25.55	F	84
41	5.5	"	"	34	32.85	F	12
42	5.0	"	"	27	30.66	W	62
43	5.0	"	"	27	26.28	F	69
44	5.0	"	"	23	23.36	W	70
45	5.5	"	"	23	23.73	F	60
46	5.5	"	"	25	23.73	F	51
47	5.5	"	"	25	28.11	F	77
48	5.0	"	"	37	36.50	W	69
49	5.5	"	"	22	25.55	F	45
50	5.0	"	"	26	28.47	W	69
51	5.0	"	"	35	23.73	F	84
52	5.5	"	"	23	29.93	F	57
53	5.0	"	"	21	29.20	W	62
54	5.5	"	"	21	31.39	F	67
55	5.5	"	"	25	31.03	F	67
56	5.0	"	"	22	25.55	W	62
57	5.5	"	"	27	35.15	F	92
58	5.5	"	"	21	24.46	F	63
59	5.0	"	"	28	25.55	W	78

Ω_{LV} = surface resistivity.

Ω_{LV} is thus the surface resistivity determined through the low voltage method of using a Wheatstone bridge. Ω_{HV} can be determined by dividing the applied RMS voltage by the recorded second-half cycle current (RMS), the first-half cycle being usually less reliable. The result of a test is either a flashover (F) or a withstand (W) and is recorded as such. The bentonite level for a few representative plates are determined by the washing method already described. The dried area is calculated by measuring, after each test, the largest and the smallest radii of the dry zone respectively and then approximating the area as an ellipse.

All the test results were listed in Table 3.2. It was found that the amount of salt used in the slurry has an important effect on the flashover voltage. This is in agreement with other published data.[1,2] The series of tests conducted here serve two purposes. Since the coating method used in this series is different from that used by McElroy and Jolly, the results of the experiments would indicate whether the method of coating was important or not. Secondly, a different testing transformer with a higher short-circuit current capability (about 10 amps) was used in these experiments, so that data-taking can be extended into the low surface-resistivity regime.

In order to render the data meaningful, the threshold flashover voltage for each surface resistivity must be determined. This can be accomplished by locating, for each applied voltage, the highest surface resistivity at which a flashover occurred. These points are plotted in Figure 3.8 where previous data have also been included. It can be seen that all the experimental points can be fitted quite well by a straight line in a log v-log Ω_s plane. This finding is significant because it seems to indicate that the same physical flashover mechanisms are operating for threshold cases. The parameter, Ω_s, can thus be used with some degree of confidence for predictions of threshold voltages.

The following section will deal with the theoretical aspects of deriving such a relation between Ω_s and v.

3.5 Theoretical Developments

3.5.1 Past Theories

The flat-plate was first designed and tested by McElroy. An idealized model of a surface discharge in series with a wet contaminant layer is shown in Figure 3.11. The discharge characteristic was represented by the expression

$$V_a = AI^{-n} (R-R_i) \tag{3.2}$$

where R is the radial distance from the tip of the arc and R_i, the radius of the inner electrode and for the conducting contaminant layer

$$V_R = B\Omega I \tag{3.3}$$

where Ω is the surface resistivity, $B = C(R_o-R)^m$ with both

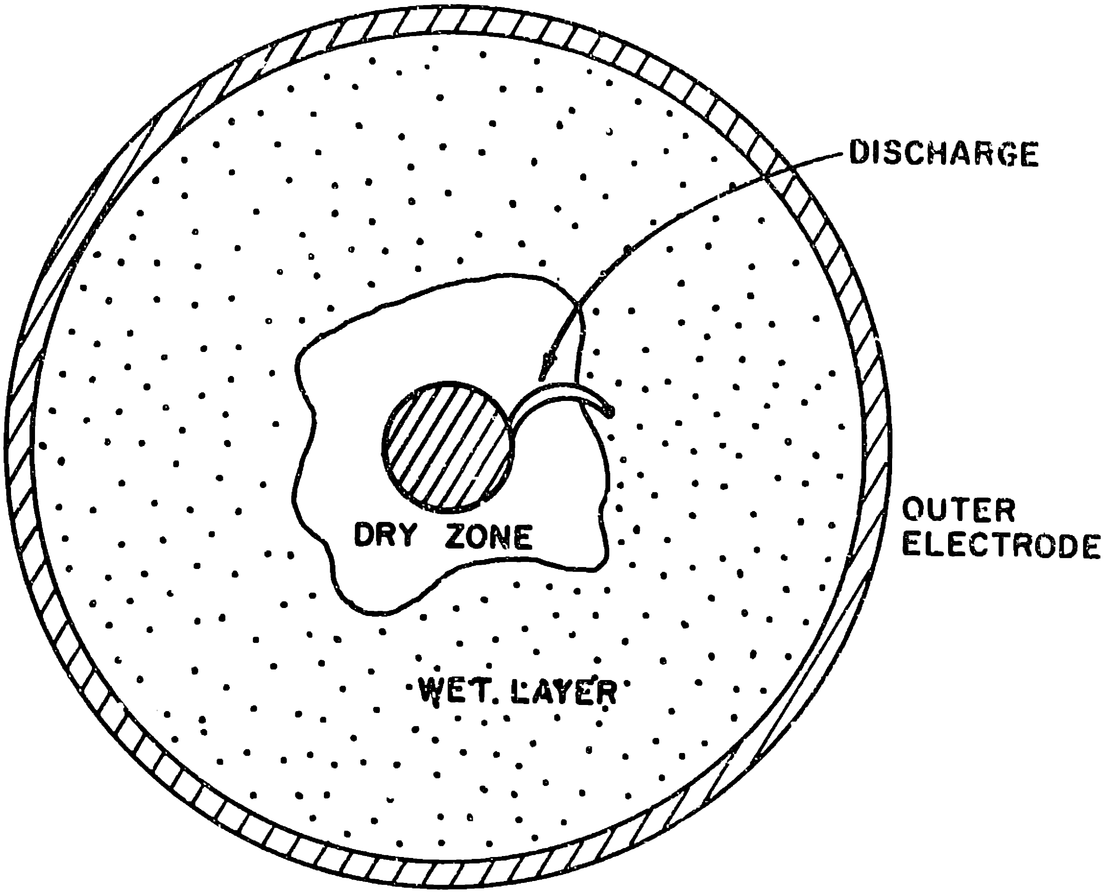

Figure 3.11 Sketch of a Flat-Plate Arc Discharge

C and m as constants and R_o, the radius of the outer electrode. The form of B assumes that it is independent of r_a, the arc root radius as well as I, the current. These simplifications were made for the sake of mathematical simplicity.

Kirchoff's voltage equation then requires,

$$V = V_a + V_R \tag{3.4}$$

Taking $\frac{\partial V}{\partial I} = 0$, will yield V_{min} as

$$V_{min} = (n+1) \left(\frac{B\Omega}{n}\right)^{\frac{n}{n+1}} [A(r-R_i)]^{\frac{1}{n+1}} \tag{3.5}$$

for a given r.

V_{crit} can then be found by setting $\frac{\partial V_{min}}{\partial r} = 0$. The constants C and m were determined experimentally and found to be 1.3×10^{-3} and 2.7 rsspectively. The value of m (= 2.7) was highly questionable and Jolly proposed m = 0 for a flat-plate, essentially eliminating the dependence of B on any physical parameter. Going through the same calculations as before and setting m = 0, he arrived at

$$X_{crit} = R_o \tag{3.6}$$

and

$$\Omega_{crit} = \frac{n}{C(AR_o)^{1/n}} \left[\frac{V}{n+1}\right]^{\frac{n+1}{n}} \tag{3.7}$$

By fitting (3.7) to experimental data, he found A to be 0.189 and n = 0.44. The value of A could be in error by 50% owing to heating of the conducting layer and the subsequent change in resistance. The value of n is low compared with other findings such as McElroy's 0.8, Wilkins' 0.76 and Claverie's 0.5. However, eq. (3.2) is never meant to be an exact representation of arc voltage and it is possible that A and n are no longer constants as the current varies over a wide range.

3.5.2 Present Approaches

Before going into deriving V_{crit}, a word or two must be said about the surface resistivity Ω. Experimentally, it is measured by two methods, the low-voltage Wheatstone bridge balancing and from the high-voltage current record, as already explained in section 3.4. Theoretically, these two values should be very close. During exploratory tests, they were found to be quite different (by as much as a factor of 2). The error was later attributed to a faulty measuring circuit, unreliable calibration of the visicorder and bad contacts between the electrodes and the wet contaminants. Once rectified, the values of Ω_{HV} and Ω_{LV} agreed to within 20%, and data taking proceeded smoothly. The values of Ω_{HV} were used in finding the $V_{crit} - \Omega$ relationship as shown in Figure 3.8, because they were thought to be generally more reliable. A third independent method has also been used to check the reasonableness of the measured values and is presented below: Consider the actual physical situation. At $t = 0$, fog is turned on and the fog droplets start drifting into the test chamber and begin depositing on the surface of a dry and coated flat-plate. As the amount of moisture increases, the salt particles embedded in the thin coating gradually start to dissolve. The resistance monitored through the bridge falls off rapidly. As time increases, more and more salt is dissolved until at a point, all the salt particles are just dissolved making the resultant solution a saturated one. This is the saturation point, and from now on, the resistance of the plate will be more or less constant. It is at this point that we perform the tests. Assuming an idealized thin coating and uniform deposition of moisture on the plate, the resistance of the flat-plate can thus be calculated. The amount of salt actually on a particular plate can be determined by the washing method, already described and will be denoted as x gm/cm^2.

The solubility of salt (NaCl) at 25°C is 357 gm/1000 c.c. The height of the moisture layer h, can thus be derived as

$$h = \frac{x}{357} 10^3 \text{ cm} \tag{3.8}$$

From Ohm's law, we have,

$$J = \frac{1}{\rho_r} E \tag{3.9}$$

and

$$I = \frac{1}{\rho_r} \int_o^{2\pi} \left(\frac{V}{R\ln(R_o/R_i)}\right) hRd\theta \tag{3.10}$$

where

$$\rho_r = \frac{1}{\sigma} = \text{resistivity in Ohm-cm}$$

Integrating (3.10) yields,

$$R_s = \frac{V}{I} = \frac{\rho_r \ln R_o/R_i}{2\pi h} \tag{3.11}$$

where R_s is the resistance measured on the bridge and $\Omega_s \equiv \rho_r/h$.

ρ_r is tabulated in the International Critical Tables[5] for various concentrations. At saturation, the molar concentration of NaCl is about 6 moles. From the tables, the highest concentration at which ρ_r is know is 5M. and hence this number is used, $\rho_r = 4.48\ \Omega$ cm at 25°C and 5M concentration.

Therefore,

$$R = \frac{4.48 \ln R_o/R_i}{2\pi h} \quad \Omega_s \tag{3.12}$$

For a typical test,

$$x = 0.036 \times 10^{-3} \text{ gm/cm}^2$$

and hence

$$h = \frac{0.036 \times 10^{-3}}{357} \times 10^3 \text{ cm}$$

$$\cong 10^{-4} \text{ cm}$$

$$R_o/R_i \simeq 5.0, \quad \ln R_o/R_i \simeq 1.6$$

so that

$$R_s \simeq 11.4 \text{ K}\Omega$$

or

$$\Omega_s \simeq 44.5 \text{ K}\Omega/\text{square}$$

These values are in reasonable agreement with the measured values of about 10 KΩ and 40 Ω/square respectively. Now that we have established reasonable confidence in the measured values of Ω, we can proceed to determine its relation with V theoretically.

The approach taken here is different from McElroy and Jolly in two important respects. They assumed that the resistance between the discharge root and the outer electrode was independent of the root position. Jolly further assumed that the resistance BΩ was also independent of current, thus setting $m = 0$. Both of these simplifying assumptions will be discarded here and a more exact approach will be attempted. The fact that a discharge root on a moist film maintains a constant current density[6,7] will be utilized here. The series resistance R will be calculated as a function of current, arc root radius, distance from outer electrode and surface resistivity. The only approximations are that the calculations are two-dimensional and the presence of the center electrode is neglected (i.e. $R_i \rightarrow 0$).

Consider eq. (3.4)

$$V = V_a + V_R \tag{3.4}$$

Letting $x = R - R_i$, we can write

$$V = A\, I^{-n}\, x + I\, R_s(x, R_o, R_a, I) \tag{3.13}$$

But

$$J = I_o/\pi R_a^2 = \text{constant} \tag{3.14}$$

so that R_a can be eliminated from (3.13) via (3.14). Consider the physical model as sketched in Figure 3.12. As the arc root moves towards the outer electrode, the flow pattern of the current will change and hence the series resistance R. It is the purpose here to solve for R_s.

The problem is essentially a surface conductance problem and can be solved by analogy. For a static case, and with no free charge, we have,

$$\nabla \cdot \varepsilon E = 0 \tag{3.15}$$

Since E is curl-free, it can be expressed as

$$E = -\nabla\phi \tag{3.16}$$

so that

$$\nabla \cdot \varepsilon \nabla\phi = 0 \tag{3.17}$$

which is Laplace's equation for constant ε. For a static conduction problem, the conservation of charge equation is used instead of (3.15):

$$\nabla \cdot J = 0 \tag{3.18}$$

From Ohm's law,

$$J = \sigma E \tag{3.19}$$

so that,

$$\nabla \cdot \sigma E = 0 \tag{3.20}$$

But, the field is still curl-free, and we arrive at an equation similar to (3.17) except ε is replaced by σ:

$$\nabla \cdot \sigma \nabla\phi = 0 \tag{3.21}$$

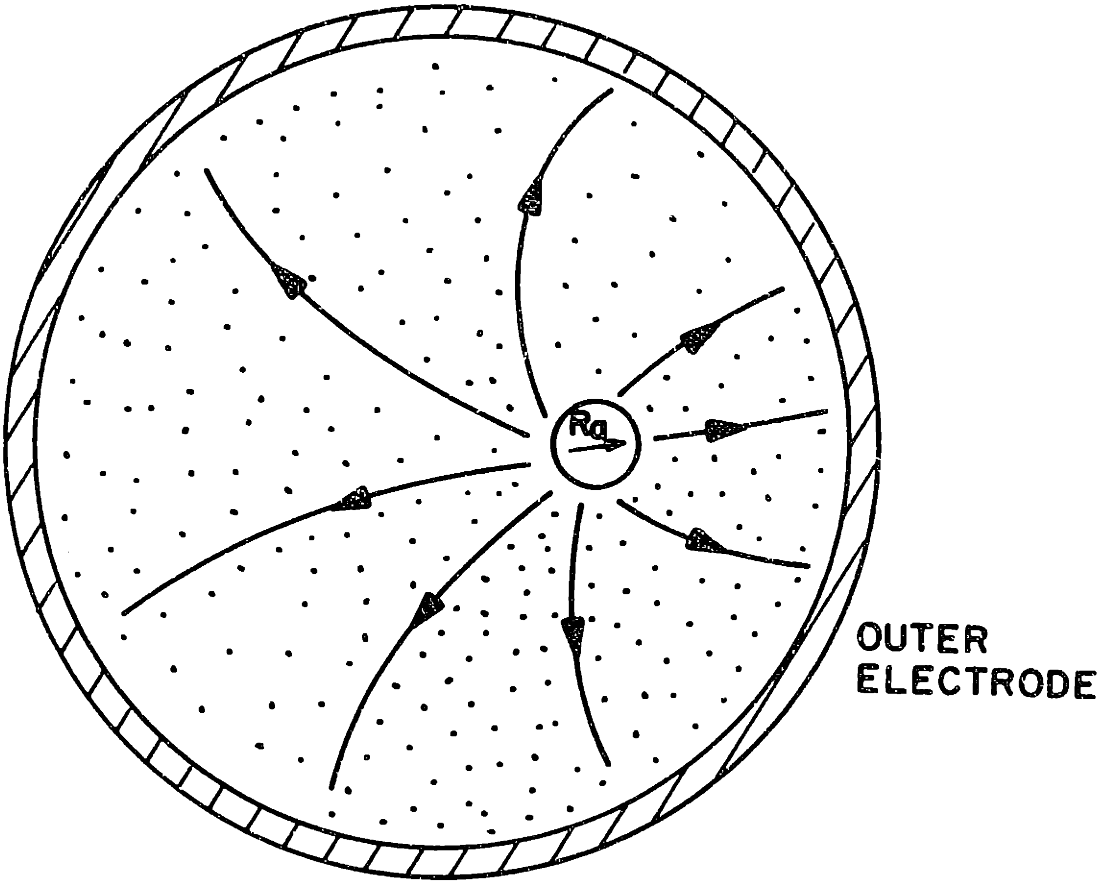

Figure 3.12 Sketch of Current Flow from Arc Root to Outer Electrode

Hence all the field problem solutions involving ε, e.g. calculation of capacitances for different electrode configurations, can be readily transformed into conductance calculations when ε is replaced by σ. Weber[8] calculated the capacitance between the cylindrical conductors, one inside the other. Denoting the radius of the inner cylinder as R_a, the outer one as R_o and their distance of separation between the two centers, x, the capacitance/unit length C can be shown to be

$$C = \frac{2\pi\varepsilon}{\cosh^{-1} \frac{x}{2R_a} [(\frac{R_o}{x})^2 - (\frac{R_a}{x})^2 -1]-\cosh^{-1} \frac{x}{2R_o}[(\frac{R_o}{x})^2 - (\frac{R_a}{x})^2 +1]} \tag{3.22}$$

Equation (3.22) can be readily transformed into conductance/unit length by substituting σ for ε. The surface resistance is thus readily arrived at

$$R_s=\Omega_s \frac{\cosh^{-1} \frac{x}{2R_a}[(\frac{R_o}{x})^2 - (\frac{R_a}{x})^2 -1]-\cosh^{-1} \frac{x}{2R_o} [(\frac{R_o}{x})^2 - (\frac{R_a}{x})^2 +1]}{2\pi} \tag{3.23}$$

where Ω_s is the surface resistivity in ohms per square. Equation (3.13) can thus be written as:

$$V = AxI^{-n}$$

$$+ \frac{I\Omega_s}{2\pi} \{\cosh^{-1} \frac{x}{2R_a}[(\frac{R_o}{x})^2 - (\frac{R_a}{x})^2 -1]-\cosh^{-1} \frac{x}{2R_o}[(\frac{R_o}{x})^2 - (\frac{R_a}{x})^2 +1]\} \tag{3.24}$$

and

$$I = \pi R_a^2 J \tag{3.25}$$

where J is a constant.

Since A and n are constants yet to be determined by matching the best fit between theory and experiment, it is appropriate to normalize the above equations so that all the quantities are rendered dimensionless. Furthermore, no a priori values need be used for numerical solution. Using standard dimensional analysis,[9] two normalizing constants can be shown to be appropriate:[10]

$$\tilde{V} = \frac{V}{A} R_o^{2n-1} J^n \tag{3.26}$$

and

$$\tilde{\Omega}_s = (\Omega_s/A) R_o^{2n+1} J^{n+1} \tag{3.27}$$

From these two constants, the other normalized variables can be deduced as follows:

$$R_a/R_o = \tilde{R}_a \tag{3.28}$$

$$x/R_o = \tilde{x} \tag{3.29}$$

$$\tilde{I} = \frac{\tilde{V}}{\tilde{\Omega}_s} = \frac{I}{R_o^2 J} = \frac{I}{I_o \pi} \tag{3.30}$$

Equation (3.16) can be reduced to

$$\tilde{I} = \pi \tilde{R}_a^2 \tag{3.31}$$

Substituting equations (3.26), (3.27), (3.28), (3.29), (3.30) and (3.31) into equation (3.24) yields

$$\tilde{V} = \tilde{x}(\tilde{I})^{-n} + \frac{\tilde{\Omega}_s \tilde{I}}{2\pi} \cosh^{-1} \frac{1}{2} \left[\frac{1}{\sqrt{\frac{\tilde{I}}{\pi}}\,\tilde{x}} - \frac{\sqrt{\tilde{I}/\pi}}{\tilde{x}} - \frac{\tilde{x}}{\sqrt{\tilde{I}/\pi}}\right]$$
$$-\cosh^{-1} \frac{1}{2}\left[\frac{1}{\tilde{x}} - \frac{\tilde{I}/\pi}{\tilde{x}} + \tilde{x}\right]\} \tag{3.32}$$

Theoretically, the method to use here is the same as used by others before, namely setting $\partial\tilde{V}/\partial\tilde{I} = 0$ to determine $\tilde{V}_{min}$. Then, taking $\partial\tilde{V}_{min}/\partial\tilde{x} = 0$ to determine $\tilde{V}_{crit}$ and $\tilde{x}_{crit}$.

A mathematical complication is encountered here, however, as the derivative taking would result in transcendental equations which cannot be solved analytically. Conceptually, these steps can be accomplished graphically as shown in Figure 3.13. Numerically, these steps can be accomplished by first fixing $\tilde{x}$ and then varying $\tilde{I}$ until a minimum $\tilde{V}$ is detected. This is the $\tilde{V}_{min}$. The process is then repeated for a different $\tilde{x}$. The maximum value of $\tilde{x}$ thus found is the $\tilde{x}_{crit}$. Corresponding to it, there are $\tilde{V}_{crit}$, $\tilde{\Omega}_{crit}$ and $\tilde{I}_{crit}$. These values can then be denormalized by choosing a specific A and n. The resulting theory is then compared with the experimental data and the best A and n thus determined. The programming techniques are included in Appendix D. The simulation results are shown in Figure 3.14.

3.5.3 Discussion of Results

First of all, it is interesting to note that for all the simulated cases, the theoretical x_{crit} when measured from the center of the plate is about 0.9 R_o. This finding indicates that the minimum distance that an arc must traverse in order to ensure a flashover is close to the full radius of the plate. The conclusion is in agreement with that of Jolly. It is different from the case of a long rod where, for a critical voltage, only a partial bridge of the rod is

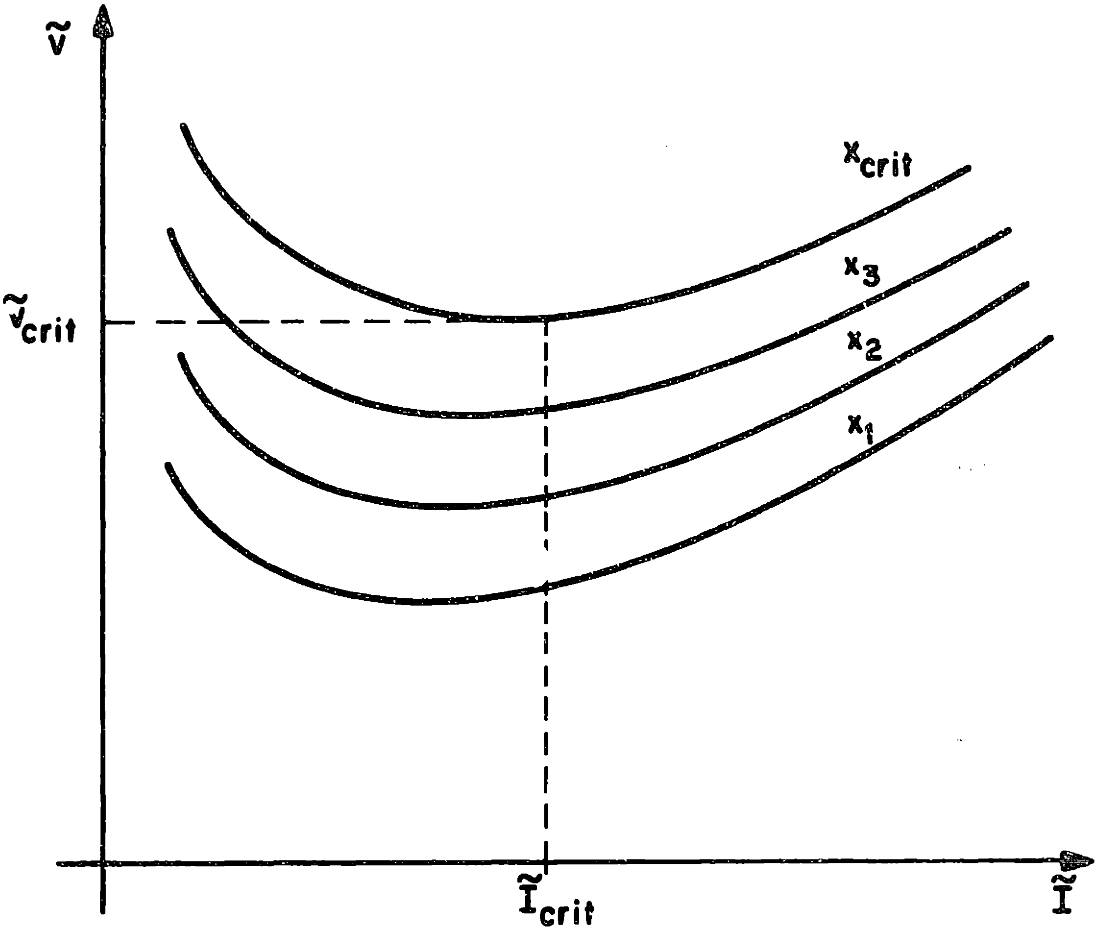

Figure 3.13 Graphical Solution of Flat-Plate Theory

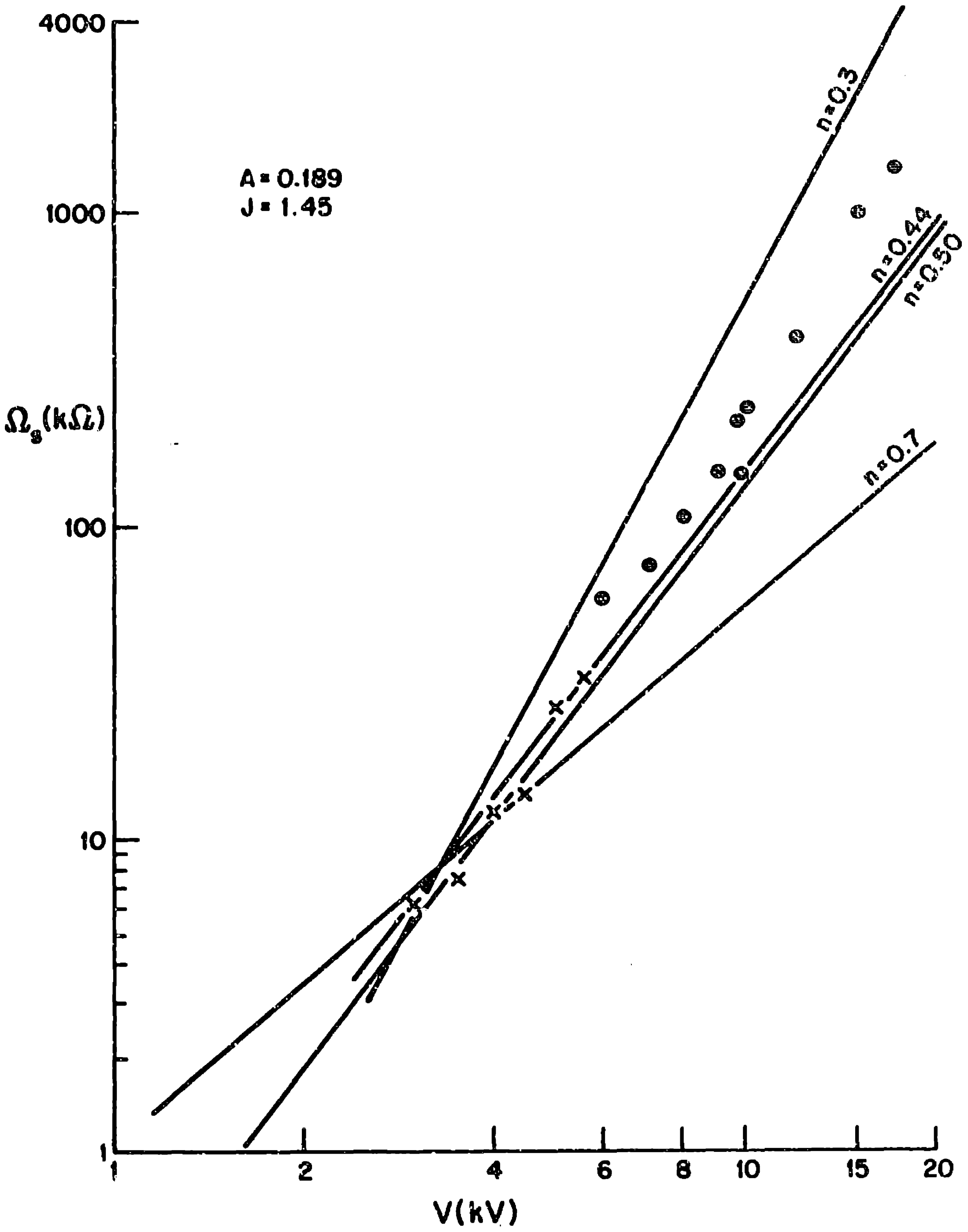

Figure 3.14 (a) Comparison between Flat-Plate Theory and Experiments

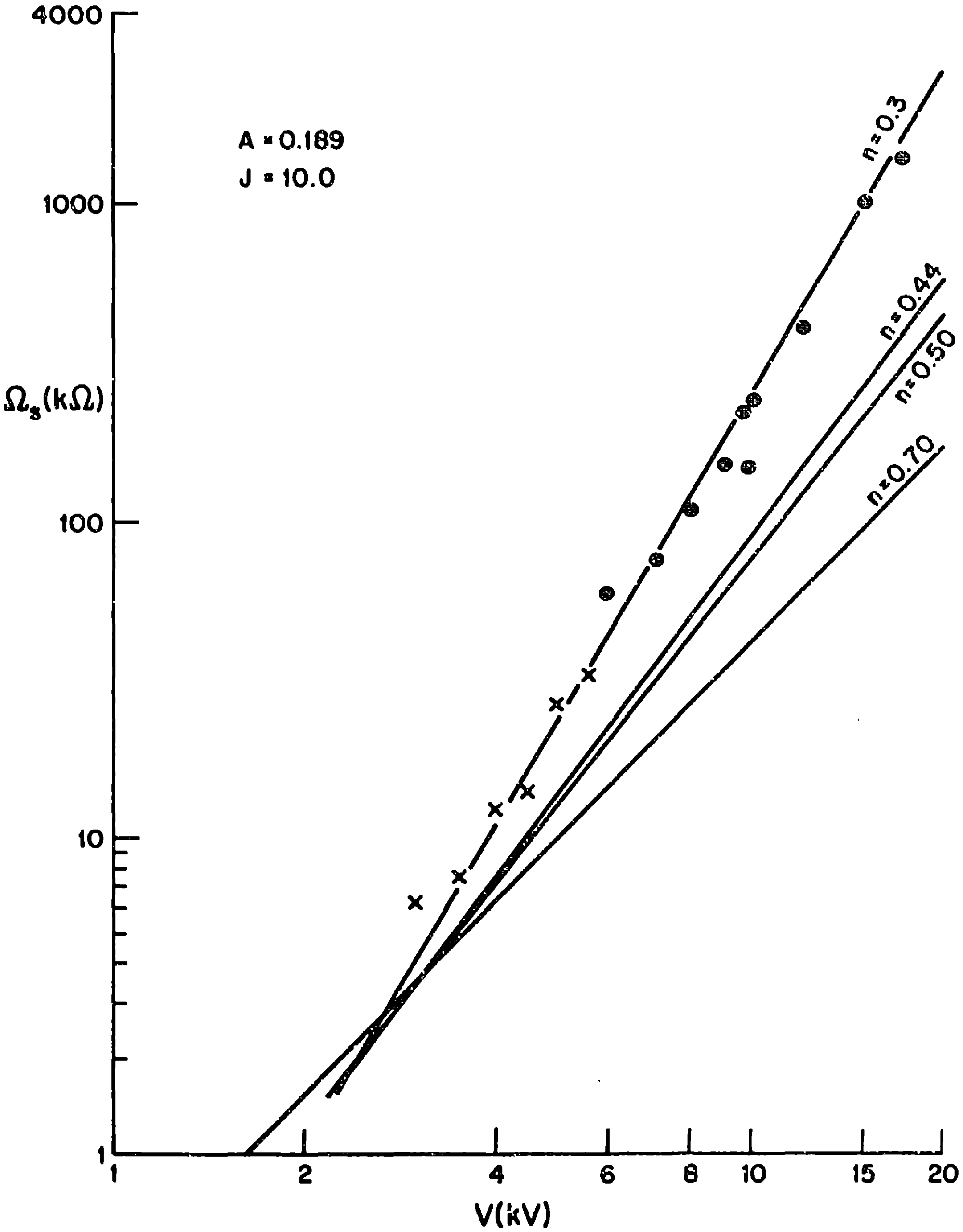

Figure 3.14 (b) Comparison between Flat-Plate Theory and Experiments

necessary to ensure a full-scale flashover.

In accordance with the philosophy of approach as outlined in Chapter I, this chapter describes an analysis of a flashover on a two-dimensional basis. The flat-plate has a more complex geometry than that of the linear model studied in Chapter II. Consequently, the theoretical approach is less sophisticated. Instead of applying a dynamic arc model, as in Chapter II, we have basically followed the paths of others by retaining the static arc model. This model, though not as powerful as the dynamic one, is still a very useful one in that it predicts a rather exact relationship between V_{crit} and Ω. This relationship has been observed experimentally. Once it has been established that the flashover of a flat-plate is both repeatable and predictable, then its usage for studying flashover processes can be expanded considerably. Other researchers (e.g. the group at the University of Southern California) have already started using it as a vehicle for contamination discharge studies.

BIBLIOGRAPHY - CHAPTER III

1. A. McElroy, "Flashover Mechanisms of Insulators With Contaminated Surfaces," Ph.D. Thesis, Department of Electrical Engineering, M.I.T., June 1969.

2. D. Jolly, "Physical Processes in the Flashover of Insulators With Contaminated Surfaces," Ph.D. Thesis, Department of Electrical Engineering, M.I.T., May, 1971.

3. Was first tried and tested by D. King and D. Jolly.

4. H.E. Remde, "Compendium on High Voltage Insulator Contamination Theory and Laboratory Test Methods," Bonneville Power Administration, High Voltage Laboratory, 1971.

5. International Critical Tables, Vol. 4, National Research Council, U.S.A., McGraw-Hill, 1926.

6. H. Näcke, "Stability of Foreign Layer Discharges and Theory of Contamination Flashover," ETZ-A, 87, pp. 577-585 (1966).

7. A. McElroy, "Current Research in the Field of Electric Arc Stability," Report No. 15, Electric Power Systems Engineering Laboratory, M.I.T., July 1969.

8. E. Weber, "Electromagnetic Theory, Dover Publications, p. 121 (1950).

9. P.W. Bridgman, "Dimensional Analysis," New Haven, Yale University Press, 1931.

10. These constants were kindly supplied by D. Jolly.

CHAPTER IV

SURFACE EFFECTS ON FLASHOVER PHENOMENON

4.1 Introduction

The previous two chapters have dealt with the flashover phenomena on idealized surfaces. The linear model substitutes the moist contaminated surface with a channel of salt water solution. The flat-plate uses an evenly coated surface gradually being wetted by fog. The surface condition is, therefore, fairly uniform and the propagation of the arc is quite independent of it. These idealized cases have been used so that theoretical models can be constructed which will then shed light on some of the physical mechanisms involved. In reality, however, a flashover process depends not only on the physical propagation mechanisms of the arc, but also, to a large extent, on the conditions of the surface during the discharge activities. High-speed movies and still pictures taken here have indicated that for most flashover cases, the arcs adhere very closely to the moist surfaces. Thus their modes of propagation can be affected by the very surfaces on which they have to propagate.

This chapter is essentially concerned with the role played by water drops accumulated on insulator surfaces in affecting flashovers. It has been generally agreed that flashovers occur only when moisture is present. Since water is by far the most readily available form of moisture in nature in the form of fog, rain, snow, ice etc., it is not surprising to find that most flashovers occur either during or after some form of precipitation. Recently, it has been reported that even sand storms might trigger insulator flashovers.[1] The details have not been published, however. The most damaging form of precipitation, as far as insulator flashovers are concerned, is probably fog since the size and momentum of the droplets are small enough so that they do not wash the insulators clean as raindrops do. Instead, they dissolve some of the surface contaminants and form a thin conducting film on the surface. The resultant leakage current will, through ohmic heating, produce dry zones around the cap and pin. Discharges will be initiated next and propagate over the rest of the moist surface as already discussed in previous chapters. If formation of the film can somehow be inhibited, then the subsequent full-scale flashover could probably be avoided.

As early as 1876, oil bath was used to interrupt the wet film on an insulator to improve performance.[2] The effectiveness of various designs of oil-bath insulators was later confirmed.[3,4] Silicone oils or polymers and silicone greases were then tried and the results were found to be satisfactory.[5-8] The primary function of the grease is to breakup the film formation so that the water drops bead up rather than spread out thin. The same can be achieved also by the use of solids such as p.t.f.e. (polytetrafluorethylene commonly known as Teflon) which have low coefficients of friction and are water-repellent. These water-repellent substances possess the unique property of preventing water drops from wetting their surfaces. For most of these substances, the drops form relatively large contact angles (for a definition, see the following section). These contact angles, however, can change when a field is applied. With the changing of contact angle, the water drops can do what they normally are incapable of doing on water-repellent surfaces; wet the surface. Hence, the electric stress can reduce the effectiveness of the water-repellent properties of the surface. Such being the case, the threshold level for flashover of an insulator can be decreased considerably. This interaction between the field and the water drops in lowering the threshold voltage for flashover will be studied in the following section.

Though greasing improves the performance of insulators remarkably, it is not, however, a permanent cure. First of all, grease has to be applied. After a year or so (at the most two years), it has to be cleaned off and reapplied as aging and chemical decomposition will drastically reduce its effectiveness. Regular application and cleaning can be very costly. It is thus desirable to understand the physical processes involved in a flashover over a greased surface so that some substitutes might be used, which retain the desirables properties of grease and eliminate the undesirable ones.

4.2 Theory of Behavior of a Water-Drop in an Electric Field

4.2.1 History of the Problem

Despite numerous reports on the performance of variously coated insulators, studies on the interaction between the water drops and the field on these surfaces are almost non-existent. Fortunately, the interaction of free water drops and an electric field has been studied in related areas such as corona and audible noise. These findings can be used as guides to our studies.

Zeleny[9] was probably the first to show experimentally that disintegration of a water drop in an electric field began as a hydrodynamical instability. Wilson and Taylor[10] detected a similar phenomenon when an uncharged soap bubble was subjected to a uniform electric field. Macky[11] and Nolan[12] showed that the same kind of disintegration occurred when a drop of water fill between a pair of charged parallel plates. Taylor later studied this instability further and found that a drop, first elongated by an electric field, became unstable when its length was 1.9 times its equatorial diameter.[13] Using the elliptic shape of the drop, he was able to calculate the critical electric field for instability and found that agreement with experiments was within 1%. His calculation is now generally accepted as a valid one in predicting the drop instability and subsequent rupture. More about it will be said in the following sections when it is applied to the case at hand.

The subject of an E-field interacting with more than one drop is a far more complex one. Davis[14] calculated the forces and field strengths between two rigid and charged spherical conductors in a uniform electric field. He presented numerical results for a number of relative sphere sizes and separations. Depending on the distance of separation between these spheres, the field intensification factor at the tips of the drop could vary from 3 to 1000. These numbers clearly demonstrate the unstable nature of the situation. As the drops elongate under electric stress, their separation decreases. The field is thus intensified and the drops deform further. This process has been repeatedly observed in the course of our work and will be reported in the experimental section. Latham and Roxburgh[15] used the intensification factors of Davis and applied them to a pair of drops in uniform field, based on Taylor's assumptions. They were able to arrive at a critical E-field for instability. Taylor[16] analyzed the problem further and concluded that the drops must be in an equilibrium state to start with before they could become unstable. Experimentally, therefore, he used two equal rings to support the drops before the field was applied. The two neighboring drops were thus physically constrained to be at rest till, without moving the constraints, the drop surfaces sprang together at a critical potential difference. Brazier-Smith[17] devised a numerical method for calculating the correct stable equilibrium shape of a conducting drop subject to electrical stress. He found the shape to be a very close approximation of the ellipsoid that Taylor used and essentially verified Taylor's analytic solutions.

From these previous studies, it is generally established that a free drop in a uniform field is first elongated and will rupture if the field is above a critical value. Because of the complex dynamics involved, it is possible only to determine the critical field for instability. The actual rupturing process cannot be described mathematically.

4.2.2 Present Theoretical Approaches

Our problem is complicated further by the physical constraints involved. These water drops are sessile drops, i.e. they are sitting on top of an insulating surface. The surface is therefore acting as an additional boundary condition. Any deformation of the drop at the interphase will be governed in part by the surface properties of the solid, such as its surface tensions with respect to water as well as air and in part by the surface tension of water itself. Thus, besides the dynamics of the bulk of the drop, we must also consider the boundary condition at the liquid/solid interface.

Below will be retraced the steps of thinking that led to the present understanding of the problem. Consider the physical set-up as shown in Figure 4.1. The water drop is located on top of an insulating surface (in the experiments, it is a piece of plexiglas). A horizontal field is applied. We want to describe how the drop reacts and how the contact angle

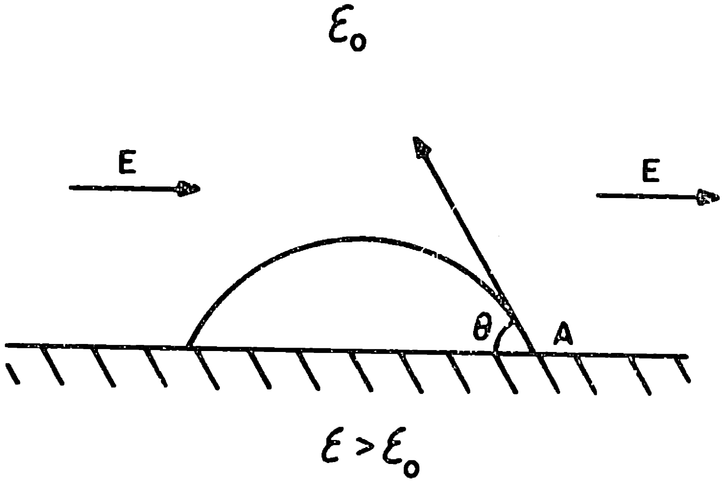

Figure 4.1 A Sessile Drop

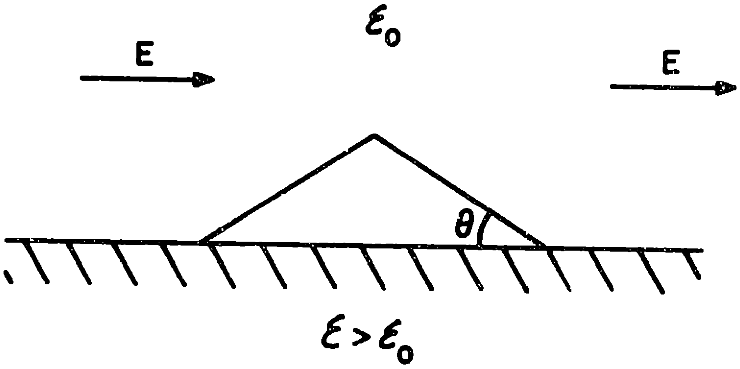

Figure 4.2 Simplified Geometry of a Sessile Drop

changes. At first, it was thought that the electric field at the solid-liquid-air interface (i.e. point "A" in Figure 2.1) could influence the contact angle by altering the surface tension forces. If that was the case, then the magnitude of the E-field at "A" would have to be determined. The solution looked deceptively simple on paper, since it involved no more than a Laplace's equation with boundary conditions. Several attempts were made to solve the field problem analytically. The Schwarz-Christoffel transformation was first tried and later the Fourier transformation. Both methods failed owing to serious questions about separability of variables in the transformed spaces. The next method used was to approximate the drop as a triangle with well-defined contact angles in the form of wedges, as shown in Figure 4.2. This shape introduced its own problems, however, and the singularities at the edges remained. At this point, even field sketching[18] was employed to provide a rough idea of the magnitude of the stress. Finally, after numerous other futile attempts, it was realized that it was not possible to obtain an analytic solution to the problem. The obstacles were the odd shape of the drop as well as the consequent singular boundary conditions. This realization forced a review of the philosophy of attacking the problem. First, it became clear that the knowledge of a field distribution for a particular configuration was not absolutely important. With the application of field, the shape of the drop would change continuously and so would the resultant field map. As it was impossible to solve for the field of even a well-defined geometrical configuration, it would be entirely hopeless to try for a shape that would be changing with the field. Secondly, the assumption that the electric field directly influenced the contact angle at the interface was not necessarily a correct one. We need to re-examine the contact angle phenomenon in a more rigorous manner, with the electric field included, if possible. Despite the difficulties encountered in calculating the fields around a drop, a two-dimensional numerical soltuion was obtainable. A program was written by D. Bosack which is capable of plotting equipotential lines for a two dimensional system of n conductors and dielectrics enclosed within a well-defined boundary. The electric fields can be subsequently calculated. Utilizing such a program, the equipotential lines for a half cylinder resting on top of a flat piece of porcelain surface ($\varepsilon \simeq 5.6\varepsilon_o$) placed between two energized parallel electrodes was simulated. The plot is shown in Figure 4.3. Another simulation without the porcelain produced almost identical results. This finding substantiates what can be reasonably expected from physical intuition alone, i.e. because the field lines are mostly parallel to the air/dielectric interface, polarization effects are not important.

4.2.3 Contact Angle Analysis

It is observed that in most instances a liquid placed on a solid will not wet it but remains as a drop having a

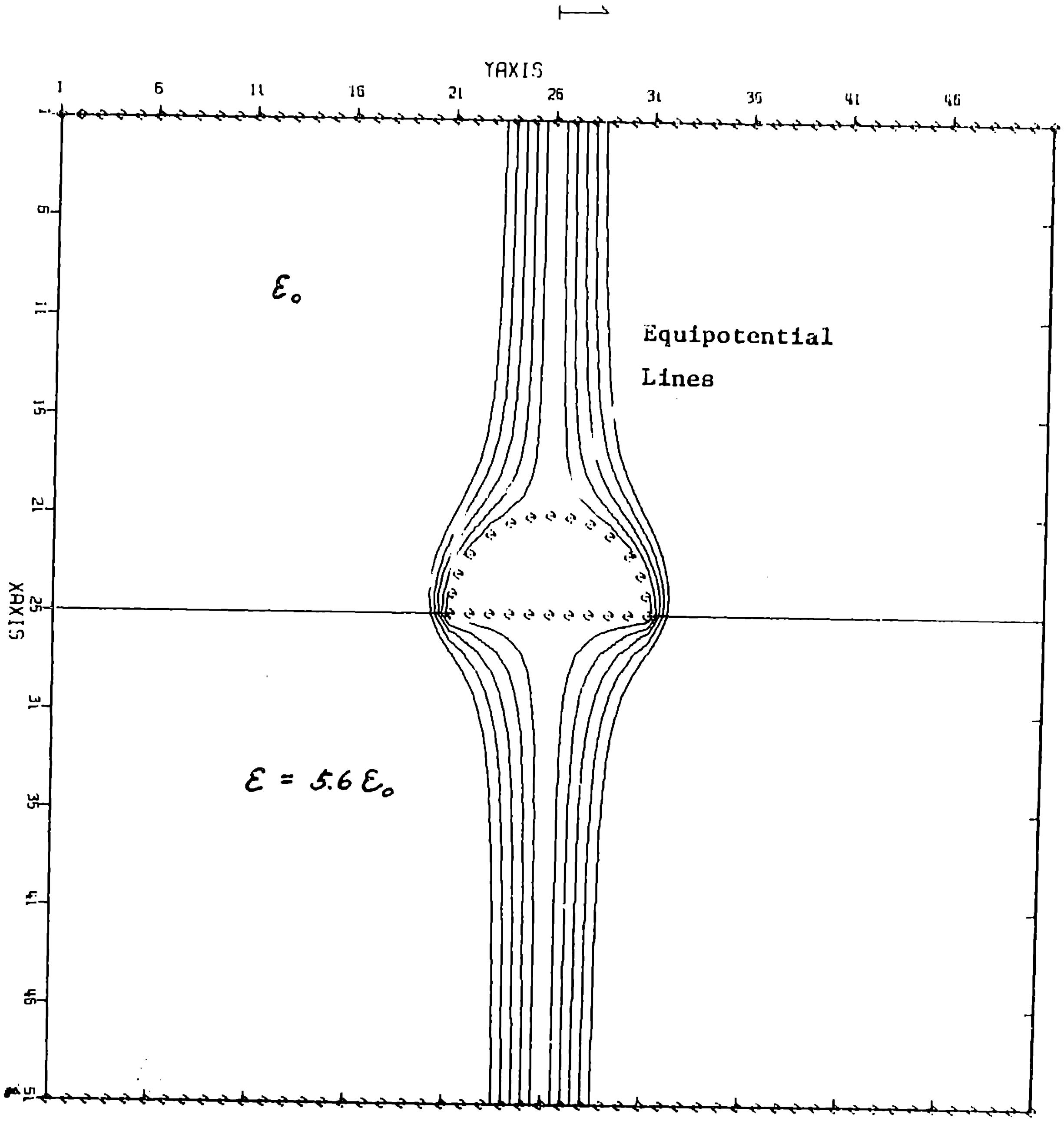

Figure 4.3 Computer Simulation of a Two-dimensional Half-Cylinder

definite angle of contact between the liquid and solid phases. In most surface chemistry textbooks, this angle is calculated by balancing the forces in the horizontal direction, as shown in Figure 4.4. The Young-Dupre equation is thus arrived at:

$$\gamma_{sa} = \gamma_{\ell s} + \gamma_{\ell a} \cos \theta \qquad (4.1)$$

Two observations should be made about the equation. First, this equation is valid when there is no other forces (such as electrical) present. If an E-field is applied, it is not clear how its effects can be incorporated into the equation without a more formal derivation. This derivation will be supplied below. Secondly, the contact angle is not uniquely definable, as the equation implies. For a particular solid and liquid, the contact angle behaves in a hysteretical manner. A vivid illustration is that of a raindrop sliding down a window pane. The advancing tip of the drop has a larger contact angle than the receding end. For obvious reasons, the upper and lower bounds are usually denoted by advancing and receding angles respectively. Hysteresis is not yet completely understood and the most commonly cited explanation is the roughness of the surface.[19] Since the hysteretic behavior of the water drop is of importance in our later theoretical and experimental work, contact angles of drop sizes of interest have been measured to illustrate a few typical values. It has been observed that drops of

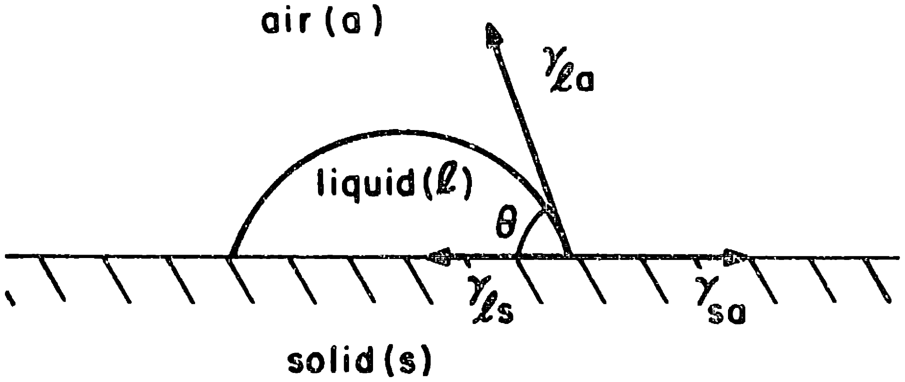

Figure 4.4 Contact Angle Illustration

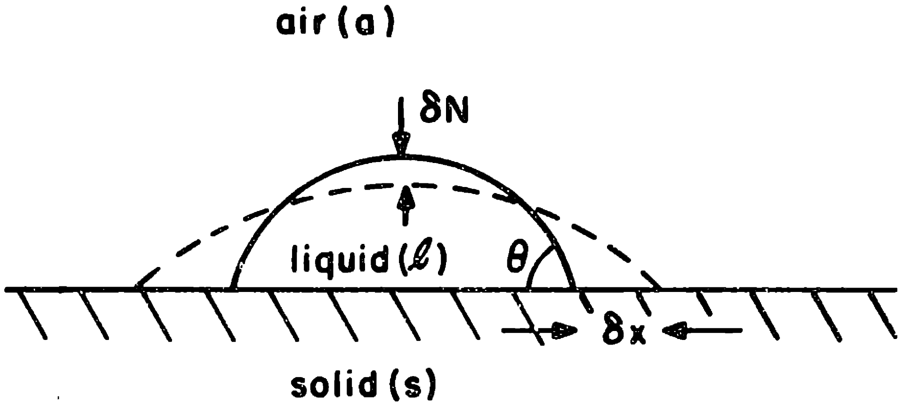

Figure 4.5 Drop under Perturbational Change

different sizes usually have different contact angles. Poynting and Thomson[20] reported a simple means of deriving a contact angle by measuring the height of a drop. By approximating the shape of a sessile drop, they showed that the following equation could be used:

$$1 - \cos \theta = \frac{g\rho h^2}{2\gamma_{\ell a}} \tag{4.2}$$

where

θ = contact angle

g = gravitational constant = 980 cm/sec^2

ρ = density of water = 1.0 gm/c.c.

h = height of drop in cm

γ = surface tension of drop = 72 dynes/cm

Drops of desirable sizes were injected from a microliter syringe onto a level, clean, and flat surface. Its height was then measured by means of a micronmeter. The contact angles could then be calculated from eq. (4.2). Tables 4.1 4.2 and 4.3 illustrate some of the measurements on a clean plexiglas plate, a Teflon plate and a greased surface. The tabulated values clearly demonstrate that the contact angle is not a uniquely determinable quantity. It is also very much dependent on the type of solid surface with which it comes in contact. Teflon and greased surfaces are much more water-repellent than a clean piece of plexiglas.

Now that we have established the hysteretical nature of contact angles, we move on to study the influence exerted by

TABLE 4.1

DETERMINATION OF CONTACT ANGLE OF WATER ON CLEAN PLEXIGLAS

volume (μℓ)	h(cm)	θ(degrees)
20	0.185	39°
40	0.198	42°
60	0.251	55°
80	0.277	61°
100	0.287	63°
120	0.307	68°
140	0.312	69°

TABLE 4.2

DETERMINATION OF CONTACT ANGLE OF WATER ON TEFLON

volume (μℓ)	h (cm)	θ (degrees)
20	0.240	57°
40	0.246	59°
60	0.271	66°
80	0.2[illegible]6	70°
100	0.290	71°
140	0.295	74°

TABLE 4.3

DETERMINATION OF CONTACT ANGLE OF WATER ON GREASED PLEXIGLAS

volume (μℓ)	h (cm)	θ (degrees)
20	0.213	46°
40	0.279	61°
60	0.297	66°
80	0.309	69°
100	0.338	76°
140	0.341	77°

the electric field. Equation (4.1) is sufficient and correct for most cases of practical interest. But, it makes the addition of other forces difficult, unless they act in a similar fashion as the surface tension (which usually is not the case, however). To consider the effects of such other forces as gravity and electric stresses, it is necessary to rederive the force balance equations in a rigorous manner from basic thermodynamics.

The system under consideration is as shown in Figure 4.5. From the second law of thermodynamics, we can write, for a pure mechanical system:

$$dU = - PdV + TdS \tag{4.3}$$

and if we use Helmholtz Free Energy,

$$F = U - TS$$

we have,

$$dF = dU - TdS - SdT$$

$$dF = - PdV + SdT \tag{4.4}$$

Energies of other origins can be added to equation (4.4), when needed. The surface tension γ can be recognized either as a force/unit length or an energy/unit area term and is related to the Helmholtz energy as follows:

$$(\partial F/\partial \Omega)_{T.V.n_i} = \gamma$$

where

Ω = surface area of interface

T = temperature

n_i = number of moles of component i

Now, for the system to be under thermodynamic equilibrium, any variation of the force energy (i.e. Helmholtz) of the system at constant temperature, volume and mass must be zero, i.e.

$$(\delta F)_{T,v,n_i} = 0 \tag{4.5}$$

where the symbol δ refers to a variation in the "virtual work" sense.

The total free energy of the system is given by

$$F = \int_V dF^V + \int_\Omega dF^\Omega + \int_V gzdm^V + \int_\Omega gzdm^\Omega \tag{4.6}$$

where

g = acceleration of gravity

dm^V = the mass of an element dV

dm^Ω = the mass of a membrane-like element $d\Omega$

z = the height of the element above a horizontal plane

We see here that the free energy is composed of two constituents, one from the bulk volume and the other from the surface which is treated as if it were a membrane.

$$\delta F = \delta \int_V dF^V + \delta \int_V dF^\Omega + \delta \int_V gzdm^V + \delta \int_\Omega gzdm^\Omega = 0 \tag{4.7}$$

For reversible variations, the variation sign can be transferred inside the integral:

$$\delta F = \int_V \delta dF^V + \int_\Omega \delta dF^\Omega + \int_V g\delta z dm^V + \int_V gz\delta dm^V$$

$$+ \int_\Omega g\delta z dm^\Omega + \int_\Omega gz\delta dm^\Omega = 0 \qquad (4.8)$$

The superscript "v" means inside the bulk of the drop; while the superscript "Ω" denotes the surface of the drop. Now,

$$dF^V = - PdV + \sum_i \mu_i \, dn_i^V \qquad (4.9)$$

where

μ_i = chemical potential of i^{th} component

$$dF^\Omega = \gamma d\Omega + \bar{\bar{T}}^e \cdot \vec{d\xi} d\Omega + \sum_i \mu_i \, dn_i^\Omega \qquad (4.10)$$

where

$\bar{\bar{T}}^e$ = electric stress tensor at the liquid air interface

$d\xi$ = displacement of liquid normal to the surface

The free energy inside the bulk of the drop is essentially unchanged before and after the application of electric field. The field acts as a surface force just like surface tension in certain respects.

Substituting (4.9) and (4.10) into (4.8)

$$\delta F = \int_v -P\delta dV + \sum_i \int_v \mu_i \delta dn_i^{\,v} + \int_\Omega \gamma \delta d\Omega$$
$$+ \sum_i \int_\Omega \mu_i \delta dn_i^{\,\Omega} + \int_v g\delta z dm^v + \int_v gz\delta dm^v$$
$$+ \int_\Omega g\delta z dm^\Omega + \int_\Omega gz\delta dm^\Omega - \int_\Omega |T^e|\,\delta(d\xi d\Omega) = 0 \qquad (4.11)$$

Because the variations of mass (due to chemical means) are independent of variations of v and Ω, eq. (4.11) can be separated into two independent equations:

$$\int_v - P\delta dV + \int_\Omega \gamma\delta d\Omega - \int_\Omega |T^e|\,\delta(d\xi d\Omega) + \int_v g\delta z dm^v$$
$$+ \int_\Omega g\delta z dm^\Omega = 0 \qquad (4.12)$$

and

$$\sum_i \int_v \mu_i \delta dn_i^{\,v} + \sum_i \int_\Omega \mu_i \delta n_i^{\,\Omega} + \int_v gz\delta dm^v + \int_\Omega gz\delta dm^\Omega = 0 \qquad (4.13)$$

Equation (4.12) contains the equilibrium condition for a drop under mechanical (including gravity) and electrical conditions. Equation (4.13) contains the conditions for chemical equilibrium in a gravitational field. This latter equation does not concern us here. This derivation here is more general than needs be for our system. For simplicity, gravity and chemical potentials will all be assumed to be zero and hence (4.13) is automatically satisfied. For a more thorough discussion of the thermodynamics involved, however, the reader is referred to References 22, 23, and 24.

Now,

$$dm^{V} = \rho dV \tag{4.14}$$

$$dm^{\Omega} = \lambda d\Omega \tag{4.15}$$

where

ρ = density of the volume element in units of mass/volume

λ = surface density of the surface element in units of mass/area

The superscripts designate the medium e.g.

a = air

ℓ = liquid

s = solid

Consider the first term in (4.12)

$$\int_{V^{\ell}} P\delta dV^{\ell} = \delta \int_{V^{\ell}} PdV^{\ell} - \cancel{\int_{V^{\ell}} \delta PdV^{\ell}}$$

and

$$\delta \int_{V^{\ell}} PdV^{\ell} = \int_{\Omega^{\ell a}} P^{\ell} \; \delta N \; d\Omega^{\ell a} \tag{4.16}$$

$\delta N^{\ell a}$ = normal component of motion of the element of liquid surface into the air

P^{ℓ} = the pressure on the element measured inside the liquid

The integral is only over the liquid-vapor interface since the solid surface is not considered to vary.

Similarly,

$$\int_{V^a} P\delta dV^a = \delta \int_{V^a} PdV^a - \int_{V^a} \delta \cancel{P} dV^a \tag{4.17}$$

$$\delta \int_{V^a} PdV^a = - \int_{\Omega^{\ell a}} P^a \ \delta N^{\ell a} \ d\Omega^{\ell a} \tag{4.18}$$

where

P^a = the pressure on the element of surface measured in the air.

The last term in (4.17) is zero because any difference in atmospheric pressure due to perturbation is discounted.

Now consider the second term in eq. (4.12):

$$\int_{\Omega^{\ell a}} \gamma^{\ell a} \ \delta d\Omega^{\ell a} = \delta \int_{\Omega^{\ell a}} \gamma^{\ell a} \ d\Omega^{\ell a} - \int_{\Omega^{\ell a}} \delta\gamma^{\ell a} \ d\Omega^{\ell a} \tag{4.19}$$

$$\delta \int_{\Omega^{\ell a}} \gamma^{\ell a} \ d\Omega^{\ell a} = \int_L \gamma^{\ell a} \cos\theta \ \delta x dL + \int_{\Omega^{\ell a}} \gamma^{\ell a} \left[\frac{1}{R_1} + \frac{1}{R_2}\right] \delta N^{\ell a} \ d\Omega^{\ell a} \tag{4.20}$$

Where dL is the element of length of the line formed by the intersection of the three surfaces and x is the virtual motion of this line normal to dL along the solid and in a direction which increases $\Omega^{\ell a}$, as shown in Figure 4.4. θ is the contact angle and R_1 and R_2 are the principal radii of curvature.

Here we see that the virtual change in surface area of liquid-air interface is composed of two terms, one right on the boundary of liquid-solid-air and the other in the rest of the liquid-air interface. The final term in Eq. (4.20) is in fact derived by Gibbs[22,23] and represents the change of area of the liquid-air interface due to the change of shape of the drop in the variation.

$$\int_{\Omega^{s\ell}} \gamma^{s\ell}\ \delta d\Omega^{s\ell} = \delta \int_{\Omega^{s\ell}} \gamma^{s\ell}\ d\Omega^{s\ell} - \int_{\Omega^{s\ell}} \delta\gamma^{s\ell}\ d\Omega^{s\ell} \qquad (4.21)$$

and

$$\delta \int_{\Omega^{s\ell}} \gamma^{s\ell}\ d\Omega^{s\ell} = \int_{L} \gamma^{s\ell}\ \delta x dL \qquad (4.22)$$

$$\int_{\Omega^{sa}} \gamma^{sa}\ \delta d\Omega^{sa} = \delta \int_{\Omega^{sa}} \gamma^{sa}\ d\Omega^{sa} - \int_{\Omega^{sa}} \delta\gamma^{sa}\ d\Omega^{sa} \qquad (4.23)$$

$$\delta \int_{\Omega^{sa}} \gamma^{sa}\ d\Omega^{sa} = - \int_{L} \gamma^{sa}\ \delta x dL \qquad (4.24)$$

The electrical term enters as follows:

$$\int_{\Omega^{\ell a}} |T^{e}|\ \delta(d\xi d\Omega) = \int_{\Omega^{\ell a}} |T^{e}|\ \delta N^{\ell a} d\Omega + \int_{L} \tfrac{1}{2}(\sigma^{f} E^{\ell as})\,\delta x dL \qquad (4.25)$$

The term $E^{\ell as}$ is the electric field at the 3-phase interface, calculated by vector addition of all the field components due to the ambient field and all the free charges except one at which the field is being calculated. This is so because a charge can never move itself through its own field. The term σ^f denotes a line charge at the 3-phase interface. Since a line charge does not exist physically, the second term in eq. (4.25) is effectively zero saving us the enormous labor of trying to calculate $E^{\ell as}$.

The transformation comes about because $\delta(d\xi) = \delta N^{\ell a}$ and the second term is due to contributions from any line charges located along the liquid air solid interface. σ^f denotes such charges in coulomb/m and $E^{\ell as}$ denotes the field existing at such a boundary.

Substituting eq. (4.17) to eq. (4.25) into eq. (4.12), we finally have,

$$\begin{aligned}&\int_{\Omega^{\ell a}} [(P^a-P^\ell)\delta N+(\frac{1}{R_1}+\frac{1}{R_2})\gamma^{\ell a}\delta N - |T^e|\delta N+g\lambda^{\ell a}\delta z-\delta\gamma^{\ell a}]d\Omega^{\ell a}\\ &+\int_{V^\ell}[\delta P+g\rho\delta z]dV^\ell + \int_L [\gamma^{s\ell}-\gamma^{sa} + \gamma^{\ell a}\cos\theta - \frac{1}{2}\sigma^f E^{\ell as}]\delta x dL\\ &+\int_{\Omega^{s\ell}}[g\lambda^{s\ell}\delta z-\delta\gamma^{s\ell}]\, d\Omega^{s\ell} + \int_{\Omega^{sa}} [g\lambda^{sa}\delta z - \delta\gamma^{sa}]d\Omega^{sa} = 0\end{aligned} \tag{4.26}$$

Since the variations are arbitrary, it is necessary and sufficient that each integrand be zero. The last two integrals vanish if the solid surface is flat and level. If we neglect gravity, the first integral yields (also neglecting any surface tension changes)

$$(P^a - P^\ell) + \left(\frac{1}{R_1} + \frac{1}{R_2}\right)\delta^{\ell a} - |T^e| = 0 \qquad (4.27)$$

This is a force balance equation that we would expect and this equation must hold for any differential surface element.

Also

$$\gamma^{s\ell} - \gamma^{sa} + \gamma^{\ell a} \cos\theta = \frac{1}{2}\sigma^f E^{\ell as} \qquad (4.28)$$

is obviously the Young-Dupree Equation with an additional electric term that we set out to derive. This term is actually zero, as already discussed above.

Here we have shown that the electric stress tensor does not contribute any term to this equation unless we have line charge accumulations along the 3-phase edge where the drop rests on the solid.

The importance of the above theoretical derivation is as follows. We have successfully separated the dynamics of the drop at the liquid/solid interface from that of the rest of the drop. Equation (4.28) describes the interfacial phenomenon, while eq. (4.27), the surface phenomenon. The latter equation is the same one as used by Taylor in arriving at his critical field. Thus, the same criterion can be used in calculating the critical field for the sessile drop provided that the boundary condition (4.28) does not affect the force balance. In the absence of any line charges, this assumption is perfectly valid. The conclusion is, therefore, very simple. The dynamics of the drop are adequately described by Taylor's criterion. The resultant change in shape of the drop will affect the magnitude of the contact angle almost the same way as a change in mass would (see Tables 4.1, 4.2, and 4.3). However, the interfacial dynamics will not have any significant effect on the behavior of the rest of the drop. The coupling is thus uni-directional. A better analogy is probably provided by the previous example of a raindrop sliding down a window pane. The external force, instead of being electrical, is gravitational. Gravity acts through the bulk instead of on the surface. This distinction, however, is not relevant. The contact angles of the raindrop have changed because of a change in the shape of drop. There is no gravitational force acting at the interfacial boundary to change the angle, because infinitesimal mass yields infinitesimal weight. Similarly, the electric field is not directly acting on the contact angle per sei, but the angle changes nevertheless because the rest of the drop is reacting to the field.

This section forms the theoretical basis for the following experimental work. For each series of experiments, a theoretical explanation will be attempted to account for the observed results.

4.3 Experiments on a Water-Drop in a Uniform Field

4.3.1 Description of Experimental Apparatus

All of the experiments to be described in this chapter used the same D.C. power supply as shown in a circuit diagram in Figure 4.6. It consisted of a .4μF capacitor bank charged by a NJE D.C. high voltage power supply. The voltage ranged from 0 to 30 kV with a maximum current of 3mA. The capacitor bank was charged through a 50Ω charging resistor and its voltage was monitored by a divider circuit. The output of the divider circuit was calibrated against an electrostatic voltmeter. The voltage was pulsed on to the testing apparatus via either an electromechanical switch or a vacuum switch. The switch was paralleled by a 2000 pf door-knob type capacitor to reduce the effects of switch bounce. The 50Ω high voltage charging resistor was made by winding two layers of oxidized copper-nickel wires in opposite directions so that the resulting inductance would be low. The interconnecting leads were made as short as possible. All these precautions were taken to minimize the oscillations of the supply voltage. The risetime of a voltage pulse was usually less than 1μs. For most experimental purposes, this time was short compared with times of interest. In some of the extreme cases, however the times to flashover did approach the 1μs limit. Such data points would have to be interpreted with this limitation in mind.

The testing chamber is shown in Figure 4.7. Connected to one side of it is the fog chamber with a fog nozzle mounted at the bottom. On the other side is the exhaust chamber for excess fog particles to escape. The fog chamber is activiated only during fogging tests. For single drop experiments in a

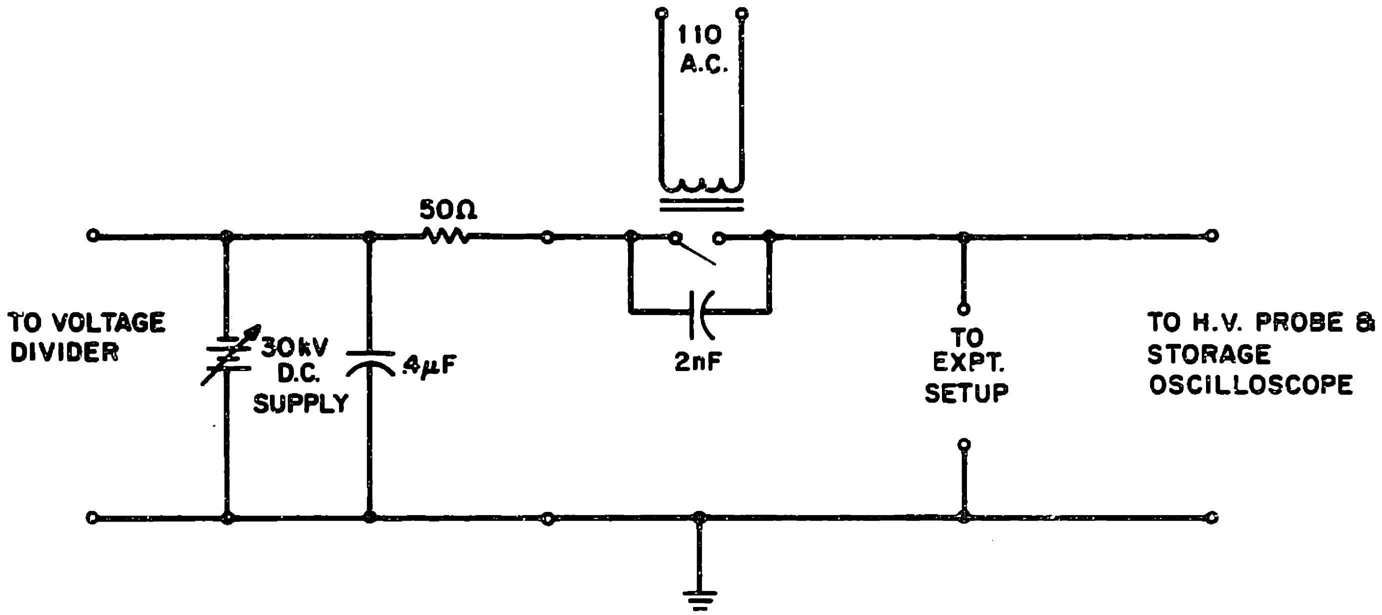

Figure 4.6 Simplified Circuit Diagram

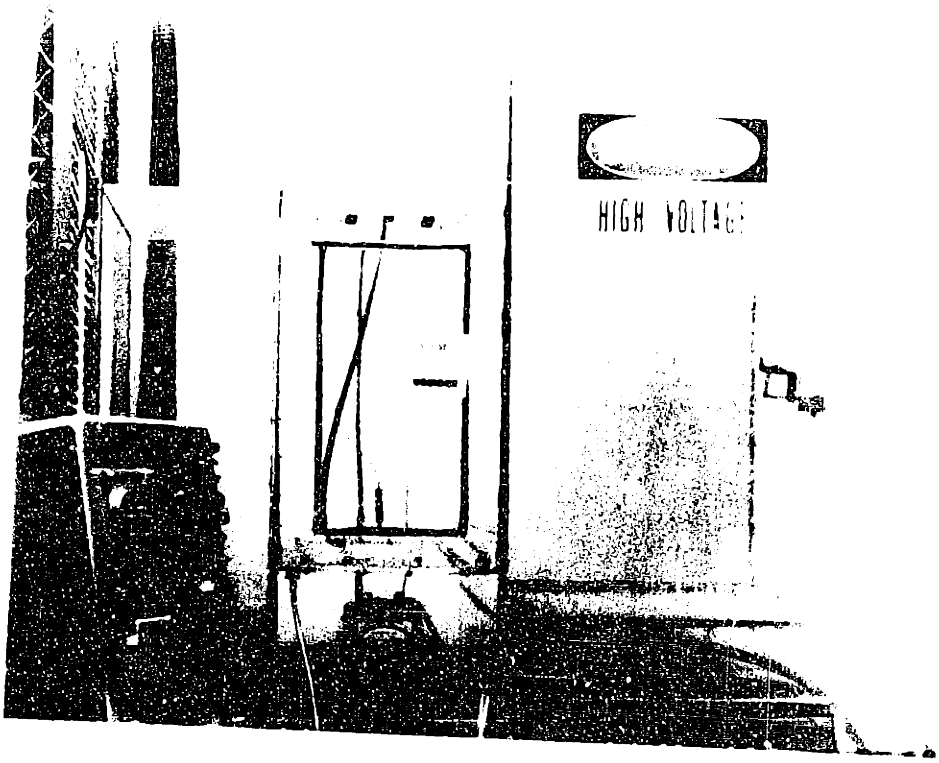
HIGH VOLTAGE

[illegible]

[illegible]

[illegible]

[illegible]

uniform field, only the middle testing chamber was used. The high voltage coaxial cable enters from the ceiling of the testing chamber.

4.3.2 Single Drop Tests in Uniform Field

The uniform field was provided by two plane parallel electrodes separated by a block of plexiglas as shown in Figure 4.8. The drop was placed on top of the plexiglas midway between the electrodes. The size of the drop for testing was picked to be 50 microliters. This was a typical size to expect when a clean piece of plexiglas was left in a dense fog for a duration of two to three hours (see section 4.4 for a calibration curve of the fog chamber). Each individual fog particle was, of course, of a minute size (around 10 microns), but these droplets would coalesce on the surface to form far larger drops as time passed. When the drop had been deposited midway between the electrodes, the apparatus was placed on a predetermined spot inside the chamber, so that the plexiglas surface was level. The high-voltage and ground leads were respectively connected and the chamber door closed. The storage oscilloscope was readied, while the capacitor bank was energized. When the desired voltage level was reached, the electromechanical switch was activated and the voltage drop was applied directly across the electrodes. Depending on the voltage level, either a flashover or a withstand would result. The voltage across the electrodes was monitored by a Tektronix High-Voltage Probe connected to the scope which was simultaneously

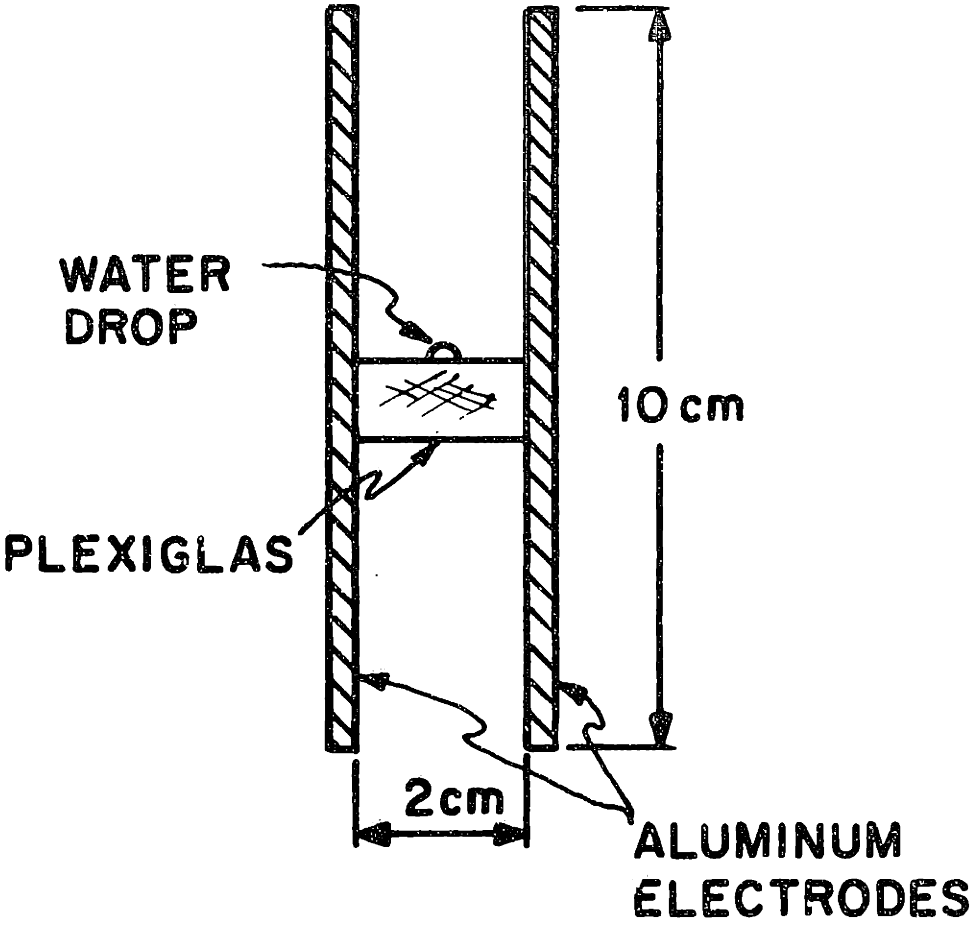

Figure 4.8 Parallel-Plate Set-up

triggered by the application of voltage. For a flashover, a typically recorded voltage trace is as shown in Figure 4.9. The vertical drop in the voltage trace indicated that a flashover had taken place. The time to this flashover was therefore the time elaspsed between the voltage application and this drop in voltage. The voltages were increased in steps of 1 kV (sometimes 2 kV) from the threshold level so that a range of times to flashover would result, covering from four to five orders of magnitude. These times to flashover τ_f are plotted on a semi-log scale as shown in Figure 4.10. On the same graph are plotted another two series of experiments for comparison. One was done with a distilled water drop on a plexiglas surface greased first with a layer of Dow Corning Five compound, commonly used for insulator coating. In the other, the liquid used was a solution of methyl chloride in distilled water ($\sim$ 0.5%) so that the drop would be about 10 times more viscous than distilled water.

4.3.3 Discussion of Theoretical and Experimental Results

The times to flashover curves in Figure 4.10 emphasize some of the important physical mechanisms operating in a flashover process. As the applied voltage increases from near a threshold value to twice that value, two distinct regimes of operation can be clearly defined. These regimes are denoted, the Townsend breakdown and the Electrohydrodynamic regimes. The Townsend breakdown regime is that case where the field is already so intense that direct discharges

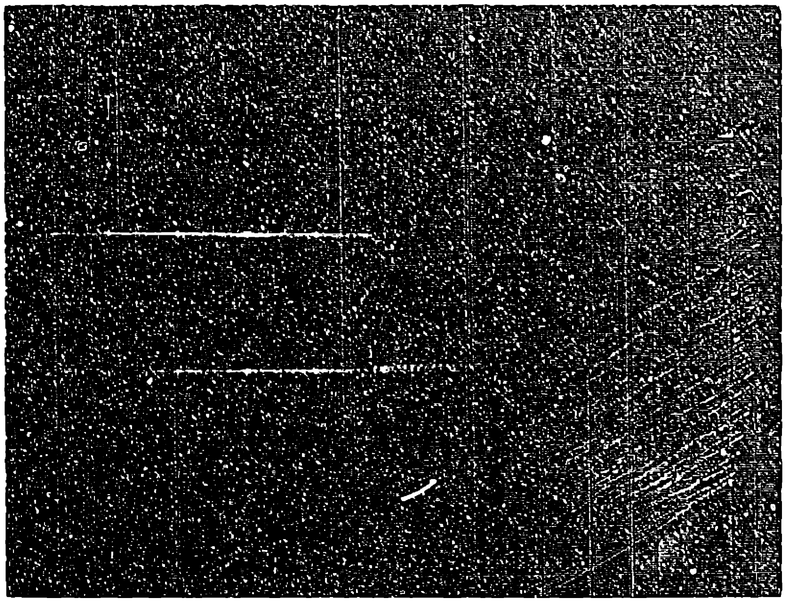

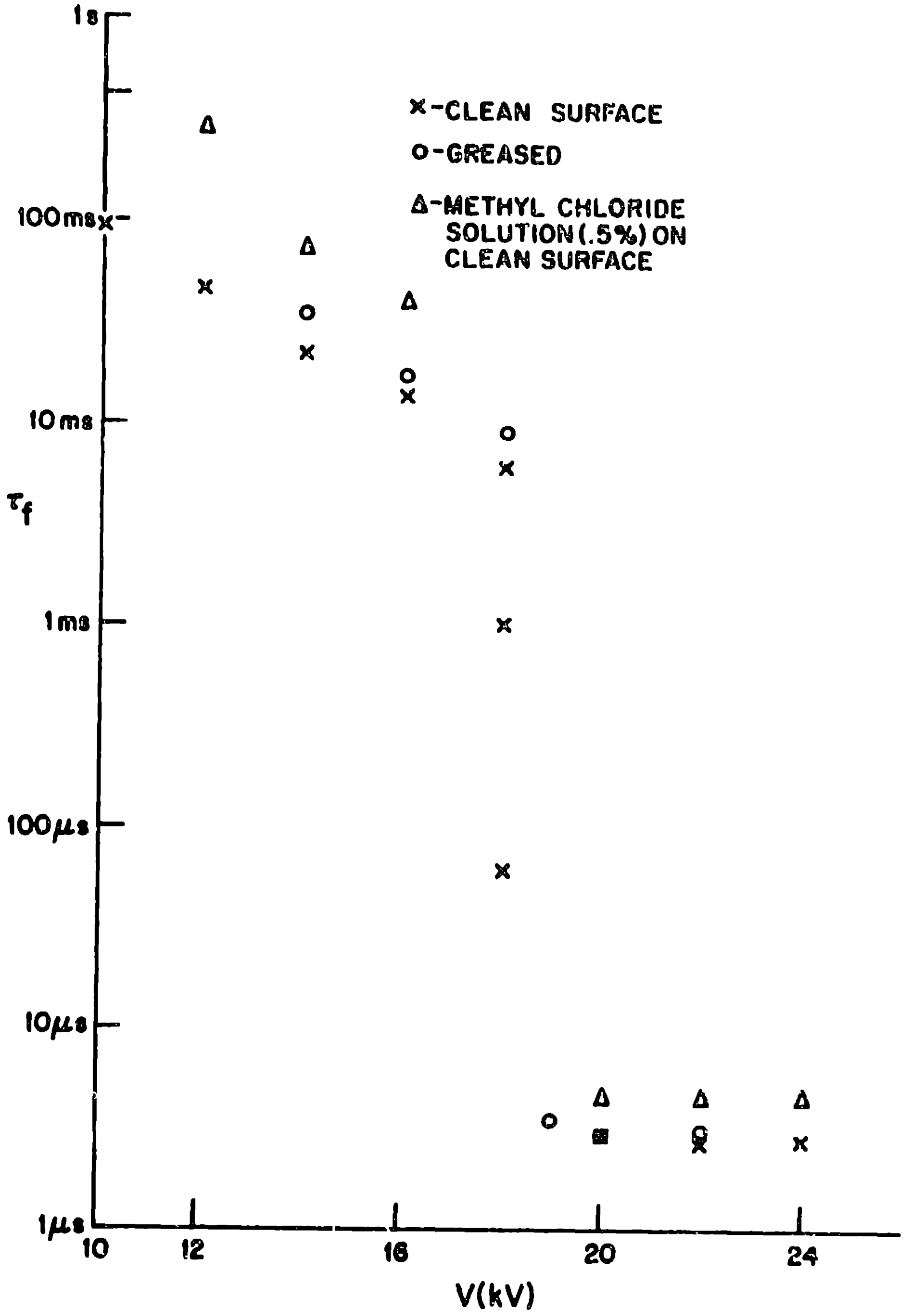

Figure 4.10 Time to Flashover for a Single Drop in Uniform Field

can be initiated between the drop and the electrodes without first deforming the drop. The electrohydrodynamic (EHD) regime occurs when the hydrodynamics of the drop plays an important role in causing flashovers. From high-speed motion pictures, it can be seen quite clearly that the drop first deforms and elongates, thus intensifying the field stress at its tip. The intensified field strengtn has a positive feedback effect on the drop, elongating it further. The process thus continues, developing into an instability until conditions are proper for an arc to strike. The resultant forces of discharge usually break up the drop. Thus, in addition to the relatively long τ_f, the breakup of the drop is another distinguishing feature of the EHD regime. In the Townsend breakdown regime, the flashover is almost instantaneous and the drop does not usually respond mechanically, so that its shape remains unchanged. To test this hypothesis on the deformation of the drop to intensify the field, a series of experiments were carried out using exactly the same experimental set-up except for the water drop which was substituted by a solder drop of roughly the same shape and volume. The use of the metallic drop ensured that no deformation was possible so that no field-intensification could result. Thus for these tests, the EHD regime was completely eliminated. This observation demonstrated that the presence of deformable water particles definitely lowers the flashover voltages. Actually, the effect is more serious than mere deformations.

The neighboring drops always seem to coalesce in such a way that filaments are formed, effectively shorting out a portion of the insulating surface. This phenomenon will be discussed further in the next section.

In section 4.2.3, it has been shown that the criterion for the instability of the bulk of the drop can be derived irrespective of the boundary condition at the interface. The boundary condition and the contact angle, in particular, however, are affected by the dynamics of the drop. Both Taylor's criterion for instability and the resultant contact angle hysteresis will now be examined.

Taylor in his paper showed that an uncharged drop, in the presence of a uniform field, will be elongated in the direction of the field. The point of instability is reached when the drop's length is 1.9 times its equatorial diameter. He approximated the shape of the drop to be an ellipsoid and derived, in c.g.s. units, the critical point for instability,

$$E_c(R_o/\gamma)^{1/2} = 1.625 \qquad (4.29)$$

where

E_c = critical electric field in e.s.u.

R_o = radius of free drop in cm

γ = surface tension in dynes/cm

Taylor's critical field E_c can be estimated for the size of drops used in our tests. For a 50 μℓ drop, R_o is about 0.35 cm and γ about 72 dynes/cm.

Equation (4.29) yields an E_c = 7.0 kV/cm.

From our experimental measurements, as shown in Figure 4.10, the thresholds of applied fields for a single drop flashover while on a plexiglas surface and for a greased surface are 5.0 kV/cm and 7.0 kV/cm respectively. Taylor's criterion thus agrees with greased surface flashover data better than with ungreased surface. This conclusion is not surprising because Taylor's critical field is substantially higher than the field normally needed to elongate the drop noticeably. His field is virtually strong enough to pull the drop physically apart. In our experimental set-up, before such a stage could be reached, the field intensification would be such that a discharge would have occurred and a flashover resulted. It therefore seems that Taylor's criterion is reasonably good when applied to a water-repellent surface such as a greased one and is too high when applied to a normal plexiglas surface. Despite its deficiencies and despite the fact that his drop is a free drop, Taylor's criterion can still be used, if one is careful, to estimate the threshold fields for flashover. This conclusion serves a useful purpose because it implies that the threshold can be approximately determined irrespective of the boundary condition at the interface. The same conclusion was reached by the theoretical derivations in section 4.2.3.

Now that a critical voltage is established, a closer look can be taken at the role of the contact angle during the instability. Based in part on high-speed motion pictures, the following dynamic mechanism known as motion via contact angle hysteresis is proposed. It has been previously discussed and measured that contact angles behave in a hysteretical manner, with a maximum and a minimum for a particular set of surface conditions. The proposed mechanism of motion is best illustrated diagrammatically, as in Figure 4.11. With no applied field, the contact angle is most likely to be somewhere between the minimum and the maximum. As soon as the field is switched on, the drop starts to elongate in the direction of the field. The base width, however, remains essentially constant in the very beginning. It is the upper part of the drop that elongates first, there being no countering forces acting against motion. This lengthening process then increases the contact angle in the same manner as the gravity increases the advancing angle of a sliding drop. The increase continues until the maximum angle allowed by hysteresis is reached. Once attained, the angle cannot increase any further. The field stress, however continues being intensified. So, at this point, the drop flattens out along the field direction, increasing its base width in contact with the surface and decreasing the contact angle. If the electrical stress continues to be increased, the above process will be repeated; an increase in contact angle and a subsequent elongation. In this way, the drop creeps along the surface towards the electrodes until an arc discharge completes the circuit and a flashover results. This process is believed to

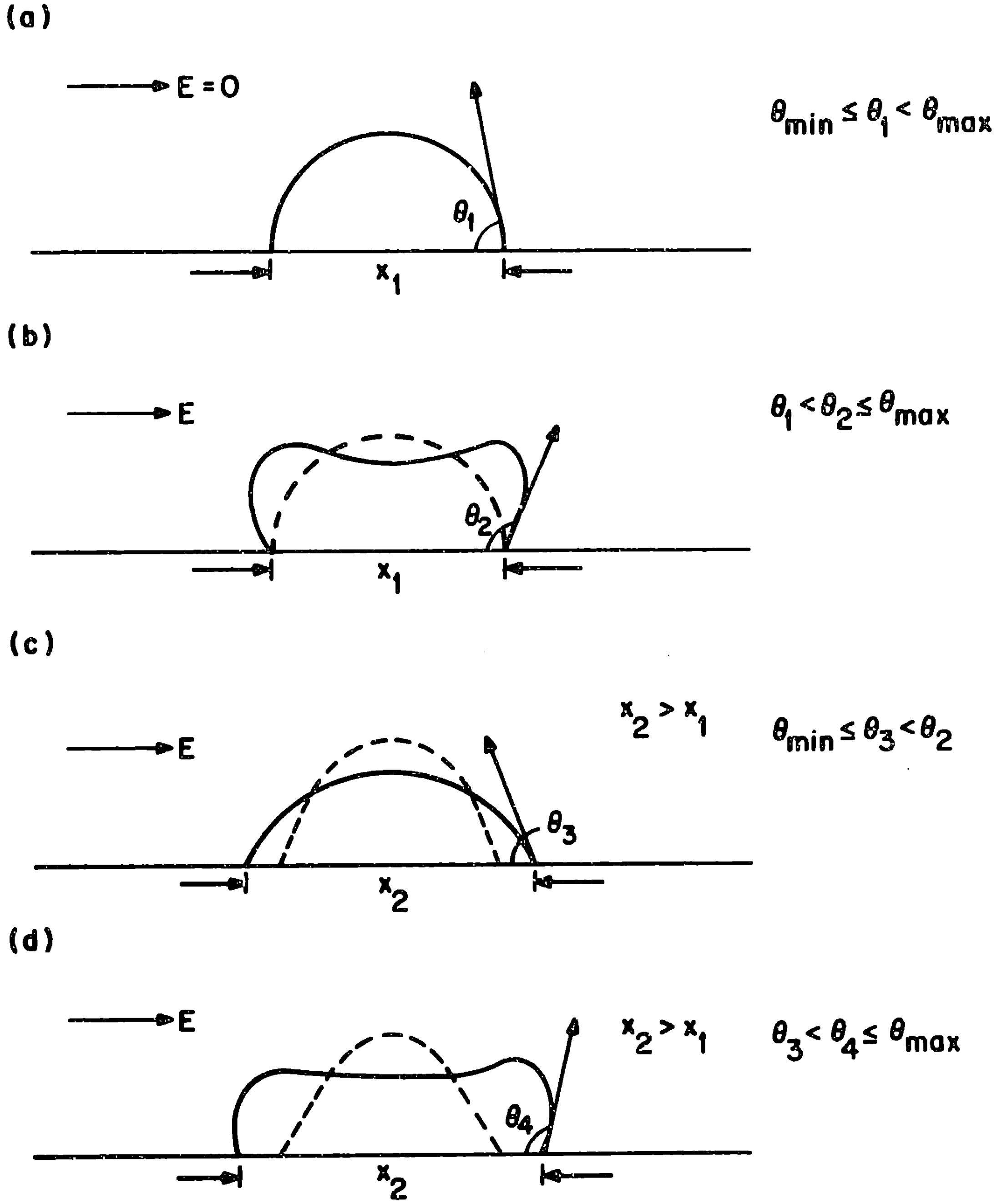

Figure 4.11 Contact Angle Hysteresis

be a valid one at least during the initial stages of elongation of the drop.

Using the critical voltage and some physics about the initial motion of the drop, one can estimate the times to flashover. For the Townsend breakdown regime, this time is essentially the transit time for an electron to bridge the air gap, assuming no transition to streamer occurs. If such a transition does occur, then the actual time would be less and the estimated time would be about the upper limit. The formative time lag for breakdown is neglected here because at such an overvoltage (> 100%), the formative time is much less than 1μs.[21]

Some estimate can now be made on the electron transit time. The applied ambient field for the Townsend breakdown is roughly 7.2 - 10.0 kV/cm. Assuming a normal atmospheric pressure of 760 mm Hg,

$$E/P \sim 9.5 - 13 \text{ kV/cm mm Hg.}$$

Corresponding to these ratios of E/P, the electron drift velocity is

$$V_{\ell} \sim 4.7 - 6.0 \times 10^{6} \text{ cm/sec.}$$

The air gap spacing that the discharge has to bridge is approximately 2.5 cm and hence the transit time is around,

$$\tau_{f} \text{ (estimated)} \simeq 0.53 \text{ μs} - 0.41 \text{ μs.}$$

The measured times to flashover for those voltage ranges were typically around 2-3 μs. The discrepancy is not really surprising, when considering the crude theory used in the estimation and more importantly, the nature of the d.c. power supply. The rise time for the voltage pulse is around 1-2 μs, so that the full supply voltage takes at least that long to reach its nominal value. If one adds 1-2 μs to the estimated τ_f, the agreement with measured data improves remarkably. The degree of agreement between these numbers is not critical; the important point is that these times to flashover have shown that the physical processes prevalent in the Townsend breakdown regime are largely electrical in nature and the drop is incapable of responding mechanically within that short duration of time. It is also clear that if a Townsend breakdown occurs, there is little that can be done to prevent it by merely improving the surface conditions, such as greasing. The breakdown probably will have to be eliminated electrically, e.g. by limiting the current.

The breakdown process in the EHD regime is more complex because of the mechanical coupling of the drop. Again, simplifications will be made here so that some reasonable estimates can be made. The force that is elongating the drop is electrical, the retarding force is the viscous drag of the fluid, and the sliding friction at the liquid/surface boundary. The above physical picture tells us that essentially only two terms are dominant, the electrical stress tensor balancing against the viscous stress tensor. Following this reasoning, a rough calculation can be made to estimate the time to flashover:

$$T^e_{ij} \simeq T^m_{ij} \tag{4.30}$$

so that

$$\frac{1}{2}\,\varepsilon_o E^2 \simeq \mu\,\frac{\partial v_x}{\partial y} \tag{4.31}$$

where

μ = viscosity of liquid used
v_x = velocity of drop
ε_o = free-space permittivity
x,y = spatial coordinate along the field direction and transverse respectively.

For simplicity, assume E is uniform and equal to applied voltage/gap distance. Now integrating (4.31) and assuming the drop to start from rest,

$$V \simeq \frac{1}{2}\,\frac{\varepsilon_o}{\mu}\,E^2 d \tag{4.32}$$

where d is the drop radius and is about 0.25cm, μ for distilled water is 0.001 Kg/sec M, and E is about 5 kV/cm. Substituting these numbers into (4.32) yields

$$V \simeq 2.7 \times 10^2 \text{ cm/sec.}$$

With a gap distance of about 1.2 cm, the time to flashover is around 5 ms.

This estimate is within our measured range for EHD regime, but is lower than some of the measured values. The reasons are clear: the crude approximations used can yield only a rough number at best; we neglected the sliding friction between the liquid/solid interface. The latter boundary condition would certainly slow down the liquid drop considerably. Another interesting point to be noted is that the time to flashover is almost directly proportional to the viscosity of the fluid used. This observation has been verified, as shown in Figure 4.10.

Despite the gross approximations used in the above calculations, reasonable estimates have resulted which shows that the physical mechanisms we proposed are probably correct. Since the two mechanisms (EHD and Townsend breakdown) are quite different, different physical means would have to be used to try reducingtheir effectiveness. For the EHD regime, surface conditions and mechanical properties of the fluid, such as viscosity, surface tension and etc. can be used to restrict the motion of the drop. For the Townsend breakdown regime, the field strength is already so intense, preventive measures are more difficult to find.

4.4 Experiments on Flat-Plate Flashover in Fog

4.4.1 Description of Experimental Apparatus

The experimental apparatus used in the tests to be described consisted of a flat-plate, similar in structure to the one described in Chapter III, but smaller in size. The diameter of the inner electrode is 6 cm. and the inner diameter of the outer electrode is 10 cm. The size of the inner electrode can be varied, if desired.

For all of the tests, fog is generated in the fog chamber shown in Figure 4.7. In order to determine how much fog is deposited per unit time on the testing apparatus and range of droplet sizes, calibration tests are first performed. The flat-plate is positioned at a pre-selected spot inside the test chamber, so that its surface is kept level. The chamber door is closed, and the air compressor turned on, supplying pressurized air at 60 psi. Water droplets are forced out by this compressed air in the form of a misty fog. A calibration test is done for each duration of fog. For each test, the drop size is measured by averaging the volume of twenty typical droplets. The density is determined by averaging the number of drops collected over a known area. Both the size and density are plotted against fogging time in Figure 4.12. With the knowledge of these calibration curves, all of the tests can be seen as a function of fogging time alone and later expressed against size and density, if necessary.

4.4.2 Flat-Plate Tests in Fog

Before data-taking began, a single drop test was repeated on the flat-plate to demonstrate that the geometry of the set-up does not affect the physical regimes of operation. The times to flashover characteristic is again determined and is shown in Figure 4.13. Next, the threshold voltage for each different surface condition is determined for a range of fogging times. The surfaces used are clean plexiglas, greased plexiglas and Teflon, respectively. For each particular fogging period, several tests are carried out to determine the threshold value. The measurements are illustrated in Figure 4.14. It can be seen that the greased surface performs best,

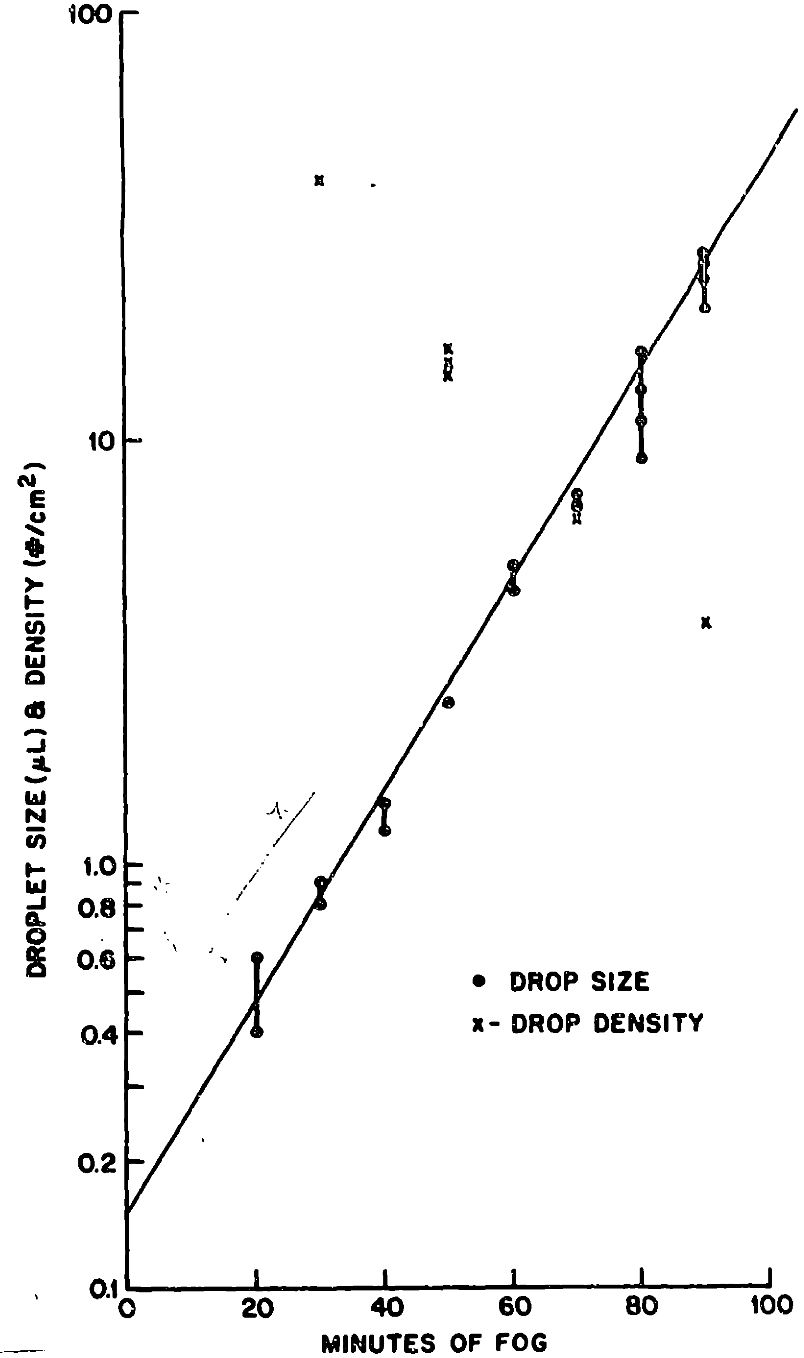

Figure 4.12 Calibration of Test Chamber in Fog

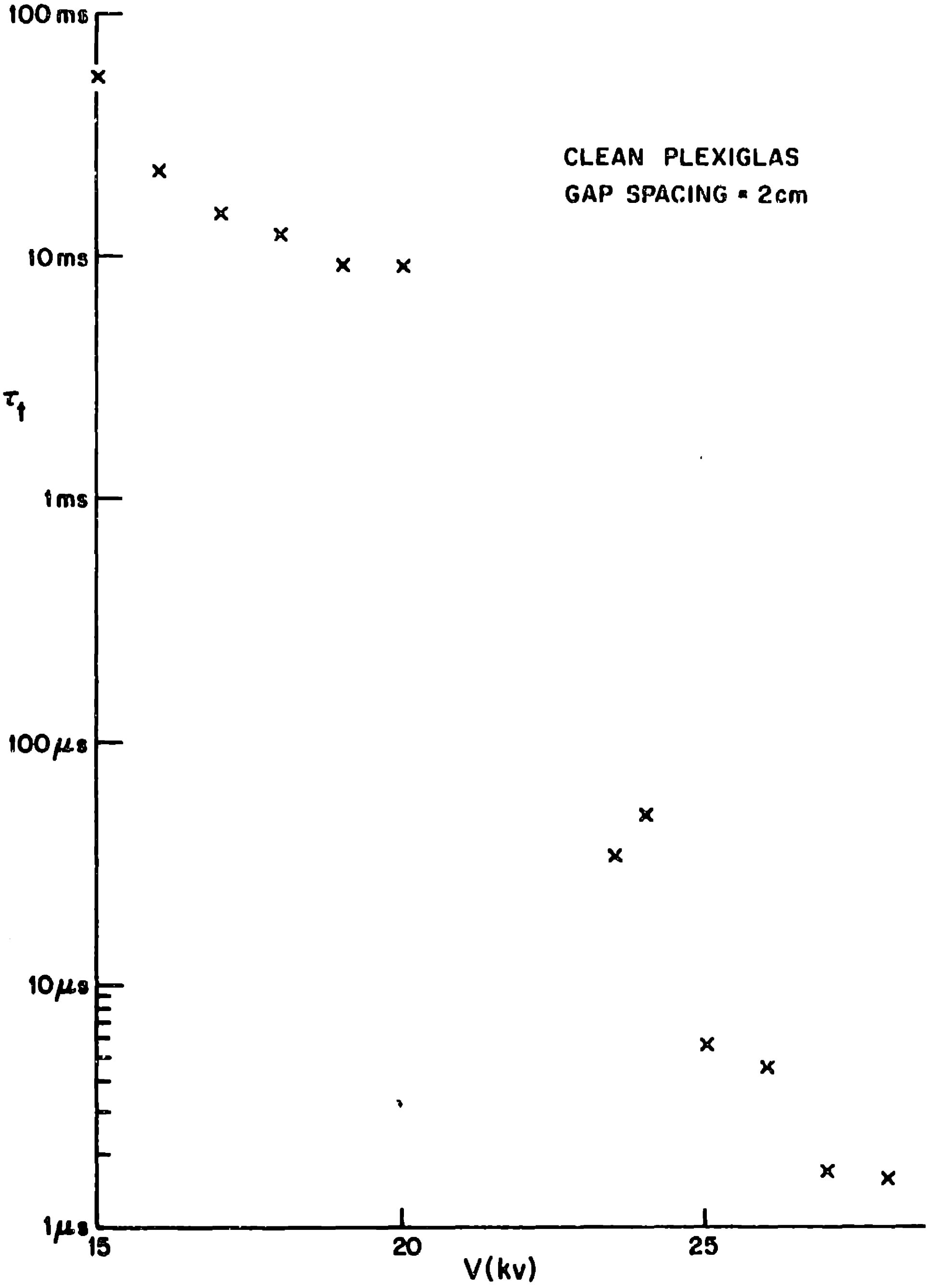

Figure 4.13 Time to Flashover for a Single Drop on a Flat-Plate

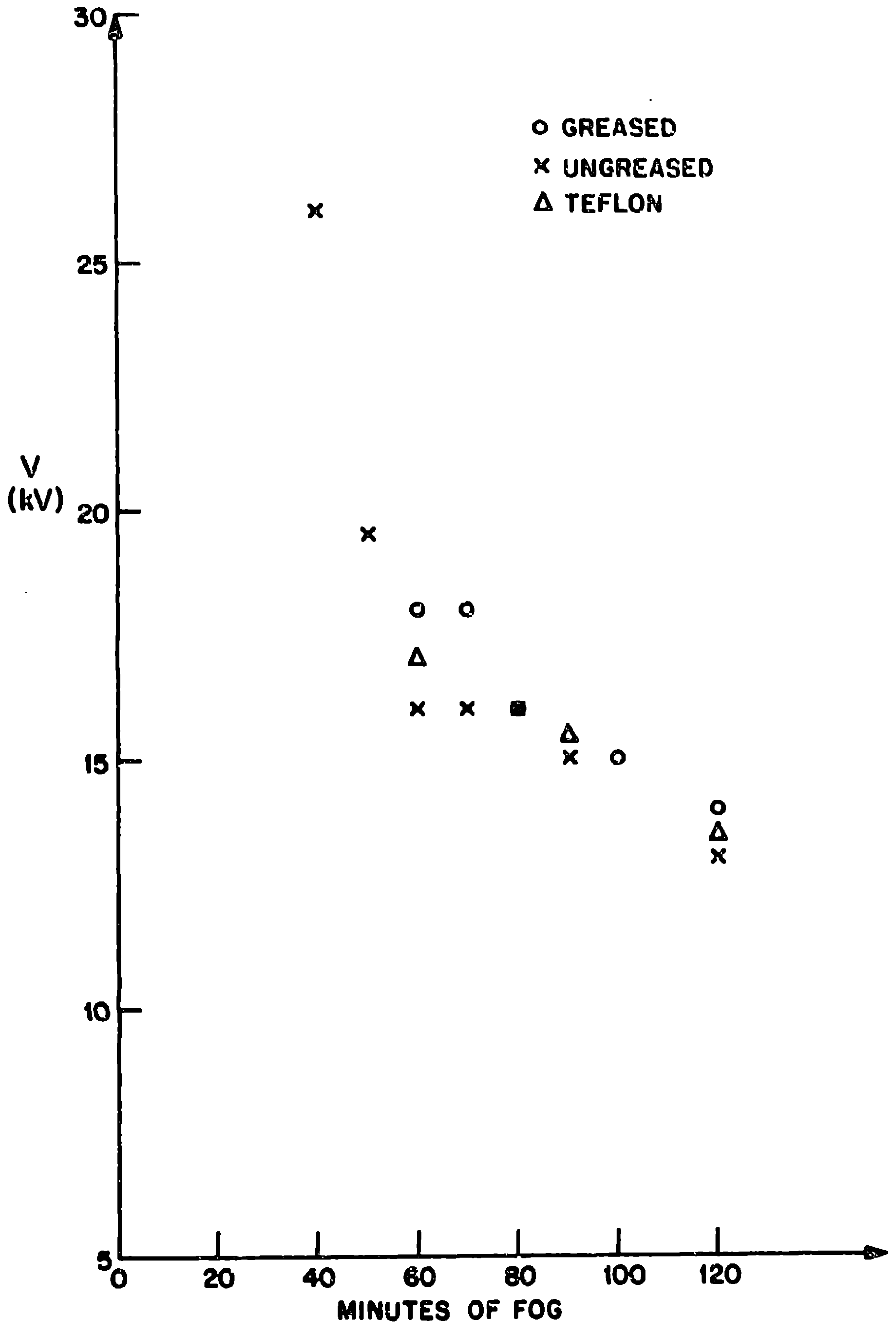

Figure 4.14 Threshold Voltage for Various Surface Conditions

Teflon next and plexiglas worst, as we would expect. Knowing the range of threshold voltages, the flat-plate test could now be carried out as follows. The plate was first thoroughly cleaned with detergent and tap water. It was then rinsed with distilled water and dried with an electric fan so that no hand wiping was necessary to avoid contamination. The electrodes were then bolted on. If a greased surface test was being performed, the Dow Corning 5-compound silicone grease was then evenly applied. A paste of grease of about 5 mm thick was first squeezed out of the Dow Corning tube. It was then divided into four equal portions and deposited on the flat-plate. The grease was evenly spread over the surface with a Kimwipe and the excess wiped off, so that only a thin layer was left on the surface. The process was repeated for every single test. Otherwise, the surface was left untouched. The flat-plate was then placed at a pre-determined position inside the test chamber to ensure that the surface was level. The high voltage terminal was clipped onto the center disc and the ground lead to the outer electrode. The chamber door was screwed on with wing nuts. The air compressor was activated and the nozzle turned on. The generated fog drifted through the filter into the test chamber, as shown in Figure 4.7. Most of the tests were performed for 40-minutes and 70-minutes durations respectively. Near the end of fogging, the d.c. power supply previously described was energized to charge up the capacitor bank. At exactly the 40-minutes mark or the 70-minutes mark (whichever the case may be), the voltage pulse was applied across the electrodes via the switch. Either a flashover or a withstand would result. The applied voltage was monitored in exactly the same way as in the single drop experiments. A Tektronix high voltage probe was used and the times to flashover were stored on the scope display. A sample display would look almost identical to the one shown in Figure 4.9 and will not be reshown here. The voltage trace registered a constant voltage level until flashover occurred when it dropped sharply. The capacitor bank was discharged in the process. The times to flashover for each fogging time and for each voltage level were recorded. A similar series of tests were run for a greased surface. Two different sizes of inner electrodes were used so that two gap distances were tested, namely 2 cm and 4 cm. The experimental results will now be discussed.

4.4.3 Discussion of Experimental Results

Figure 4.15 illustrates the measurements for both the clean surface and the greased surface, with a gap distance of 2 cm and 40 minutes of fog. First, it can be seen that the two regimes of operation, EHD and Townsend breakdown are also quite apparent in the flat-plate tests. Secondly, the greased surface does perform better than the ungreased one. These conclusions are similar to the ones we reached after the single drop tests. Despite the presence of numerous neighboring drops, the basic physical processes that govern the behavior of each individual drop appears to be the same as

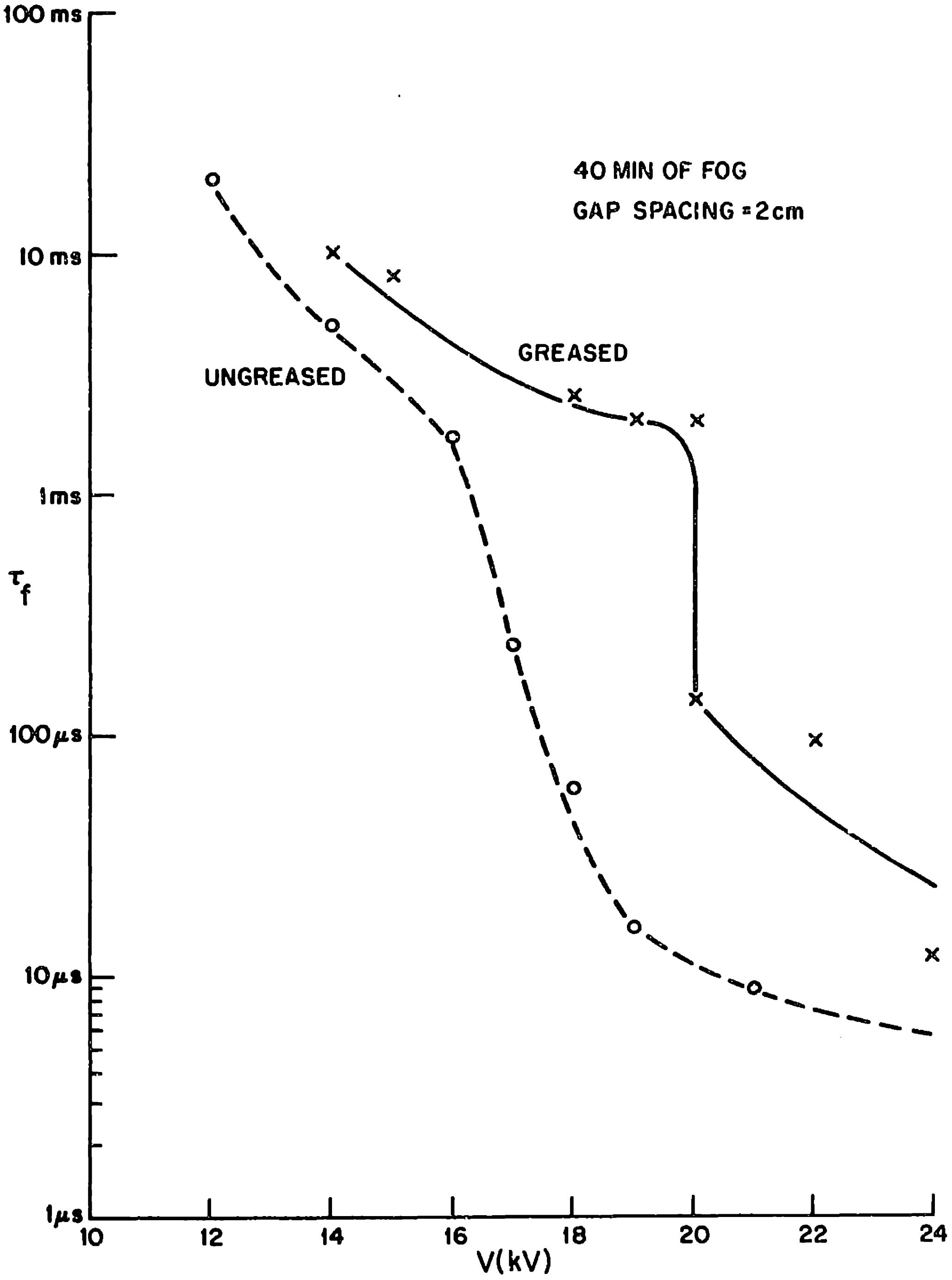

Figure 4.15 Time to Flashover for a Flat-Plate in Fog

before. For the EHD regime, the field intensification and subsequent elongation sequence is still present. The presence of neighboring drops close by probably increases the intensification factor even more. Davis' calculations showed that for two very close drops, an intensification factor of a 1000 is possible. Because of the enhanced field and because of the presence of these numerous drops, an important phenomenon was observed consistently during tests of an ungreased surface. The observation was recorded on nearly all of the withstand cases, when the voltage applied was not high enough for a flashover. Before application of voltage, the droplets are rather evenly deposited on the surface. After a withstand test, most of these individual drops coalesced forming chains or filaments. A typical measurement shows that a filament can be formed by a collection of ten to twenty drops, by merely applying the voltage only once. The filaments thus formed, completely alters the original state of the plate. This surface would now flashover at a much lower voltage than the original one. This process is denoted by filamentation and is detrimental to the insulating strength of an on-line insulator. The surface of an insulator is usually under constant electrical stress, and water drops, once deposited on the surface, will tend to coalesce, forming filaments. As moisture accumulation increases, filaments become longer. The insulating strength decreases accordingly. A flashover can thus occur considerably below the expected nominal voltage. With reduced insulating strength per unit, more insulators would be needed. A new and clean insulator usually performs much better than an old and contaminated one, partly because the new unit still retains much of its water-repellent properties, and thus is capable of preventing filamentation. A contaminated one, on the other hand, has a far more wettable surface, allowing filamentation to occur with ease. Greasing is one method of retaining the water-repellent properties of a surface. Since the drops bead up on such a surface, it is harder for them to coalesce with each other and form a filament. Not surprisingly, this is exactly what was observed during greased surface tests. After a withstand test, very little filamentation is observed and most of the drops seem to retain their original shapes. As a result, the reduction in flashover threshold voltage is small, only around 10%. For the ungreased surface, the reduction can be as much as 30-40%. Test results for a Teflon surface are more erratic and less repeatable, probably owing to frequent occurrence of discharges in the small air gaps between the electrode and the Teflon surface. The qualitative observation is that a Teflon surface ranks below the greased surface and above the ungreased one.

The test procedure was repeated for 70-minutes fogging time (Figure 4.16) and a smaller inner electrode (gap distance = 4 cm). The general behavior of the times to flashover characteristics is similar to the ones shown in Figure 4.15 and will not be discussed again.

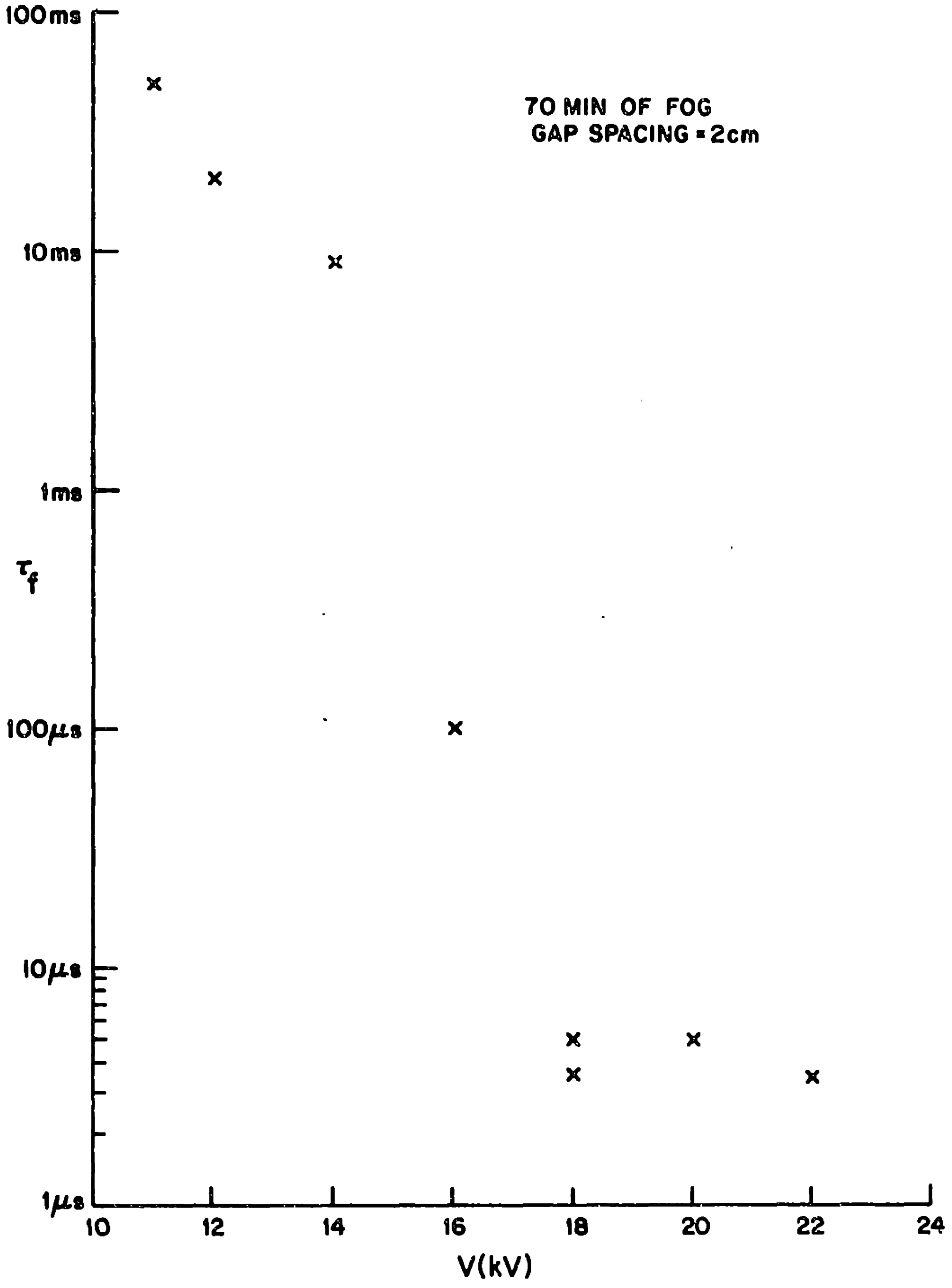

Figure 4.16 Time to Flashover for a Flat-Plate in Fog

BIBLIOGRAPHY - CHAPTER IV

1. J. Dillard, private communication, Westinghouse Corp.

2. W.C. Johnson and S.E. Phillips, "Insulators for Telegraph wires", British Patent 3534, 1876.

3. J.S. Forrest, "The Electrical Characteristics of 132 kV Line Insulators Under Various Weather Conditions," J. IEE, 1936, 79, Pt. II, p. 401.

4. J.S. Forrest, "Characteristics and Performance in Service of High-Voltage Porcelain Insulators," ibid., 1942, 89, Pt. II, p. 60.

5. M. Yamamoto and K. Ohashi, "The salt Contamination of the External Insulation of High-Voltage Electric Apparatus and Its Counter Measures," Trans. Amer. Inst. Elect. Engrs., 1961, 80, p. 380.

6. J.E. Conner and A.D. Lantz, "The Insulator Contamination Problem as Influenced by Silicone Surface Coatings," ibid., 1958, 77, Pt. III, p. 1101.

7. H.P. Harris, "Four Measures Minimize an Unusual Case of Insulator Contamination," Elect. World, 1954, 142, p. 80.

8. T. Seta, "Combatting the Contamination Problem by Applying Grease-Like Water-Repellent Substance," ETJ Japan, 1962, 7 (2), p. 73.

9. J. Zeleny, "Instability of Electrified Liquid Surfaces," The Phys. Rev., Vol. 10, #1, second series, July 1917, p. 1-6.

10. C.T.R. Wilson and G.I. Taylor, "The Bursting of Soap-Bubbles in a Uniform Electric Field," Phil. Soc. Proc. 22, p. 728 (1924).

11. W.A. Macky, "The Deformation of Soap Bubbles in Electric Fields," Phil. Soc. Proc. Vol. XXVI, p. 421-428, 1931.

12. J.J. Nolan, Proc. Roy. Irish Acad., 37, p. 28, 1926.

13. G. Taylor, "Disintegration of Water Drops in an Electric Field," Proc. Royal Soc. A. 280, p. 384 (1964).

14. M.H. Davis, "Two Charged Spherical Conductors in a Uniform Electric Field: Forces and Field Strength," Journ. Mech. and Applied Math., 17, p. 499 (1964).

15. J. Latham and I.W. Roxburgh, "Disintegration of Pairs of Water Drops in an Electric Field," Proc. Roy. Soc. A295, pp. 84-97, 1966.

16. G. Taylor, "The Coalescence of Closely Spaced Drops When They are at Different Electric Potentials," Proc. Roy. Soc. A306, pp. 423-434 (1968).

17. P.R. Brazier-Smith, "Stability and Shape of Isolated and Pairs of Water Drops in an Electric Field," The Physics of Fluids, Vol. 14, #1, pp. 1-6, 1971.

18. P. Moon and D. Spencer, Field Theory for Engineers, D. Van Nostrand Co., Inc., Princeton, New Jersey, 1961.

19. A.W. Adamson, "Physical Chemistry of Surfaces," Interscience Publishers, 1960.

20. Poynting and Thomson, Properties of Matter, p. 89 (1929).

21. E. Nasser, Fundamentals of Gaseous Ionization and Plasma Electronics, Wiley and Sons, Inc., New York, 1971.

22. J.W. Gibbs, "The Scientific Papers," Vol. 1, Thermodynamics, Longmans, Green and Co., 1906.

23. Commentary on the scientific writings of J.W. Gibbs, Vol. 1, Thermodynamics, edited by Donnan, F.G. and Haas, A., Yale University Press, 1936.

24. B.A. Pethica and T.J.P. Pethica, "The Contact Angle Equilibrium" in Second International Congress of Surface Activity, Vol. III, Academic Press, New York, New York, p. 131 (1957).

CHAPTER V

HIGH-SPEED PHOTOGRAPHIC STUDIES OF FLASHOVERS

5.1 Introduction

During the course of this work, high-speed photography was used extensively to capture the discharge activities in slow motion. Some of the proposed ideas reported in the previous chapters are in fact, based on observations of this nature. Because of space limitations, only a few of the highlights are shown here. The cases to be shown are the one-dimensional model, the flat-plate and an insulator flashover respectively.

5.2 Linear Model Flashover

The linear model used is essentially the same one as described in Chapter II. The voltage applied is 20 kV (a.c.) and is much higher than the threshold value. The flashover process is almost instantaneous. The film speed is 1000 frames/sec. so that the frames are spaced at 1 ms intervals. Figure 5.1(a) illustrates three frames when the water surface is acting as an anode. Note that the arc tip is very much diffused and not much propagation is observed during this half-cycle. Figure 5.1(b) shows the last four milliseconds when the flashover is being completed. The water electrode is in its cathode phase. The velocity of propagation has picked up considerably during these few milliseconds. These pictures clearly illustrate a significant difference in propagation velocities for different polarities. This

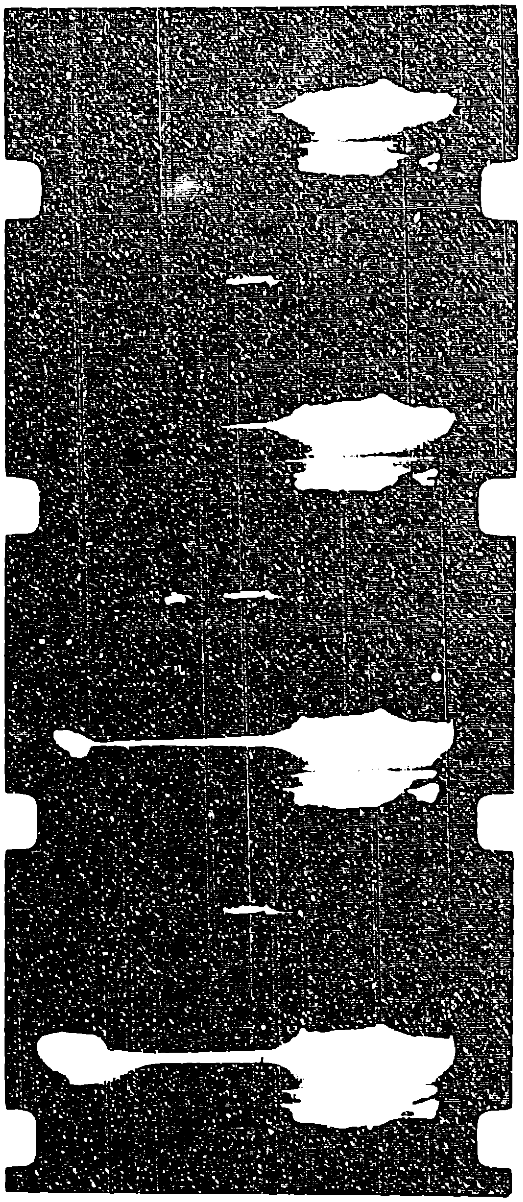

feature has been incorporated into our theories through the assumption that the power input at the arc tip is dependent on the electrode fall voltages (either cathode or anode).

5.3 Flat-Plate Flashover

Figures 5.2(a) and (b) display a sequence of events observed during a flat-plate test. The testing procedure has already been adequately described in Chapter III. In this particular test, the slurry used consists of a mixture of 50 gm. of bentonite, 2 gm. of NaCl and 1 liter of distilled water. The voltage applied is 4.5 kV and the film speed is 3000 frames/sec. The flashover process lasts 26 cycles since application of voltage. The vertical trace on the film is the superimposed current trace which also functions as a polarity indicator.

Figure 5.2(a) shows the initial discharges which are more or less symmetrically spaced around the inner electrode. As the discharges lengthen, their number decreases until only two main arcs remain. These two are very much branched at their tips and cathode-spot-like structures can be discerned under close examination as in Figure 5.2(b). This observation substantiates the assumption that discharge current enters the wet layer at more than one contact point. Figure 5.3 illustrates a typical flashover when the arc completely bridges the electrodes.

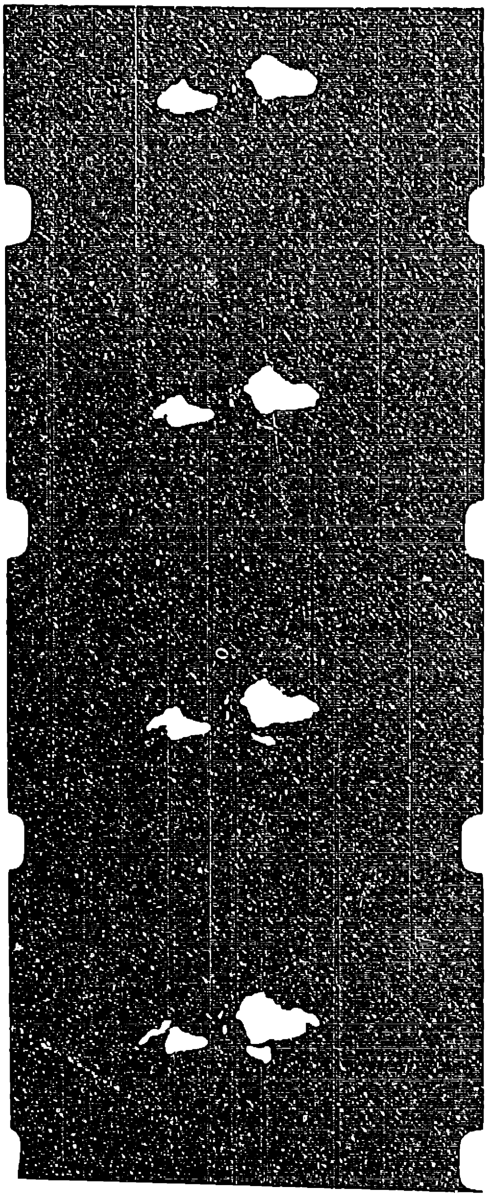

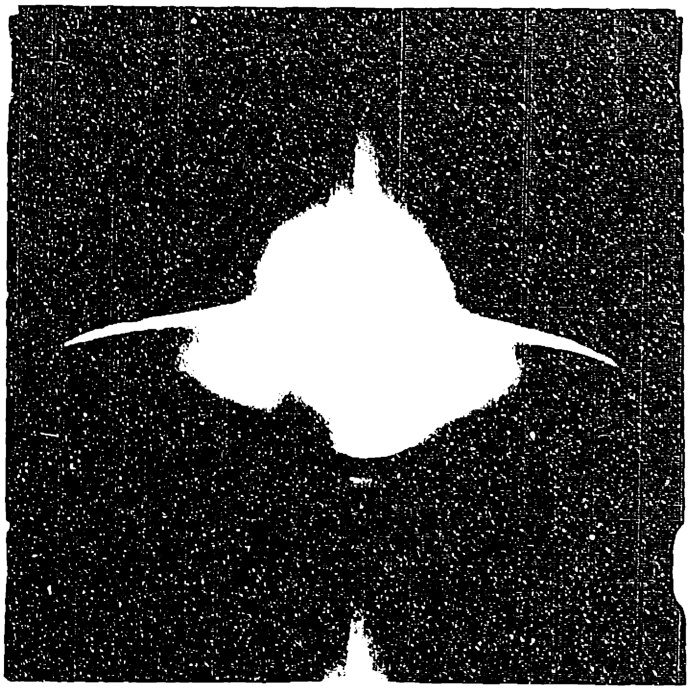

5.4 Insulator Testing

One of the main conclusions of Chapter II is that the electrode fall voltages plays a major part in the physical mechanisms of arc propagation. The higher the cathodic or anodic voltages, the greater will be the energy input at the arc tip and the faster will the arc propagate. Unfortunately, water is a very poor secondary emitter and hence has a very high cathodic voltage, much higher than metallic electrodes (see section 2.7). This is the reason why arcs can propagate much faster on water than on metal. To take advantage of this fact, metallic strips known as "arc stoppers" can be placed at strategic places where arcs can come in contact with them. Once in contact, the reduced electrode fall voltages will decrease the energy input at the arc tip and either slow down or stop the propagation. An example of the use of arc stoppers is described below for an insulator test. Actual insulator testing is an area which has not been reported in this study so far, mainly because most of the tests are exploratory in nature. In this test, the insulator is first artificially contaminated by spraying on its cleaned surface a mixture of bentonite and salt. The insulator, while still dripping wet, is placed in a vertical position in the test chamber and tested. Figure 5.4(a) shows the geometry of the set-up. It can be seen that both the bottom and the side of the insulator are visible. Two thin pieces of aluminum strips have been taped onto the inner sides of the two outermost skirts before spraying and testing. The metallic surfaces can reduce the cathode fall voltage considerably and could therefore prevent the propagation process from being completed. It is the purpose to study the effects of these metallic "arc stoppers". Figure 5.4(b) displays four frames (∿ 1.3 ms) of initial discharges on the bottom surface, just after the application of voltages. Figure 5.4(c) shows the flashover . The metallic arc stoppers, in this test, do not yield any significant improvement. One of the reasons is that these bands act as equipotential surfaces so that new arcs can be developed which can eventually flashover. Studies are now under way to redesign these arc stoppers in such a fashion so that undesirable arcing can be eliminated.

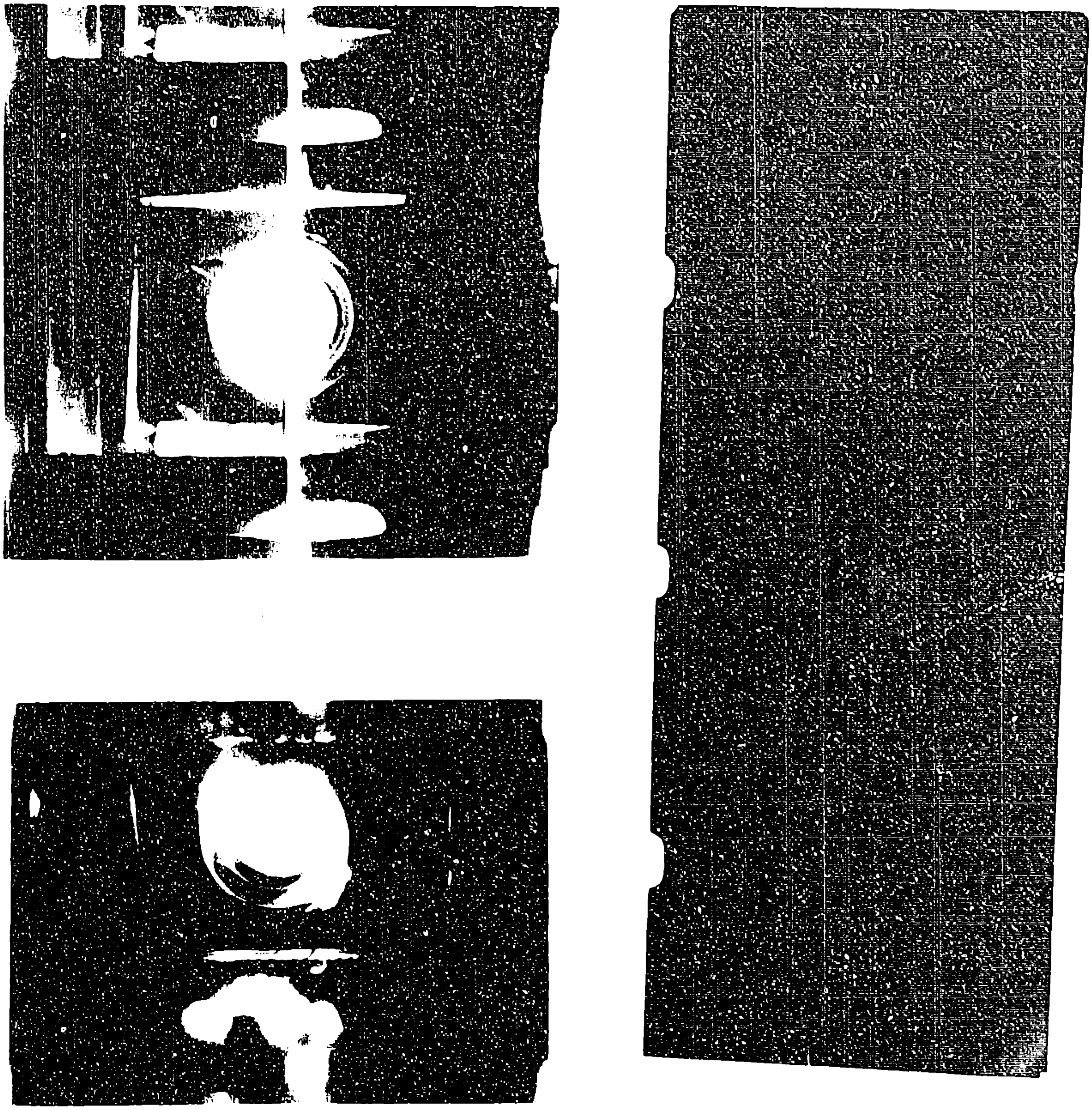
a
b

[illegible]

CHAPTER VI

SUMMARY, CONCLUSIONS AND SUGGESTIONS FOR FUTURE RESEARCH

6.1 Summary and Conclusions

Contamination flashover of outdoor suspension insulators is a result of the following sequence of events: - Deposition of pollutants and moisture making the surface conducting, formation of dry zones; initiation of arc discharges across these dry zones and propagation of discharges over the wet contaminated surface to trigger a flashover. This thesis has attempted to study the last stages of a flashover, namely, the mechanisms of arc propagation and the surface conditions which can affect them. In order to single out their salient features, simplified models are constructed so that mathematical limitations are reduced to a minimum.

In Chapter II, a linear model is investigated. Geometrically as well as mathematically, it is the simplest model. Two comprehensive theories are constructed. Each has incorporated a dynamic arc model into its formulation. One uses Mayr's arc model, while the other uses Phillips' model (later revised by Los). Mayr's cylindrical arc model is first utilized for its simplicity. However, because of its implicit limitations, it is felt that a more refined model is needed. Los modified Phillips' cylindrical arc model into a bi-cylindrical one which is more suitable for the case at hand. The physical set-up is described fully in Chapter II. Essentially, however, it consists of an cylindrical arc propagating over a liquid surface which is approximately at constant temperature. The use of the bi-cylindrical coordinates greatly simplifies the mathematics since one of the coordinates can be treated as isothermal lines. The resultant model is based on perturbational analysis and yields more realistic arc time constants. Both of these arc models are time dependent and their inclusion insures that the theories cover the full duration of a flashover process - from application of voltages to eventual flashover. Besides these dynamic arc models, another important feature of both theories is the proposed growth mechanism equation. This equation is derived from the conservation of energy and essentially stipulates that the main mechanism behind arc propagation occurs at its tip where the energy dissipated creates new ionization of the surrounding air and new arc paths. The energy input at the tip, however, is governed by the polarity of the water surface beneath it. When the surface is a cathode, the electrode fall voltage is higher than when it is an anode and the energy input is proportionately greater. This, in turn, predicts that the velocity of propagation is much faster for a cathode surface than for an anode one. This prediction is found to be in agreement with experimental observations.

Both theories are simulated on a computer and the simulation results are then compared with experimental observations. Both have compared favorably with experimental measurements. Theory II (Phillips' model) is, however, more useful, because all the input quantities can be pre-determined and the outputs are directly usable. In theory I, one or two parameters are not known a priori and can only be determined after an experiment has been performed. Its usefulness is therefore more limited. Except for the arc modeling, both theories have incorporated the same physical principles. Their good agreement with experimental data indicates that some of the proposed physical mechanisms are probably in operation. The proposed arc motion via energy input at the tip is especially significant. It is for this reason that a study is carried out to investigate further this cathode region. Based on the principles of glow discharge, a theoretical model is constructed to simulate the cathode fall regime for a water surface. The predicted values agree with measured values obtained both here at MIT and elsewhere. This model is also capable of simulating metallic electrodes. Its simulated cathodic voltages are also found to agree remarkably well with published data. These agreements have provided added confidence in the validity of the model.

The findings of Chapter III can have a significant bearing on the design of counter measures to prevent flashovers. Since the electrode fall voltages are found to play a vital role in the propagation of a discharge, methods can be devised to reduce that voltage drop. It is known that a water electrode has a much higher cathodic voltage than a metallic one. Thus if metallic strips can somehow be judiciously located at various strategic spots around the cap and pin, the arc discharges, once in contact with them, will find it more difficult to further propagate. It is with this in mind that the so-called "arc stoppers" were tested, an example being shown in Chapter V. There, a continuous metallic band, attached to the outer skirts, is intended as one type of stoppers. Some problems exist, however, one being that the stopper itself can become an additional site for discharge activities. Thus the shapes and locations of the stoppers must be carefully selected. The technique is still in the process of being improved, but preliminary studies for both the linear model and real insulators indicate that promising results can be forthcoming. The use of arc stoppers represents one of the practical benefits derived from studying the growth mechanism of an arc discharge.

Chapter III considers a two-dimensional simulation of an insulator, namely, a flat-plate. Because of the more complex geometry involved, the theory developed is only a static one. Nevertheless, it is more refined than previously proposed ones, because it takes into account the changing surface resistance as the arc root propagates from the inner electrode towards the outer one. The theory is compared with experimental results and good agreement is found. The tests are performed with a new coating technique, and because of higher short circuit current capabilities, data points were taken for lower critical resistivities than previously possible. The results, however, are in general agreement with previous studies and the theory, therefore, can apply to all the available experimental data. It is encouraging to note that, despite the simplications of the model, the static theory still provides a useful guideline to flashover criteria. Since the flat-plate tests can be standardized fairly easily, its use in studying contamination flashover should be encouraged. The effects of levels of contamination, presence of different salts, and presence of insoluble particulates such as sand can thus be studied in a controlled manner. The principal physical mechanisms can be detected without undue geometrical complication. Eventually, a dynamic model can possibly be developed.

Chapter IV studies the effects of surface conditions on flashover. Fog droplets are probably the most damaging to the insulation strength of a contaminated insulator. Most of the droplets are deposited on the surface and remain there. These droplets will elongate in the presence of electric fields and coalesce to form filaments, further reducing the insulating strength of a unit. The first part of Chapter IV investigates the elongation process in detail for a single drop. It is observed that a flashover can be completed via one of two processes, either the EHD process or the Townsend breakdown process. Inside the EHD regime, the electric field is less intense and the drop continues elongating and further intensifying the field, until a flashover finally results. A theory, known as "motion via contact angle hysteresis" is proposed for the observed behavior. In the Townsend breakdown regime, the field strength is sufficient for immediate breakdown without deforming the drop first. As a result, the flashover process is completed in far less time. Since Townsend breakdown is purely an electrical phenomenon, the only way to prevent it from occurring would be to reduce the field. For the EHD regime, however, the dynamics of the water drop plays an important role. Therefore, more alternatives of prevention are possible. One way is to apply grease so that the drops will find it more difficult to react to the applied field. It has been demonstrated by others that a greased surface performs better than an ungreased one.

The second part of Chapter IV extends the investigation of surface phenomenon into a two-dimensional case - the flat-plate - under fog. Tests indicate that the same regimes of operation are present in this case and filamentation is clearly present. The reduction in flashover voltage due to the filamentation is also drastically evident (∿ 30%). The application of grease reduces filamentation and improves the performance. The use of grease, however, has its own limitations. Because of aging and chemical decomposition, grease has to be manually cleaned off and reapplied once every two years or so. Clearly, a more permanent substitute should be found. Preliminary tests have indicated that the performance of a Teflon surface ranks above an ungreased surface but below a greased one. Materials such as Teflon therefore, deserve more investigation. However, substitutes such as these and semi-conducting glaze must also withstand other mechanical and electrical requirements before they can be used on a wide scale.

Chapter V records some of the highlights of experimental observations with high-speed photography. These photographs support some of the proposed theoretical developments as reported in the thesis text. Since flashover is such a rapid process, the use of high-speed photography has proved to be an invaluable aid to the studies.

6.2 Suggestions for Future Research

Since the main purpose of studies of this nature is to improve the performance of an insulator, major efforts should be directed towards finding a practical solution. Preliminary studies have indicated the possible utilization of arc stoppers. This line of research should be further pursued. Arc stoppers of different shapes and size should be investigated to decide on an optimum design.

For a majority of contamination flashover research, sodium chloride is probably the most commonly used salt. While its presence is undoubtedly common, it is by no means the only salt present in natural contaminants. With industrial pollution on the increase, other less common salts such as calcium sulphate and magnesium sulphate should also be included. It may be possible to define some kind of an equivalent salt density if conductivity is the only criterion. Without studying at least a few more salts, however, it is too early to make such a generalization.

Flat-plate tests using d.c. voltages should be performed so that polarity effects can be studied. With the advent of high voltage d.c. lines, it is important to establish d.c. insulation levels relative to a.c. levels so that comparison between the two can be easily made.

Thermal effects concerned with film heating play a role in flat-plate tests, since dry zones are always formed first. The importance of the drying effect and heating at the arc root tip should be further studied.

As already discussed in this thesis, surface conditions can drastically affect the performance of an insulator. With the introduction of semi-conducting insulators, porcelain is no longer the only acceptable surface material. More materials research should be directed towards finding a suitable substitute for porcelain so that its surface is more water-repellent. Or, a permanent coating might be devised so that the mechanical strengths of porcelain can be combined with a material of more desirable surface properties. If the idea of using arc stoppers is successful, the surface coating can have these stoppers embedded in them. In this way two counter measures can be incorporated into one single design.

A more extensive series of tests for naturally contaminated insulators should be performed and standardized so that test results from simplified versions in laboratory can be compared with them. In this way, the usefulness of each model can be determined.

APPENDIX A

COMPUTER PROGRAM FOR DYNAMIC THEORY I

This appendix lists the program for a numerical solution of Dynamic Theory I in section 2.5.2. The system of equations are as shown in Table 2.3. Since all the equations are normalized, all inputs are in the form of dimensionless numbers. These are denoted as A, B, and C respectively in the program. All the outputs are also in normalized form and must be denormalized for physical interpretation. The simulation is carried out on IBM 370/165, using IBM's Continuous System Modeling Program.

```
LABEL      ARC  VELOCITY  CALCULATIONS  I
CONSTANT  A=1.90
CONSTANT  B=0.18
CONSTANT  C=20.0
INITIAL
       Q0=ALOG(W)
       W=C*(A-B)**2.0
       RA0=C*EXP(-Q0)
DYNAMIC
       Y=RA/C
       Q=-ALOG(Y)
       I=(1.0-B/A-B/(A*RA)+1.0/RA)/(1.0+(1.0-X)/RA)
       IA=(1.0-B/A-I*(1.0-X))/(RA*X)
       DXDT=A*B*IA/Q
       X=INTGRL(0.01,DXDT)
       DRADT=RA*(1.0-RA*(IA**2.0)*(A**2.0))
       RA=INTGRL(RA0,DRADT)
METHOD  TRAPZ
CONSTANT  DELT=1.0E-02, FINTIM=2.0E+01
PRINT  I,RA,IA,Q,DXDT,X
END
STOP
```

APPENDIX B

COMPUTER PROGRAM FOR DYNAMIC THEORY II

This appendix lists the program for a numerical solution of Dynamic Theory II in section 2.6.2. The system of equations are as shown in Table 2.6. The input quantities for each simulations are V (volts), r (Ωcm), ℓ(cm) and Q (Joules). The output quantities are current and velocity respectively. The simulation is carried out on IBM 370/165, using IBM's Continuous System Modeling Program.

```
LABEL      ARC  VELOCITY  CALCULATIONS  II
CONSTANT  VE=800
CONSTANT   VO=8000
       L=10.0
INITIAL
       A=0.10
       QO=0.10
       XO=0.00
       RAO=52.0*(R*L)**1.42/(A**0.58*(VO-VE)**1.42)
DYNAMIC
       T=1.0/(RA**3.*IA**2.*A**2.*0.5*(RA*A**2.0)**(-1.27))
       EO=(52.0*(A**2.0*RA)**0.42)**(0.705)/A
       DRADT=RA*(1.0-(IA*RA/EO)**2.0)/T
       RA=INTGRL(RAO,DRADT)
       DQDT=IA**2.0*RA-52.0*(IA/A)**0.58
       Q=INTGRL(QO,DQDT)
       DXDT=VE*IA/Q
       X=INTGRL(XO,DXDT)
       I=(VO-VE)*(1.0+R/RA)/(R*L+R**2.0*(L-X)/RA)
       IA=(VO-VE-I*R*(L-X))/(RA*X)
METHOD  TRAPZ
TIMER  DELT=1.0E-06,  FINTIM=2.0E-02
PRINT  I, RA, IA, Q, DXDT, X
END
STOP
```

APPENDIX C

COMPUTER PROGRAM FOR CATHODE FALL REGION SIMULATION

This appendix lists the program for a numerical solution of cathode fall voltage simulation. The system of equations are summarized in Table 2.8. As already described in the text, all the integrations are carried out towards the cathode surface so that the boundary conditions are specified at the anode side of the cathode fall regime. The critical quantity to be determined is the cathode fall voltage V_c. The simulation is carried out on IBM 370/165, using IBM's Continuous System Modeling Program.

```
LABEL      CATHODE  VOLTAGE  FALL  CALCULATIONS
CONSTANT Q=1.62E-19,EPSIL=0.885E-11,NO=2.69E+25,UE=4.0E-02,...
       UI=2.0E-04, P=760.0
INITIAL
       GAMAEO=-1.00E+25
       GAMAIO=-(1.0E-01)*GAMAEO
       EO=1.0E+05
       VIO=UI*EO
       VEO=-UE*EO
FUNCTION  SIGMA1=0.0E+00,0.0E+00,...
                 2.0E+03,3.4E-05,2.2E+03,5.2E-05,2.4E+03,1.34E-04,...
       2.6E+03,2.34E-04,2.8E+03,4.30E-04,3.0E+03,9.10E-04,3.1E+03,...
       1.36E-03,3.2E+03,2.01E-03,3.3E+03,3.05E-03,3.4E+03,4.5E-03...
       ,3.5E+03,6.05E-03,3.6E+03,8.2E-03,4.0E+03,1.67E-02,...
       5.0E+03,5.54E-02,6.0E+03,1.27E-01,7.0E+03,2.24E-01,8.0E+03,...
       3.40E-01,9.0E+03,4.91E-01,1.0E+04,6.37E-01,1.1E+04,8.1E-01,...
       1.2E+04,1.02E+00,1.3E+04,1.24E+00,1.4E+04,1.48E+00,1.54E+04,...
       1.6E+00,1.6E+04,1.76E+00,2.0E+04,2.5E+00,4.0E+04,6.0E+00,...
       6.0E+04,8.0E+00,8.0E+04,9.4E+00,1.0E+05,1.04E+01
DYNAMIC
       VE=-UE*(E/P)*P
       VI=UI*(E/P)*P
       E=INTGRL(EO,DEDX)
       DEDX=Q/EPSIL*(GAMAI/VI-GAMAE/VE)
       GAMAE=INTGRL(GAMAEO,Y)
       GAMAI=GAMAE+GAMAIO-GAMAEO
       Z=AFGEN(SIGMA1,E/P)
       Y=-P*GAMAE*Z*100.0
       NI=GAMAI/VI
       NE=GAMAE/VE
       NNET=NI-NE
       K=GAMAE/GAMAI
       V=-INTGRL(0.0,E)
PRINT    E, VE, VI, GAMAE, GAMAI, NI, NE, NNET, K, V
TIMER  DELT=1.00E-07, FINTIM=5.00E-05
TIMER  PRDEL=2.00E-07
```

```
METHOD   TRAPZ
       END
```

APPENDIX D

COMPUTER PROGRAM FOR FLAT-PLATE SIMULATION

This appendix lists the program for a numerical solution of the system of equations developed in section 3.5.2. The essential feature of the program is the detection of a minimum current as a function of applied voltage. The maximum of these minimum currents is then located by varying the parameter, x, the arc propagation distance. Once the critical current and distance are determined, the critical voltage can be derived for each particular surface resistance. The programming language used is Fortran IV GI.

```
C         FLAT-PLATE  CALCULATIONS
        REAL  I, K, N
        DIMENSION  V(400)
        N=0.48
        X=0.92
        WRITE(6,100)   X
        W=0.00
        DO 30 M=1,100
        W=W+1000.0
        WRITE(6,300)   W
         I=0.00
        DO 10 J=1,200
        I=I+0.0001
        Y=(1.0/((I/3.14)**0.5*X)-(I/3.14)**0.5/X-X/((I/3.14)**0.5)/2.0
        Z=(1.0/X-I/(3.14*X)+X)/2.0
        YA=Y+((Y)**2.0-1.0)**0.5
        ZA=Z+((Z)**2.0-1.0)**0.5
        YB=ALOG(YA)
        ZB=ALOG(ZA)
        K=YB-ZB
        V(J)=X*(I)**(-N)+W*I*K/6.28
        IF(J.EQ.1)GO TO 10
        DELTA=V(J)-V(J-1)
        IF(DELTA)10,10,20
10        CONTINUE
20      WRITE(6,200)  I, V(J)
30      CONTINUE
100     FORMAT(1H1,F10.5)
200     FORMAT(1H ,2E20.6)
300     FORMAT(1H ,F10.5)
       STOP
        END
```

BIOGRAPHICAL DATA

T.C. Cheng was born in Shanghai, China and received his secondary school education at Wah Yan College, Hong Kong. He attended the Massachusetts Institute of Technology, from 1965 until 1974, receiving the B.S. degree in 1969, and M.S. and E.E. degrees in 1970, all in Electrical Engineering. From 1969 - 1971, he was a Teaching Assistant in the Department of Electrical Engineering. From 1971-1972, he received a M.I.T. fellowship. From 1972 on, he was a Research Assistant with the Electric Power Systems Engineering Laboratory.

Mr. Cheng was employed, during the summer of 1967, by the M.I.T. Research Laboratory of Electronics to detect experimentally the presence of ozone in outer space. During the summer of 1968, he worked for the M.I.T. Continuum Electromechanics Laboratory, studying surface instabilities. In the summer of 1969, he worked for Holograph Corp., Cambridge, Mass. developing a new product for marketing. In 1971, he served as a consultant to Environmental Research and Technology, Inc., Lexington, Mass. for air precipitator design.

T.C. Cheng is a member of IEEE, Eta Kappa Nu, Tau Beta Pi and Sigma Xi.